INFORMATION TO USERS

This manuscript has been reproduced from the microfilm master. UMI films the text directly from the original or copy submitted. Thus, some thesis and dissertation copies are in typewriter face, while others may be from any type of computer printer.

The quality of this reproduction is dependent upon the quality of the copy submitted. Broken or indistinct print, colored or poor quality illustrations and photographs, print bleedthrough, substandard margins, and improper alignment can adversely affect reproduction.

In the unlikely event that the author did not send UMI a complete manuscript and there are missing pages, these will be noted. Also, if unauthorized copyright material had to be removed, a note will indicate the deletion.

Oversize materials (e.g., maps, drawings, charts) are reproduced by sectioning the original, beginning at the upper left-hand corner and continuing from left to right in equal sections with small overlaps.

Photographs included in the original manuscript have been reproduced xerographically in this copy. Higher quality 6" x 9" black and white photographic prints are available for any photographs or illustrations appearing in this copy for an additional charge. Contact UMI directly to order.

Bell & Howell Information and Learning
300 North Zeeb Road, Ann Arbor, MI 48106-1346 USA
800-521-0600



Reproduced with permission of the copyright owner. Further reproduction prohibited without permission.

Reproduced with permission of the copyright owner. Further reproduction prohibited without permission.

MICROWAVE SPECTROSCOPY AND MODELING OF WEAKLY BOUND DIMERS AND TRIMERS

by

Rebecca A. Peebles

A dissertation submitted in partial fulfillment
of the requirements for the degree of
Doctor of Philosophy
(Chemistry)
in The University of Michigan
2000

Doctoral Committee:

Professor Robert L. Kuczkowski (Chair)
Professor Mark M. Banaszak Holl
Professor Anthony H. Francis
Professor Lawrence L. Lohr
Professor Jens Zorn

Reproduced with permission of the copyright owner. Further reproduction prohibited without permission.

UMI Number: 9977235

UMI®

UMI Microform9977235
Copyright 2000 by Bell & Howell Information and Learning Company.
All rights reserved. This microform edition is protected against
unauthorized copying under Title 17, United States Code.

Bell & Howell Information and Learning Company
300 North Zeeb Road
P.O. Box 1346
Ann Arbor, MI 48106-1346

Reproduced with permission of the copyright owner. Further reproduction prohibited without permission.

For my father,
In loving memory

Reproduced with permission of the copyright owner. Further reproduction prohibited without permission.

ACKNOWLEDGMENTS

First, I'd like to thank Dr. Kuczkowski without whose help, encouragement and willingness to let me join his group I wouldn't have been able to do all of this. I'd also like to thank Professor Norman Craig at Oberlin College who was responsible for developing my initial interest in molecular spectroscopy and who has shown willingness and eagerness to help me in my career ever since. Thanks go to the Kuczkowski group and to several visitors who have helped me in my studies over the course of my time at Michigan. I'd also like to thank the members of my committee: Dr. Francis, Dr. Lohr, Dr. Banaszak Holl and Dr. Zorn for being interested and willing to be part of this. Also, Professor Banaszak Holl provided assistance when I was starting to use the Jaguar *ab initio* program, and Professor Lohr helped me with the *ab initio* calculations and Gaussian 94. The Computer Services staff in the Chemistry Department (Mike Kitson, Dr. Todd Raeker, and Bill Custer) have also been a huge help with both computational and hardware problems. Professor Helen Leung at Mount Holyoke College was kind enough to let me use some of her data in the work on $HCCH{\bullet}N_2O$ and provided lots of helpful advice with that project and on the running of Herb Pickett's spectrum fitting program. I am grateful to Gail Potrykus for her assistance and patience with papers, printing, photocopying and other things too numerous to list. I'd like to acknowledge the financial support for this research which came from the National Science Foundation Experimental Physical Chemistry Division, a University of Michigan and US Department of Education GAANN fellowship, a Sloan Summer Research Fellowship from the University of Michigan Center for the Education of Women and the Alfred P. Sloan Foundation, and a Margaret Sokol Fellowship from the University of Michigan

Reproduced with permission of the copyright owner. Further reproduction prohibited without permission.

Chemistry Department. I'd like to thank my parents for their support, inspiration and patience over the years. Finally, many thanks go to Sean for initially teaching me how to run the spectrometer, and for his constant help, inspiration, caring, patience, love and concern since the day I joined the Kuczkowski group. I couldn't have done any of it without you. Thank you.

Reproduced with permission of the copyright owner. Further reproduction prohibited without permission.

TABLE OF CONTENTS

DEDICATION ii

ACKNOWLEDGEMENTS iii

LIST OF TABLES viii

LIST OF FIGURES xi

LIST OF APPENDICES xiii

CHAPTER

I. INTRODUCTION 1

Thesis Proposition 12
References for Chapter I 13

II. THE OCS TRIMER: ISOTOPIC STUDIES, STRUCTURE AND DIPOLE MOMENT 15

Introduction 15
Experiment 16
Results 17
A. Spectra 17
B. Dipole Moment 18
C. Structure 21
Discussion 23
A. Experimental Summary 23
B. Empirical Structure Trends 24
Summary 27
References for Chapter II 29

III. MICROWAVE SPECTRUM AND STRUCTURE OF THE $(CO_2)_2N_2O$ COMPLEX 31

Introduction 31
Experiment 32
Results 35
A. Spectra 35
B. Nuclear Quadrupole Hyperfine Structure 35
C. Dipole Moment 36
D. Structure 38
Discussion 41

Reproduced with permission of the copyright owner. Further reproduction prohibited without permission.

Conclusion 44
References for Chapter III 46
IV. MICROWAVE SPECTRA, DIPOLE MOMENT, AND STRUCTURAL ANALYSIS OF N_2O•SO_2 48
Introduction 48
Experiment 50
Results 50
A. Spectra 50
B. Dipole Moment 54
C. Structure 56
Discussion 61
A. Structure Inferences 61
B. Structure Comparisons 62
Summary 63
References for Chapter IV 65
V. $(N_2O)_2$•SO_2: ROTATIONAL SPECTRUM AND STRUCTURE OF THE FIRST VAN DER WAALS TRIMER CONTAINING SULFUR DIOXIDE 67
Introduction 67
Experiment 68
Results 69
A. Spectra 69
B. Dipole Moment 71
C. Structure 72
Discussion 77
Summary 80
References for Chapter V 82
VI. ISOTOPIC STUDIES, STRUCTURE AND MODELING OF THE NITROUS OXIDE•ACETYLENE COMPLEX 84
Introduction 84
Experiment 85
Results 87
A. Spectra 87
B. Dipole Moment 88
C. Structure 90
Discussion 94
Summary 96
References for Chapter VI 97
VII. SEMI-EMPIRICAL AND *AB INITIO* MODELING OF WEAKLY BOUND DIMERS AND TRIMERS 99
Introduction 99
Theoretical Methods 100
A. Semi-empirical Calculations Using the ORIENT Model 100
B. *Ab initio* Calculations 101

Reproduced with permission of the copyright owner. Further reproduction prohibited without permission.

OCS Trimer Calculations 103
$(CO_2)_2N_2O$ Calculations 107
$N_2O \cdot SO_2$ Dimer 110
$(N_2O)_2 \cdot SO_2$ Calculations 113
Acetylene-N_2O 118
General Conclusions 122
References for Chapter VII 125
APPENDICES **127**

Reproduced with permission of the copyright owner. Further reproduction prohibited without permission.

LIST OF TABLES

Table

II.1 Spectroscopic constants for the assigned isotopes of $(OCS)_3$ 18

II.2 Stark coefficients for OCS trimer transitions 19

II.3 Dipole moment components for OCS trimer 20

II.4 Principal axis coordinates for OCS trimer 21

II.5 Experimental structural parameters for OCS trimer 22

III.1 Spectroscopic constants for the seven isotopes of $(CO_2)_2N_2O$ 33

III.2 Dipole moment data for the normal and $^{15}N_2O$ isotopomers of $(CO_2)_2N_2O$ 37

III.3 Principal axis coordinates for the two possible structures of $(CO_2)_2N_2O$ 39

III.4 Structural parameters for the two possible structures of $(CO_2)_2N_2O$ 40

IV.1 Spectroscopic constants for $N_2O{\bullet}SO_2$ isotopomers with substitution in N_2O only 51

IV.2 Spectroscopic constants for isotopomers of $^{15}N_2O{\bullet}SO_2$ with isotopic substitution of SO_2 52

IV.3 Experimental and predicted dipole moment components for $N_2O{\bullet}SO_2$ 54

IV.4 Stark coefficients for the $N_2O{\bullet}SO_2$ upper tunneling doublet 55

IV.5 Structural parameters for four inertial fits for $N_2O{\bullet}SO_2$ 56

IV.6 Principal axis coordinates for four possible $N_2O{\bullet}SO_2$ structures 57

V.1 Spectroscopic constants for $(N_2O)_2{\bullet}SO_2$ 69

V.2 Stark coefficients for $(^{15}N_2O)_2{\bullet}SO_2$ 71

V.3 Dipole moment components for $(N_2O)_2{\bullet}SO_2$ 72

Reproduced with permission of the copyright owner. Further reproduction prohibited without permission.

V.4 Structural parameters for two possible $(N_2O)_2 \bullet SO_2$ configurations 73

V.5 Principal axis coordinates for two possible $(N_2O)_2 \bullet SO_2$ structures 75

VI.1 Spectroscopic constants for $HCCH \bullet N_2O$ 86

VI.2 Stark coefficients for $HCCH \bullet N_2O$ 89

VI.3 Dipole moment components for $HCCH \bullet N_2O$ 90

VI.4 Structural parameters for $HCCH \bullet N_2O$ 92

VI.5 Principal axis coordinates for $HCCH \bullet N_2O$ 93

VII.1 Predicted structural parameters for $(OCS)_3$ 105

VII.2 Predicted structural parameters for $(CO_2)_2N_2O$ 109

VII.3 Predicted structural parameters for $N_2O \bullet SO_2$ 111

VII.4 Predicted structural parameters for $(N_2O)_2 \bullet SO_2$ 115

VII.5 Relative energies of N_2O/SO_2 combinations predicted by ORIENT 117

VII.6 ORIENT structural parameters for $HCCH \bullet N_2O$ 119

VII.7 *Ab initio* structural parameters for $HCCH \bullet N_2O$ 121

A.1 Transition frequencies for $(^{18}OCS)_3$ 128

A.2 Transition frequencies for $(O^{13}CS)_3$ 130

B.1 Transition frequencies for normal $(CO_2)_2N_2O$ 132

B.2 Transition frequencies for $(^{13}CO_2)_2N_2O$ 134

B.3 Transition frequencies for $^{13}CO_2 \bullet {}^{12}CO_2 \bullet N_2O$ 135

B.4 Transition frequencies for $^{12}CO_2 \bullet {}^{13}CO_2 \bullet N_2O$ 137

B.5 Transition frequencies for $(CO_2)_2{}^{15}N_2O$ 138

B.6 Transition frequencies for $(CO_2)_2N_2{}^{18}O$ 140

B.7 Transition frequencies for $(CO_2)_2{}^{15}N^{14}NO$ 141

C.1 Transition frequencies for upper frequency tunneling components of $N_2O \bullet SO_2$ 146

Reproduced with permission of the copyright owner. Further reproduction prohibited without permission.

C.2 Transition frequencies for lower frequency tunneling components of $N_2O{\bullet}SO_2$ 147

D.1 Transition frequencies for normal $(N_2O)_2{\bullet}SO_2$ 148

D.2 Transition frequencies for $(^{15}N_2O)_2{\bullet}SO_2$ 150

D.3 Transition frequencies for $^{15}N_2O{\bullet}^{14}N_2O{\bullet}SO_2$ 152

D.4 Transition frequencies for $^{14}N_2O{\bullet}^{15}N_2O{\bullet}SO_2$ 153

D.5 Transition frequencies for $(^{15}N_2O)_2{\bullet}^{34}SO_2$ 154

E.1 Transition frequencies for $HCCH{\bullet}N_2O$ 156

F.1 Distributed multipole moments for OCS 158

F.2 Distributed multipole moments for CO_2 and N_2O used in $(CO_2)_2N_2O$ and $HCCH{\bullet}N_2O$ calculations 158

F.3 Distributed multipole moments for SO_2 159

F.4 Distributed multipole moments for N_2O with bond centers 160

F.5 Distributed multipole moments for HCCH 160

Reproduced with permission of the copyright owner. Further reproduction prohibited without permission.

LIST OF FIGURES

Figure

I.1 Schematic diagram of the University of Michigan Fourier transform microwave spectrometer 4

I.2 Spectrum of two transitions of $(OCS)_3$ 6

II.1 Anti-parallel and predicted parallel configurations for $(OCS)_3$ 15

II.2 Parallel OCS dimer configurations 25

II.3 Anti-parallel OCS dimer configurations 26

III.1 Two possible experimental structures for $(CO_2)_2N_2O$ 31

III.2 CO_2 dimer and $(CO_2)_2$ faces of trimers 42

III.3 Experimental CO_2-N_2O configurations 43

IV.1 Experimental structures of CO_2-SO_2, OCS-SO_2 and CS_2-SO_2 49

IV.2 Parameters used to define the N_2O•SO_2 structure 56

IV.3 Four possible experimental structures for N_2O•SO_2 59

IV.4 Dimers of SO_2 with linear molecules 63

V.1 Experimental structure (Structure I) of $(N_2O)_2$•SO_2 74

V.2 Second possible experimental structure (Structure II) of $(N_2O)_2$•SO_2 76

V.3 Experimental N_2O•SO_2 structure and $(N_2O)_2$•SO_2 faces 78

VI.1 Structure of HCCH•N_2O 91

VII.1 Four ORIENT structures for $(OCS)_3$ 103

VII.2 Two ORIENT structures for $(CO_2)_2N_2O$ 107

VII.3 ORIENT structure for N_2O•SO_2 110

Reproduced with permission of the copyright owner. Further reproduction prohibited without permission.

VII.4 Second and third highest energy ORIENT structures for $(N_2O)_2 \bullet SO_2$..... 114

Reproduced with permission of the copyright owner. Further reproduction prohibited without permission.

LIST OF APPENDICES

Appendix

A. Transition frequencies for OCS trimer 128

B. Transition frequencies for $(CO_2)_2N_2O$ 132

C. Transition frequencies and experimental details for $N_2O \cdot SO_2$ 144

D. Transition frequencies for $(N_2O)_2 \cdot SO_2$. 148

E. Transition frequencies for $HCCH \cdot N_2O$ 156

F. Distributed multipole moments used in ORIENT semi-empirical calculations 158

Reproduced with permission of the copyright owner. Further reproduction prohibited without permission.

CHAPTER I

INTRODUCTION

Weak forces between molecules are of fundamental importance to the understanding of many aspects of chemistry. Hydrogen bonding is critical in biological systems and is responsible for the unique properties of liquid water. It is also a significant factor in the interactions between many molecules in the gas phase and in solution. Weaker van der Waals forces are also important in determining how molecules will interact with each other. Since the first step in a reaction usually involves the meeting of two or more molecules, a knowledge of the forces governing the interaction of the monomers can lead to insight into their reaction mechanism. Intermolecular interactions are particularly important in the Earth's atmosphere where many molecules interact and react with each other at relatively low temperatures. If a thorough quantitative understanding of the intermolecular forces in small clusters of molecules is gained, it should ultimately be possible to extrapolate this knowledge to larger clusters and eventually to condensed phases. The most important aspect of the forces to understand, if a comprehension of very large groups of molecules is desired, is the small changes that occur as more and more monomers are added to a system.

A good way to learn about these forces is to study weakly bound dimers and trimers. The structures of these complexes can be very useful in helping to understand intermolecular forces. Although many dimer structures have been studied (the SO_2 complexes in a recent review by Kuczkowski and Taleb-Bendiab, for instance[1]), prior to the research reported in this thesis, few trimers had been studied at high resolution. The majority of these were combinations of water and rare gas atoms with other small

Reproduced with permission of the copyright owner. Further reproduction prohibited without permission.

molecules (for example: N_2O-Ne_2,[2] $(H_2O)_2$-CO_2,[3] $(CO_2)_2$-H_2O,[4,5] Ne-C_6H_6-H_2O,[6] Ar_3-HF[7]). A few homo-molecular trimers of linear triatomic molecules had been studied by IR and microwave spectroscopy [$(CO_2)_3$,[8,9] $(N_2O)_3$,[10] $(OCS)_3$,[11] $(HCCH)_3$,[12] $(HCN)_3$[13]], but the only hetero-molecular trimer of linear triatomics that had been examined in the microwave region was $(CO_2)_2$-HCN.[14] The tetramer $(CO_2)_3$-HCN had also been studied, but the spectral assignment was relatively simple compared to the systems described in this thesis because the complex was a symmetric top.[15] Recent projects presented in this dissertation and in other publications[16-23] are the first systematic microwave studies of the more complex trimers of linear and bent monomers.

There are several ways to examine how molecules interact. High resolution spectroscopic techniques can be used to probe the structures of small clusters of molecules. Infrared spectroscopy gives information about both the structure and vibrational motions of a complex and can be used to detect relatively large clusters, but the resolution of the method can be too low to give definitive structural information. Other methods of laser spectroscopy also often have resolution limits too low for direct structure determination, although other properties of van der Waals complexes can be probed. The high resolution of microwave spectroscopy, however, gives pure rotational spectra which lead to accurate structural information for small complexes. The only limitations for this method are that the cluster of interest must have a dipole moment and must not be too heavy, since this will shift the spectrum out of the frequency range of the spectrometer. This method will be described in more detail below and applied to several dimer and trimer systems in Chapters II – VI. Once the configurations of dimers and trimers have been determined experimentally, they can be examined and compared, elucidating structural trends and providing information about what types of interactions govern the structures.

The weakly bound complexes that are studied are very floppy systems with the constituent monomers constantly experiencing large amplitude vibrational motions. The

Reproduced with permission of the copyright owner. Further reproduction prohibited without permission.

experimental structures that are obtained for these systems are vibrational averages rather than static equilibrium configurations such as would result from *ab initio* calculations. Information on the dynamic aspects of the complexes is difficult to extract from the microwave spectroscopic data, although it can be obtained from the centrifugal distortion constants of relatively simple systems.[24] Some clusters display tunneling motions or internal rotation, and the spectral perturbations from these motions can be used to obtain data such as barrier heights and tunneling frequencies.[25] The effect on microwave data of the large amplitude motions present in a complex is frequently more subtle than the large perturbations caused by tunneling motions. While these smaller effects occasionally lead to difficulties in obtaining the structures that are necessary for comparison purposes, they can give valuable data of their own. For instance, a large standard deviation in a least-squares fit of the structure of a complex to its moments of inertia is an indication that the internal motions in the complex are relatively large, while very small values for the distortion constants in a fit indicate that the complex is relatively rigid. The interpretation of these data is qualitative, however, and thus difficult to perform with confidence. Detailed dynamic information about van der Waals complexes is best determined with alternative infrared techniques such as those mentioned in the last paragraph, since they detect the vibrational transitions of a molecule.

Microwave spectroscopy measures the pure rotational spectra of molecules. These spectra result from transitions between quantized rotational energy levels. The positions of the levels are determined in part by the moments of inertia, where, by convention, $I_a < I_b < I_c$, and I_a is the moment of inertia about the a axis, etc. The quantum number J is used to designate total angular momentum, and K_a and K_c are the approximate projections of the total angular momentum on the a and c inertial axes, respectively. Since the projections are approximate, the K quantum numbers are not "true" quantum numbers, but rather "pseudo quantum numbers" that behave sufficiently well to be useful in the interpretation and prediction of spectra. Rotational transitions

Reproduced with permission of the copyright owner. Further reproduction prohibited without permission.

occur between adjacent J levels ($\Delta J = \pm 1$; $\Delta K_a = \pm 1$ and/or $\Delta K_c = \pm 1$) or within a single J level ($\Delta J = 0$; $\Delta K_a = \pm 1$ and/or $\Delta K_c = \pm 1$) and are only visible in the microwave when the molecule has a dipole moment. Structural information can be obtained, because the transition frequencies depend on the rotational constants (A, B and C) of the molecule as well as on the quantum numbers J, K_a and K_c. The rotational constants are inversely proportional to the moments of inertia about the principal axes ($B = \hbar^2/2I_b$, in Joules) and thus can be related to molecular structure since moments of inertia depend on intermolecular distances [$I_x = \sum_i m_i\left(y_i^2 + z_i^2\right)$ for the x-inertial axis and atom i with mass m and coordinates (x, y, z)].

Since a complex or molecule only has three unique moments of inertia, only three

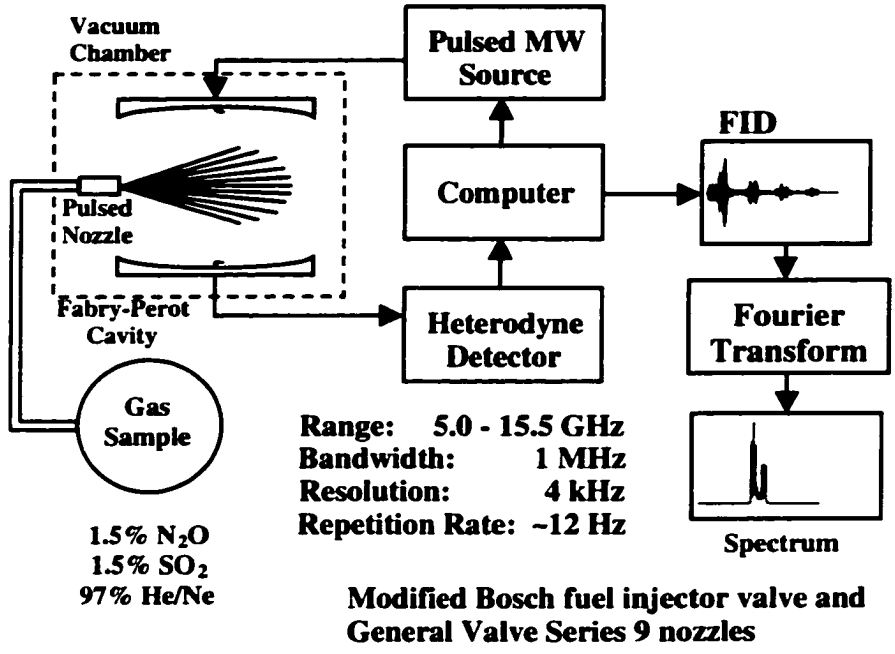


Figure I.1. Schematic diagram of the University of Michigan FTMW spectrometer.

pieces of structural information can be obtained from its spectrum. The reasonable assumption that monomer structures do not change upon complexation minimizes the number of parameters to be determined in a dimer or trimer, but it is usually necessary to

Reproduced with permission of the copyright owner. Further reproduction prohibited without permission.

obtain additional data to determine all of the structural parameters of the complex. Isotopic substitution of one or more atoms in the system, with the assumption that this does not change the structure, provides additional equations that can be used in the structure determination process. For example, it should be possible to determine the configuration of a trimer requiring nine parameters (a trimer of three linear monomers) by assigning three isotopic species for a total of nine moments of inertia. In practice, though, the number of isotopes required to determine a structure uniquely is usually larger because of the least-squares structure fitting process that is used. For trimers of linear monomers, five to seven isotopic species are typically required to obtain a structure of comparable quality to that of a dimer. If the trimers are more complex, containing bent or three dimensional molecules, the required number of isotopes can be even larger. For this reason, the study of trimers has been constrained primarily to systems containing rare gas atoms, water and linear monomers. Once systems of three linear monomers have been thoroughly explored, slightly more complex systems with one bent molecule can be attempted. Eventually enough experience with these systems will make it possible to assign even more complex trimers.

Rotational spectra are measured with a Balle-Flygare type Fourier transform microwave (FTMW) spectrometer.[26, 27] The apparatus consists of a large evacuated chamber (Fabry-Pérot cavity) containing two movable, concave, spherical mirrors that are adjusted until the microwave radiation forms a standing wave between them. A short gas pulse is followed by a pulse of microwave radiation which is delivered to the cavity by an L-shaped antenna in the center of one mirror. If the radiation is at the frequency of a rotational transition of the sample, the interaction between the dipole moment of the sample and the radiation in the cavity causes a macroscopic polarization of the gas. The rotation of the sample molecules with the frequency of the polarizing radiation and with their dipoles aligned parallel to each other emits radiation at the transition frequency. The emitted radiation, which decays over time as the macroscopic polarization dissipates,

Reproduced with permission of the copyright owner. Further reproduction prohibited without permission.

is detected by the antenna which was used for the initial microwave pulse. The decay of the radiation in the spectrometer cavity over time is termed a free induction decay (FID), and a Fourier transform of this signal gives a frequency domain spectrum. The band width of the spectrometer is about 1 MHz, so transitions within about ±500 kHz of the excitation frequency should be detected.

The gas sample contains about 1.5% of each of the sample components, with the remainder consisting of either argon or "first run" He/Ne (10:90) carrier gas. A sample backing pressure of 2 – 3 bar is used with a chamber pressure of about 10^{-6} torr. The

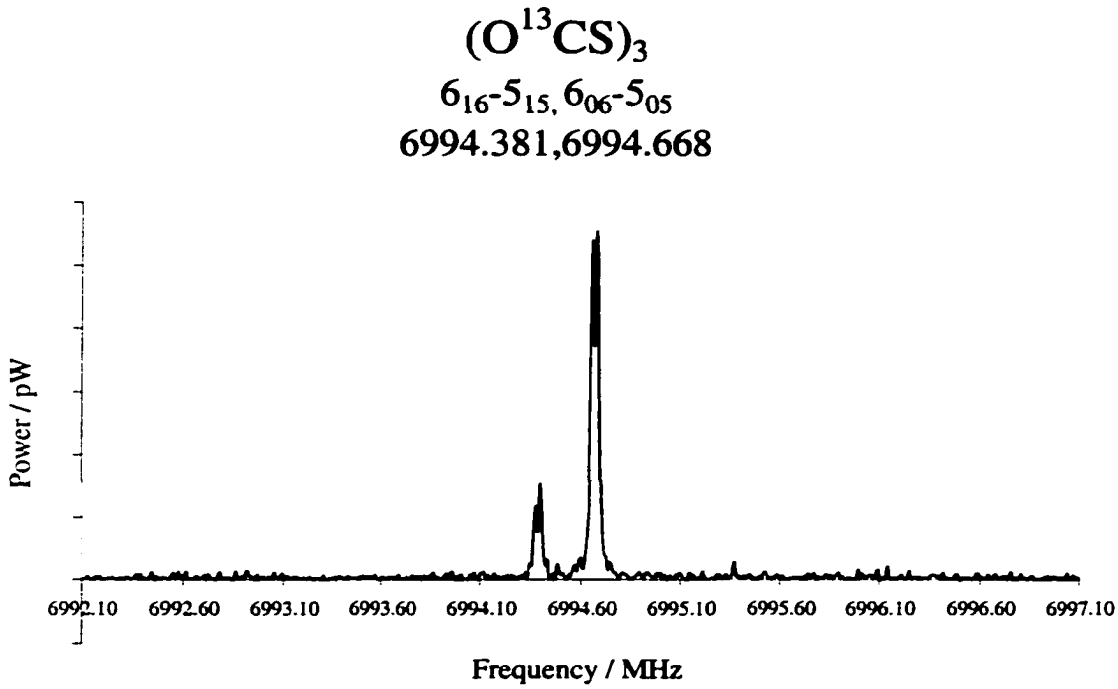


Figure I.2. Two transitions of $(OCS)_3$, a typical trimer.

sample is injected into the spectrometer cavity through a pulsed nozzle with a circular orifice of about 0.7 mm diameter. This nozzle is either a modified Bosch fuel injector valve or a General Valve Series 9 nozzle which is manufactured for spectroscopic applications. Complexes form when two or three molecules collide in the nozzle and then encounter a third (or fourth) body which carries away excess energy allowing the

Reproduced with permission of the copyright owner. Further reproduction prohibited without permission.

original cluster to stick together. The third body is usually a rare gas atom which has been added to the sample for this purpose. After the expansion, which has a rotational temperature of about 3 K, the system is essentially collision free, so any complexes that were formed in the nozzle are frozen out and stable. The valve is aligned perpendicular to the axis of microwave propagation, because this arrangement eliminates doubling of the transitions due to the Doppler effect. The frequencies of rotational transitions measured in this way are typically reproducible to within about 4 kHz, and they have a full width at half maximum of about 30 kHz. For dimer transitions the signal-to-noise (S/N) ratio is usually in excess of 20 after about 100 gas pulses, while trimers are much weaker with a S/N of 5 – 10 in about 500 gas pulses. Recent upgrades to the Michigan spectrometer based on software and hardware from the University of Kiel[28] allow automatic scanning of large regions of the spectrum. A typical scan during a trimer search uses a frequency step size of about 200 kHz and averages the spectra of 300 – 500 gas pulses at each frequency. Figure I.1 is a schematic diagram of the spectrometer and Figure I.2 shows two transitions of $(O^{13}CS)_3$ (^{13}C enriched).

The general procedure for assigning the spectrum of a weakly bound complex involves first using model structures to predict the spectrum and then using the spectrometer to search for transitions in regions of the spectrum where several lines are predicted. Model structures can be obtained from semi-empirical or *ab initio* calculations or by making an educated guess based on similar complexes and chemical intuition. A search range that is likely to have transitions from several possible structures is chosen. Once a region of 1.5 – 2 GHz has been scanned, and possible transitions identified, it is necessary to determine which transitions belong to the spectrum of interest. The first step in doing this is to perform mixing tests where one component at a time is removed from the sample (assuming a mixed dimer or trimer is desired). If a line is observed when only one sample component is present, it cannot be due to the complex of interest. After a number of transitions requiring both sample components have been identified in this

Reproduced with permission of the copyright owner. Further reproduction prohibited without permission.

manner, it is possible to attempt to assign them by comparing with one or more of the predicted spectra.

While mixing tests help to eliminate transitions that are not due to the desired complex, it would be helpful to have a tool that assists in the actual quantum number assignment of the transitions. This tool can be found in the Stark effect. When an electric field is applied to the region of the molecular expansion, a rotational transition will split into a number of components corresponding to different values of the quantum number M ($M = 0, \pm1, \ldots, \pm J$). Normally the M components are degenerate, but the application of an electric field lifts this degeneracy, and each component will have a frequency shift that is related to the dipole moment of the molecule, the value of M, the magnitude of the applied field, and the rotational constants. Thus, by measuring the Stark effect of an unassigned transition, the value of J for that transition can be determined from the number of components observed. The spacing between the components and the speed at which the frequencies change with applied field can also help identify the K_a and K_c pseudo quantum numbers of a transition. Ultimately, once an assignment has been accomplished, the dipole moment of the complex can be determined from the Stark effect measurements. This often leads to structural information and can give insight into whether there is a significant amount of induction in a complex.

The Stark effect is measured by applying voltages up to ±7 kV to two parallel steel mesh plates located just outside of the Fabry-Perot cavity of the spectrometer. These plates measure about 50 cm x 50 cm and are spaced about 30 cm apart. The electric field is calibrated by measuring the Stark effect of the $J = 1 - 0$ transition of OCS at 12162.98 MHz and assuming a dipole moment of 0.7152 D.[29]

Once the spectra of several isotopomers of a complex have been measured, it is usually possible to determine its structure by least-squares fitting of the moments of inertia to the structural parameters. This gives an r_0 (average) structure, since ground state vibrational motions are not accounted for. If substitutions of single atoms have been

Reproduced with permission of the copyright owner. Further reproduction prohibited without permission.

performed, then it is also possible to obtain r_s (substitution) coordinates for these atoms. This procedure uses Kraitchman's equations[30] and gives coordinates of the substituted atom in the principal axis system of the parent species. After a structure has been determined, it is compared with similar dimer and trimer species, leading to insight into the intermolecular forces present in the complexes. Comparison with theoretical predictions, as previously indicated, is also useful.

Theoretical methods can be used in addition to spectroscopy to gain insight into intermolecular interactions and to aid in spectral assignment. Both *ab initio* and semi-empirical techniques give information about how molecules interact. In addition to the prediction of structures, these methods can be used to calculate properties such as interaction energies, the dipole moment, higher multipole moments and barrier heights. While the dipole moment can be determined experimentally, the other quantities are more easily calculated. The relative contributions of electrostatic, dispersion, repulsion and induction forces to the total interaction energy of a complex can lead to insight into why it has a certain configuration or why seemingly similar systems often exhibit different structures.

In practice, semi-empirical calculations have been more effective than *ab initio* techniques at predicting the configurations of small complexes. Semi-empirical methods combine experimental and *ab initio* data to predict the structures and properties of molecular clusters. Electrostatic interactions are often modeled with *ab initio* distributed multipole analyses (DMA's) which calculate series of multipole moments (point charges, dipoles, quadrupoles, etc.) placed on each atom (and occasionally other points) in a molecule. Models for dispersion, repulsion and induction interactions often originate with experimental data. The simple Buckingham-Fowler model,[31,32] for example, uses a DMA to calculate electrostatic interactions and places hard spheres at the van der Waals radii of the atoms to model repulsive terms. One monomer simply rolls around the surface of the other until the electrostatic interactions are optimized. The success of this

Reproduced with permission of the copyright owner. Further reproduction prohibited without permission.

model on a variety of systems is an indication of the dominance of electrostatic interactions in the angular orientation of most dimers.[31 - 34] Other semi-empirical models include more complex dispersion-repulsion terms that incorporate several empirically determined constants. One of these more complicated models is the basis of the ORIENT semi-empirical program.[35] This program uses a DMA to represent the electrostatic interactions and atom-atom terms with an exp-6 form to represent dispersion and repulsion. Induction can be added to a calculation via *ab initio* distributed polarizabilities or by placing experimental point molecular polarizabilities on each monomer. The ORIENT model has been quite successful at predicting dimer and trimer structures[16, 19, 36, 37] and will be discussed in detail in Chapter VII. Other semi-empirical models for the study of van der Waals complexes have also been developed,[38, 39] but none has been systematically applied to an extensive series of related systems. The model developed by Muenter has been used in a range of situations, though,[11, 38, 39] and it will also be examined further in Chapter VII.

Ab initio calculations are a second way of modeling the intermolecular interactions in dimers and trimers. These computations model atoms and molecules by combining functions (basis sets) that approximate electron orbitals. This method is often less successful than semi-empirical models at predicting the structures of weakly bound complexes. There are several reasons for this. First, it is often necessary to use large basis sets that include polarization functions in order to model intermolecular interactions effectively. Also, since dispersion interactions often play a large role in determining the structures of weakly bound complexes, the inclusion of electron correlation can be an important factor in obtaining accurate *ab initio* results. Methods that take this into account are quite complicated. The result of these difficulties is that calculations on van der Waals molecules are usually large and therefore computationally expensive. If a search for the global minimum energy structure is to be carried out by performing calculations from several molecular starting orientations the expense and time consumed

Reproduced with permission of the copyright owner. Further reproduction prohibited without permission.

are greatly magnified. These factors often make it impossible to carry out calculations at a level sufficient to give accurate results. A third complication is that the potential energy surfaces for dimers and trimers are often very flat, meaning that the forces on the atoms change little with relatively large changes in geometry. This makes it difficult to achieve convergence in geometry optimizations, again increasing computation time and also making it difficult to obtain useful results from a calculation. Newer methods such as density functional theory help make *ab initio* calculations a more feasible option. In a relatively short computation time, they give results comparable to higher level methods that account for electron correlation. The problem of flat potential energy surfaces is often impossible to solve, though. Attempts at implementing *ab initio* methods to study some specific dimer and trimer systems will be discussed further in Chapter VII which will also give more specific computational details and highlight some of the difficulties encountered.

Although semi-empirical and *ab initio* methods can be used to predict structures and properties of small molecular clusters, and spectroscopic methods can be used for structure determination, the best way to gain an understanding of intermolecular forces is by comparison of experimental and theoretical structures. The differences are an indication of where theoretical models are inaccurate, and these discrepancies show where our understanding of intermolecular forces is incomplete. The development of models that predict the structures of dimers correctly, and then predict the small structural changes that occur in a dimer when a third body is added to the system, will indicate a good understanding of intermolecular forces, suggesting that larger systems may be modeled accurately. Also, correct prediction of the structures of a wide range of complexes indicates that the interaction model must be a relatively good representation of the intermolecular forces present. The following chapters will detail the assignments of several dimer and trimer species and will compare their structures with those of other relevant clusters. In the final chapter, the performance of semi-empirical and *ab initio*

Reproduced with permission of the copyright owner. Further reproduction prohibited without permission.

models on these complexes will be examined, and some general conclusions will be drawn.

Thesis Proposition

This thesis will examine weakly bound trimers containing linear and bent triatomic molecules and compare the structures of these van der Waals complexes with those predicted by a semi-empirical model and with *ab initio* calculations. Some of the first systems beyond homo-molecular trimers will be studied. The use of linear monomers in $(OCS)_3$ and $(CO_2)_2N_2O$ will minimize the number of structural parameters to be determined in these complex systems, making it possible to study a sufficient number of isotopic species that the structures can be determined accurately. In $(N_2O)_2{\bullet}SO_2$, the first high resolution study of a trimer containing the bent SO_2 molecule will be an initial step toward understanding more complex systems containing several nonlinear molecules. Examination of the dimers $N_2O{\bullet}SO_2$ and $HCCH{\bullet}N_2O$ will enhance the knowledge gained from the trimer studies and provide useful theoretical results. Comparison of trimer structures with other dimers and trimers will elucidate structural trends which in turn will assist in the development and testing of intermolecular interaction theories.

Reproduced with permission of the copyright owner. Further reproduction prohibited without permission.

References for Chapter I

[1] R. L. Kuczkowski and A. Taleb-Bendiab in *Structures and Conformations of Nonrigid Molecules*, J. Laane, *et al*, eds. (Kluwer Academic Publishers, The Netherlands, 1993).

[2] N. S. Ngari and W. Jager, J. Chem. Phys. **111**, 3919 (1999).

[3] K. I. Peterson, R. D. Suenram and F. J. Lovas, J. Chem. Phys. **94**, 106 (1991).

[4] K. I. Peterson, R. D. Suenram and F. J. Lovas, J. Chem. Phys. **90**, 5964 (1989).

[5] H. S. Gutowsky and C. Chuang, J. Chem. Phys. **93**, 894 (1990).

[6] E. Arunan, T. Emilsson and H. S. Gutowsky, J. Chem. Phys. **99**, 6208 (1993).

[7] H. S. Gutowsky, T. D. Klots, C. Chuang, J. D. Keen, C. A. Schmuttenmaer and T. Emilsson, J. Am. Chem. Soc. **107**, 7174 (1985).

[8] M. J. Weida and D. J. Nesbitt, J. Chem. Phys. **105**, 10210 (1996).

[9] G. T. Fraser, A. S. Pine, W. J. Lafferty and R. E. Miller, J. Chem. Phys. **87**, 1502 (1987).

[10] R. E. Miller and L. Pedersen, J. Chem. Phys. **108**, 436 (1998).

[11] J. P. Connelly, A. Bauder, A. Chisholm and B. J. Howard, Mol. Phys. **88**, 915 (1996).

[12] D. Prichard, J. S. Muenter and B. J. Howard, Chem. Phys. Lett. **135**, 9 (1987).

[13] K. W. Jucks and R. E. Miller, J. Chem. Phys. **88**, 2196 (1988).

[14] H. S. Gutowsky, J. Chen, P. J. Hajduk and R. S. Ruoff, J. Phys. Chem. **94**, 7774 (1990).

[15] H. S. Gutowsky, P. J. Hajduk, C. Chuang and R. S. Ruoff, J. Chem. Phys. **92**, 862 (1990).

[16] R. A. Peebles, S. A. Peebles and R. L. Kuczkowski, Mol. Phys. **96**, 1355 (1999).

[17] S. A. Peebles and R. L. Kuczkowski, Chem. Phys. Lett. **286**, 421 (1998).

[18] S. A. Peebles and R. L. Kuczkowski, J. Chem. Phys. **109**, 5276 (1998).

[19] S. A. Peebles and R. L. Kuczkowski, J. Phys. Chem. **102**, 8091 (1998).

[20] S. A. Peebles and R. L. Kuczkowski, Chem. Phys. Lett. **308**, 21 (1999).

Reproduced with permission of the copyright owner. Further reproduction prohibited without permission.

[21] S. A. Peebles and R. L. Kuczkowski, J. Chem. Phys. **111**, 10511 (1999).

[22] S. A. Peebles and R. L. Kuczkowski, J. Mol. Struct., accepted for publication.

[23] R. A. Peebles and R. L. Kuczkowski, J. Phys. Chem. **103**, 6344 (1999).

[24] A. Taleb-Bendiab, M. S. LaBarge, L. L. Lohr, R. C. Taylor, K. W. Hillig, II, R. L. Kuczkowski and R. K. Bohn, J. Chem. Phys. **90**, 6949 (1989).

[25] A. Taleb-Bendiab, K. W. Hillig, II and R. L. Kuczkowski, J. Chem. Phys. **97**, 2996 (1992).

[26] T. J. Balle and W. H. Flygare, Rev. Sci. Instrum. **52**, 33 (1981).

[27] K. W. Hillig, II, J. Matos, A. Scioly and R. L. Kuczkowski, Chem. Phys. Lett. **133**, 359 (1987).

[28] J.-U. Grabow, Ph.D. Thesis, University of Kiel, Kiel (1992).

[29] J. S. Muenter, J. Chem. Phys. **48**, 4544 (1968).

[30] J. Kraitchman, Am. J. Phys. **21**, 17 (1953).

[31] A. D. Buckingham and P. W. Fowler, J. Chem. Phys. **79**, 6426 (1983).

[32] A. D. Buckingham and P. W. Fowler, Can. J. Chem. **63**, 2018 (1985).

[33] A. McIntosh, A. M. Gallegos, R. R. Lucchese and J. W. Bevan, J. Chem. Phys. **107**, 8327 (1997).

[34] S. A. Peebles and R. L. Kuczkowski, J. Mol. Struct. **436 – 437**, 59 (1997).

[35] A. J. Stone, A. Dullweber, M. P. Hodges, P. L. A. Popelier and D. J. Wales, *ORIENT: A program for studying interactions between molecules*, Version 3.2, University of Cambridge (1995).

[36] R. A. Peebles, S. A. Peebles, R. L. Kuczkowski and H. O. Leung, J. Phys. Chem. **103**, 10813 (1999).

[37] S. A. Peebles and R. L. Kuczkowski, J. Mol. Struct. **447**, 151 (1998).

[38] T. A. Hu, L. H. Sun and J. S. Muenter, J. Chem. Phys. **95**, 1537 (1991).

[39] J. S. Muenter, J. Chem. Phys. **94**, 2781 (1991).

Reproduced with permission of the copyright owner. Further reproduction prohibited without permission.

CHAPTER II

THE OCS TRIMER: ISOTOPIC STUDIES, STRUCTURE AND DIPOLE MOMENT

Introduction

The OCS trimer was first studied by FTMW techniques in 1996 by Connelly, *et al*[1]. The cluster, containing three linear triatomics, was a major advance in the study of

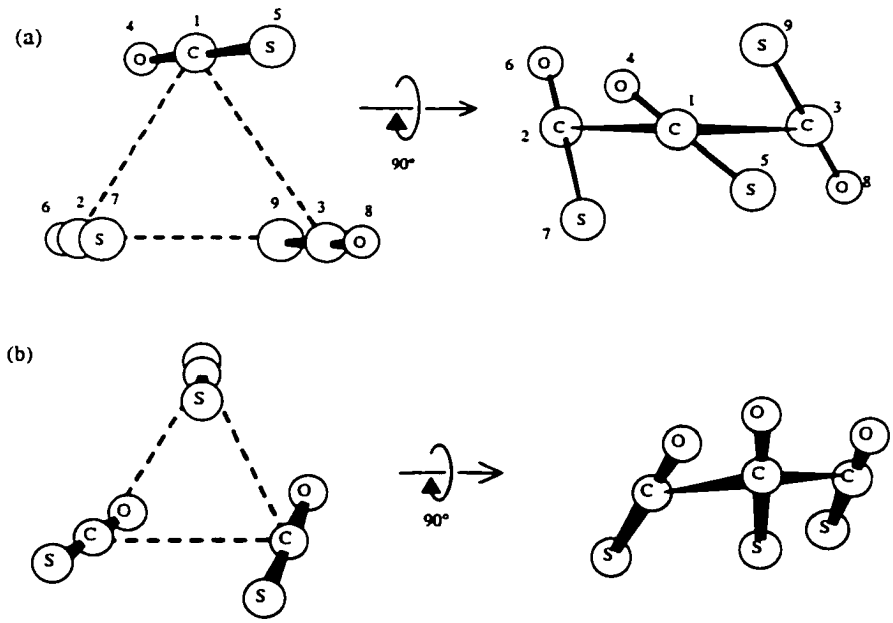


Figure II.1. (a) The anti-parallel experimental structure for OCS trimer. In the left-hand view, the three carbon atoms are in the plane of the page. A rotation of 90° about an axis in the C-C-C plane brings the top OCS above the page and the other two below, giving the view on the right. In this view, all three OCS molecules are nearly parallel to the plane of the page. (b) The semi-empirical prediction for the parallel form of OCS trimer. Alignment is as in (a).

structurally complex trimers by microwave spectroscopy. The only equally complex

Reproduced with permission of the copyright owner. Further reproduction prohibited without permission.

trimer that had been studied by the FTMW technique was $(CO_2)_2HCN$, which, along with $(CO_2)_3HCN$, was studied by Gutowsky and co-workers.[2, 3]

A lack of isotopic data hampered the initial study of $(OCS)_3$. Examination of only the normal isotopomer made a unique structure determination impossible; however, semi-empirical modeling identified two possible isomers, illustrated in Fig. II.1, that were consistent with the observed rotational constants (Table II.1). The modeling pointed to a preference for an anti-parallel barrel-like structure over a parallel model in which the three OCS dipoles would reinforce each other. This chapter reports the assignment of two additional isotopomers of the trimer, measurement of the dipole moment, and a structural analysis. Semi-empirical calculations which further confirm the experimentally determined structure are discussed in Chapter VII. The observed barrel-like configuration is similar to other mixed trimers of linear triatomic molecules recently studied in this laboratory and elsewhere. These include $(CO_2)_2OCS$,[4, 5] $(OCS)_2CO_2$,[6] $(CO_2)_2N_2O$[7] (Chapter III) and $(CO_2)_2HCN$.[2] As with these and other previously studied homo-molecular trimers, like $(CO_2)_3$[8] and $(N_2O)_3$,[9] the relationship of known dimers to the structure of the larger complex is easily recognized and will be discussed. Examination of this relationship can elucidate structure trends which can lead to a better understanding of intermolecular forces.

Experiment

The spectra of two isotopomers of $(OCS)_3$ were observed in the 5.5 – 12.0 GHz range on the Balle-Flygare type Fourier transform microwave spectrometers at the University of Michigan. The spectrometers and experimental method were discussed in greater detail in Chapter I. The ^{18}OCS (93.4% ^{18}O) and $O^{13}CS$ (99% ^{13}C, 12% ^{18}O) were obtained from Isotec. A typical transition of the $(^{18}OCS)_3$ isotopomer had a signal-to-noise ratio of about 7 in 300 gas pulses, while transitions of the $(O^{13}CS)_3$ isotopomer

Reproduced with permission of the copyright owner. Further reproduction prohibited without permission.

generally required about 500 gas pulses to obtain the same quality of signal. Several transitions of both species were considerably weaker, requiring about 1000 gas pulses to obtain a good signal-to-noise ratio. The difference in intensity between the two isotopes can be attributed to the lower isotopic enrichment in the $O^{13}CS$ sample. Although transitions of the normal species show a small splitting (usually a few tens of kilohertz) due to interconversion between the two enantiomers of the chiral complex,[1] the only splitting observed in this study was in the 6_{16}-5_{15} and 6_{06}-5_{05} transitions of $(O^{13}CS)_3$ (Fig. I.2). These two transitions were split by about 20 kHz each, which is about the limit of resolution of the spectrometer.

Results

A. Spectra

For $(^{18}OCS)_3$, 21 *a*-type and 10 *c*-type transitions were observed, while for $(O^{13}CS)_3$ 22 *a*-type and 9 *c*-type transitions were observed. The frequencies of these transitions are given in Appendix A. The transitions of each isotopomer were fit to a Watson A-reduction Hamiltonian in the I^r representation.[10] The resulting spectroscopic constants for both isotopes and the normal species are given in Table II.1. For the $(O^{13}CS)_3$ isotopomer, δ_K was not well determined, so it was fixed at the value of δ_K from the $(^{18}OCS)_3$ isotopomer. This improved the quality of the fit slightly and had little effect on the other distortion constants. Two lines believed to be the 6_{06}-5_{05} and 6_{16}-5_{15} transitions of $(^{18}O^{13}CS)_3$ were observed in the $O^{13}CS$ sample (which is estimated to be 12% $^{18}O^{13}CS$), but the rest of the spectrum of this isotope remains unassigned due to the low intensity of the lines.

Reproduced with permission of the copyright owner. Further reproduction prohibited without permission.

Table II.1 Spectroscopic constants for the assigned isotopes of $(OCS)_3$.

	$(^{16}O^{12}CS)_3$ [a]	$(^{18}O^{12}CS)_3$	$(^{16}O^{13}CS)_3$
A / MHz	847.97958(2)	813.3787(2)	837.5555(3)
B / MHz	736.17579(2)	708.4134(2)	728.1778(3)
C / MHz	574.32591(1)	553.1467(2)	565.3423(2)
Δ_J / kHz	0.45440(9)	0.4134(22)	0.4566(27)
Δ_{JK} / kHz	0.1571(5)	0.1822(91)	0.129(16)
Δ_K / kHz	0.3013(5)	0.2309(79)	0.301(15)
δ_J / kHz	0.06797(4)	0.0583(12)	0.0680(17)
δ_K / kHz	0.0339(3)	0.0545(59)	0.0545[d]
N [b]	137	31	31
$\Delta\nu_{rms}$ [c]	0.51	1.16	2.19

[a] from reference 1
[b] N = number of lines in fit
[c] $\Delta\nu_{rms}$ in kHz where $\Delta\nu = \nu_{obs} - \nu_{calc}$
[d] fixed at value from $(^{18}OCS)_3$

B. Dipole Moment

In order to guide the assignment of the isotopomers, the dipole moment of the normal isotopic species was measured. This ought to provide insight on the preferred structural isomer, since three parallel OCS molecules should give a total dipole of about three times the OCS monomer moment, while the anti-parallel arrangement should have a

Reproduced with permission of the copyright owner. Further reproduction prohibited without permission.

Table II.2 Stark coefficients for OCS trimer transitions.

Frequency / MHz	$J'_{Ka'Kc'} - J''_{Ka''Kc''}$	$\|M\|$	$\Delta\nu / \varepsilon^2$ [a]	Obs – Calc [a]
6355.5492	$5_{24} - 4_{23}$	1	2.301	0.025
		2	8.666	–0.446
6369.5275	$4_{32} - 3_{22}$	3	–5.360	–0.189
6648.6140	$5_{33} - 4_{32}$	1	0.652	0.045
		2	2.463	0.091
		3	5.187	–0.125
7852.9891	$5_{33} - 4_{23}$	3	–9.001	–0.149
		4	–15.836	–0.106
7885.3043	$6_{34} - 5_{33}$	2	1.212	0.082
		3	2.692	0.149

[a] units of 10^{-5} MHz cm^2 V^{-2}

dipole moment about equal to that of one OCS monomer. Stark effect measurements on 10 components of 5 transitions were least-squares fit to calculate the dipole moment of the complex. To reduce possible complication from non-linear second order Stark effects, transitions with intermediate K values were measured. These transitions should be the least affected by such behavior, and when plotted showed little if any deviation from linearity. The *b*-component of the dipole moment was predicted to be very small, and when it was included in the fit resulted in a small, negative value for μ_b^2. This indicated that the component was, indeed, too small to be determined from the data available. The fact that *b*-type transitions were not seen after 60,000 gas pulses was further indication of the small value of μ_b. A maximum possible value of μ_b is 0.2 D, based on the assumption that this dipole moment component could contribute no more

Reproduced with permission of the copyright owner. Further reproduction prohibited without permission.

that 20 kHz of a total 1 MHz shift for the fastest moving Stark effect measured. It was found that $\mu_a = 0.537(10)$ D, $\mu_c = 0.373(2)$ D and $\mu_{tot} = 0.653(8)$ D. The Stark coefficients for the measured transitions are summarized in Table II.2, and the dipole moment data is shown in Table II.3. The experimentally determined dipole moment components give values consistent with the anti-parallel model identified in both this and the previous work.[1] In these models the experimental monomer dipole moments are projected onto the principal axes of a plausible trimer structure. The dipole moment components predicted by projecting the monomer moments onto the principal axes of our experimental structure (see below) and the parallel and anti-parallel models of Connelly[1] are given in Table II.3 for comparison. The possibility that the structure can be the parallel form is essentially eliminated by the dipole moment data. The results also suggest small polarization effects which increase μ_a and decrease μ_c by about 0.15 D compared to the experimental structure.

Table II.3 Dipole moment components for OCS trimer.

		Projected Values [a]		
	Experiment	Experimental Structure	Anti-parallel Model Connelly, *et al* [b]	Parallel Model Connelly, *et al* [b]
μ_a / D	0.537(10)	0.391	0.6	1.5
μ_b / D	0.00(20)[c]	0.023	0.05	0.02
μ_c / D	0.373(2)	0.517	0.4	1.4
μ_{tot} / D	0.653(8)	0.649	0.72	2.1

[a] Projection of OCS monomer dipole moments onto the principal axes of the experimental or semi-empirical structure.
[b] Reference 1.
[c] Uncertainty based on the assumption that the *b*-component of the dipole moment contributes at most 20 kHz of a 1 MHz total shift to the fastest Stark effect measured.

Reproduced with permission of the copyright owner. Further reproduction prohibited without permission.

C. Structure

Figure II.1(a) illustrates a model and numbering scheme for the experimental anti-parallel structure. The parallel structure [Fig. II.1(b)] is similar with the OCS molecule that contains C3 rotated by about 180° from its orientation in Fig. II.1(a). The $(^{18}OCS)_3$

Table II.4 Principal axis coordinates (Å) for the experimentally determined structure of OCS trimer.

	a	*b*	*c*
C1[a]	1.08070	1.68607	–0.64283
C2	–2.25260	0.31900	–0.03202
C3	0.88452	–1.98819	0.29479
O4	0.25388	1.92442	–1.41492
S5	2.20003	1.36340	0.40240
O6	–2.55231	0.16991	–1.13859
S7	–1.84685	0.52082	1.46604
O8	1.37954	–2.04039	1.33824
S9	0.21438	–1.91753	–1.11782
M1[b]	1.45697	1.57760	–0.29149
M2	–2.11620	0.38684	0.47155
M3	0.65925	–1.96444	–0.18006

[a] Atom numbering as in Figure II.1.
[b] M1, M2 and M3 are the center of mass of the OCS molecules with C1, C2 and C3, respectively.

Reproduced with permission of the copyright owner. Further reproduction prohibited without permission.

isotopic shift data, and the dipole moment data, are only consistent with the anti-parallel form.

Nine parameters defining the structure of the OCS trimer were fit to the nine moments of inertia from the normal species and the two enriched isotopomers using techniques for solving a set of non-linear simultaneous equations. The structures of the OCS monomers were held fixed at their experimental values, with $r_{O\text{-}C}$ = 1.1561 Å and $r_{C\text{-}$

Table II.5 Experimental structural parameters for $(OCS)_3$.

	Experimental
C1-C2 / Å [a]	3.654
C1-C3 / Å	3.797
C2-C3 / Å	3.908
C1-C2-C3 / °	60.2
C2-C3-C1 / °	56.6
C3-C1-C2 / °	63.2
S5-C1-C3 / °	70.9
S7-C2-C1 / °	82.8
O8-C3-C2 / °	116.5
S5-C1-C3-C2 / ° [b]	136.4
S7-C2-C1-C3 / °	80.0
O8-C3-C2-C1 / °	89.9
S5-C1-C3-S9 / °	−156.2
S7-C2-C1-S5 / °	32.7
S9-C3-C2-S7 / °	−178.8

[a] Atom numbering as in Figure II.1.
[b] The signs of the dihedral angles are consistent with the definition in Reference 13.

Reproduced with permission of the copyright owner. Further reproduction prohibited without permission.

$_S$ = 1.5651 Å.[11, 12] The fitted parameters were the C1-C2 and C2-C3 distances, the angles C1-C2-C3, S5-C1-C3, S7-C2-C1 and O8-C3-C2, and the dihedral angles S5-C1-C3-C2, S7-C2-C1-C3 and O8-C3-C2-C1. Since this is a minimum data set with nine moments of inertia and nine structural parameters, the fit is exact, with no statistical fitting errors or redundancy checks from fitting extra equations. The principal axis coordinates derived from the fit are given in Table II.4, and the nine fitted parameters are given in Table II.5[13]. An uncertainty can be estimated by holding one structural parameter fixed while fitting the other eight parameters to the nine moments of inertia. This was done three times using each of the three coordinates that define the relative positions of the carbon atoms as the fixed parameter. The calculations led to standard deviations of between 0.001 and 0.003 amu•Å^2 in the fitted moments. This suggests that statistical errors caused by the effects of large amplitude motions on the moments of inertia are not a complication. Nevertheless, the derived parameters are so called effective parameters in the ground state and they may deviate markedly from equilibrium values which are estimated to be within 0.05 Å for distances and about 5° in angles.

As a redundancy check of the derived structure, the spectrum of the ($^{18}O^{13}CS)_3$ species was predicted. Two transitions believed to belong to this species were found at 6737.035 MHz and 6737.337 MHz (6_{16}-5_{15} and 6_{06}-5_{05}), approximately 800 kHz from the predicted frequencies. Their low intensity discouraged further exploration of this assignment.

Discussion

A. Experimental Summary

The original study of OCS trimer[1] established that the complex had a structure in which the three monomers are aligned roughly side-by-side, but there was insufficient

Reproduced with permission of the copyright owner. Further reproduction prohibited without permission.

experimental data to determine whether the three sulfur atoms were pointing in the same direction (parallel structure) or whether one of the sulfur atoms pointed in the opposite direction to the other two (anti-parallel structure). The new isotopic shift data reported here clearly establishes that the anti-parallel conformer has been observed. The dipole moment results confirm this. Table II.3 compares the experimental values of the dipole moment components with the values projected on the principal axes for this structure using the dipole moments of the OCS monomers (0.7152 D[14]). These results are in reasonable agreement but indicate that some modest polarization effects also occur.

B. Empirical Structure Trends

It is of interest to study the small changes that occur in dimers upon addition of a third body to the system. For this reason, each of the three faces of the OCS trimer is compared to the corresponding dimer. The parallel face, where both sulfur atoms are pointing in the same direction, is examined first. An experimental structure is not available for the parallel OCS dimer, although there has been evidence of its existence in MBERS studies,[15] so a comparison with a semi-empirical model structure is made instead. This structure was predicted using parameters that accurately reproduce the known, non-polar OCS dimer[16] center of mass separation. Details of the semi-empirical model are given in Chapter VII. Both the trimer and the predicted dimer structure have the two OCS units tipped away from a parallel arrangement, with the sulfur atoms farther apart than the oxygen atoms, a logical size effect. Various distances and angles are compared in Figure II.2 (a, b). While the dimer is predicted to have a planar structure, the trimer face is twisted noticeably from planarity with a S5-C1-C2-S7 dihedral angle of 32.7°.

The recent determination of the $(OCS)_2$-HCCH structure[17, 18] provides another complex with which to compare the polar $(OCS)_2$ face of OCS trimer. This complex with

Reproduced with permission of the copyright owner. Further reproduction prohibited without permission.

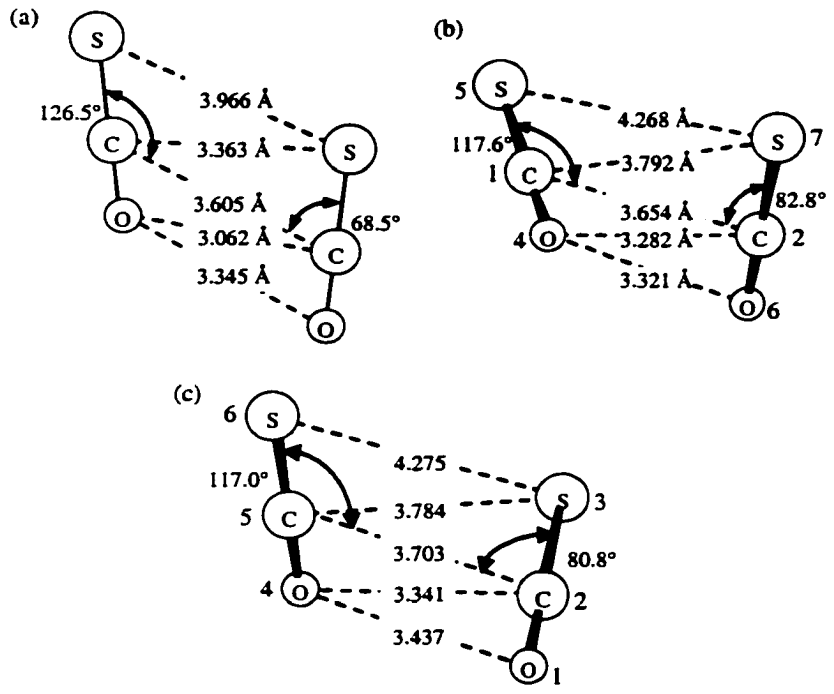


Figure II.2. OCS dimer structures: (a) semi-empirical model, polar, (b) experimental, parallel $(OCS)_2$ face of OCS trimer. The trimer face has a S7-C2-C1-S5 dihedral angle of 32.7°, (c) the $(OCS)_2$ face of $(OCS)_2$-HCCH (Ref. 18). The S6-C5-C2-S3 dihedral angle is 38.0°.

acetylene is the only other known trimer in which a polar OCS dimer fragment is isolated. This fragment is shown in Figure II.2(c). Comparison with II.2(b) shows very good agreement between both the distances and the angles. This is a good indication that if a polar form of $(OCS)_2$ exists, its structure will be similar to the faces of the two trimers where a polar fragment has been isolated. The similarity between the structures also gives us confidence that the experimental $(OCS)_3$ configuration is correct.

The two anti-parallel faces of the trimer are compared with the non-polar dimer structure[16] in Figure II.3. It can be seen that both trimer faces have the OCS molecules tipped away from the parallel alignment that is observed in the dimer. Also, the planar structure of the dimer is lost in the trimer faces, although the change is significantly larger on the face in II.3(a) than that in II.3(b). The former deviates from planarity by 33.8°, while the latter deviates by only 1.2°. It is interesting to note that the face that is

Reproduced with permission of the copyright owner. Further reproduction prohibited without permission.

nearly planar has a much larger tilt away from the parallel structure of the dimer than the

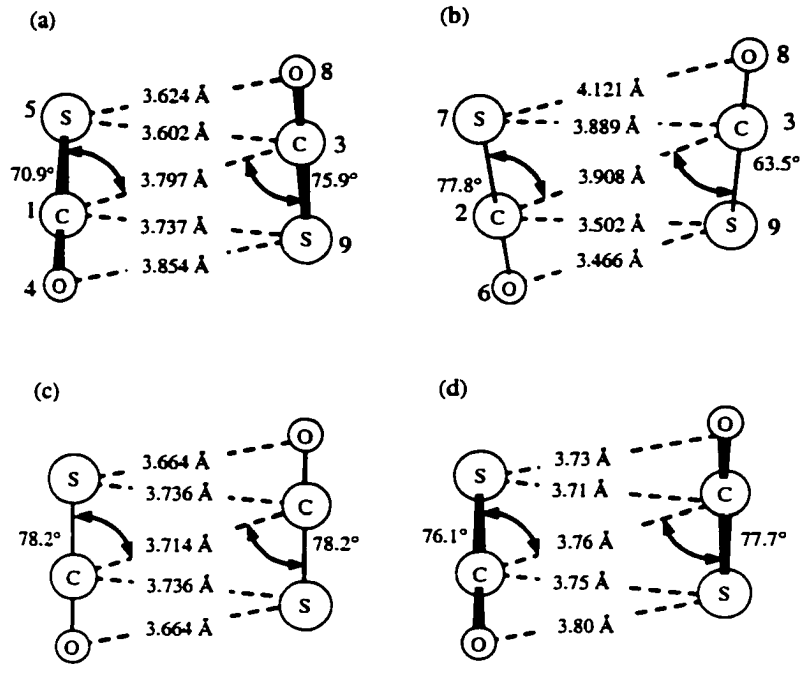


Figure II.3. (a,b) The two anti-parallel $(OCS)_2$ faces of OCS trimer. The S5 C1 C3 S9 dihedral angle is -156.2°, and the S9-C3-C2-S7 dihedral angle is -178.8°, (c) the experimental structure of OCS dimer (Reference 16), (d) the $(OCS)_2$ face of $(OCS)_2CO_2$. The O-C-C-S dihedral angle is 34.0° (Reference 6).

face that has a large dihedral angle but which otherwise reproduces the intermolecular C-C and C-S distances of the parallel dimer more closely.

The phenomenon of one face of a trimer having significantly larger changes from the comparable dimer structure than a second face of the trimer is also observed in other, similar trimer complexes. Some examples are $(CO_2)_2N_2O$,[7] $(OCS)_2CO_2$,[6] and $(CO_2)_2OCS$,[4,5] all recently studied in this laboratory. This interesting effect will be discussed further in Chapter III.

Dihedral angles between adjacent monomers, particularly on the trimer faces that most closely resemble the known dimer structures, can also be compared. The dihedral angle of the $(OCS)_2$ face of $(OCS)_2CO_2$ is 34.0° (O-C-C-S), which is only 0.2° different

Reproduced with permission of the copyright owner. Further reproduction prohibited without permission.

from the angle of 33.8° observed in $(OCS)_3$. The O-C-C-O angle of the $(CO_2)_2$ portion of $(CO_2)_2N_2O$ is also similar to these two dihedrals, with a value of 33.4°. This trend is broken, though, by the O-C-C-O dihedral angle in $(CO_2)_2OCS$, which has the considerably smaller value of 7.7°. Other trimers with similar structures, such as $(CO_2)_2HCN$,[2] $(CO_2)_2H_2O$,[19, 20] $(N_2O)_3$[9] and $(CO_2)_3$,[8] also have dihedral angles that are considerably different from the ~34° angle seen in the complexes discussed here. Thus, perhaps the similarity between the dihedral angles of $(OCS)_3$, $(CO_2)_2N_2O$ and $(OCS)_2CO_2$ is no more than a coincidence. It is possible that the angle of ~34° might be common in other trimers containing an $(OCS)_2$ face, but there are presently no other known trimers containing two anti-parallel OCS molecules to compare.

The OCS dimer portion of $(OCS)_2CO_2$ (Figure II.3(d)) can be compared with the OCS dimer face of $(OCS)_3$ that is shown in Figure II.3(a). While no parameters differ very greatly, "third body effects" in the OCS dimer unit of $(OCS)_3$ are readily apparent. The larger sulfur and the electrical asymmetry in the third OCS molecule cause the OCS dimer face to be more distorted than in $(OCS)_2CO_2$.

Summary

It has been determined that the OCS trimer has a barrel-like anti-parallel structure. This configuration is similar to that proposed by Connelly, *et al* in a previous paper, and it conforms to a pattern of structures seen in other trimers of linear monomers. Structures with this triangular arrangement of monomers are common and include CO_2 trimer,[8] N_2O trimer,[9] $(CO_2)_2H_2O$,[19, 20] $(CO_2)_2HCN$,[2] $(CO_2)_2N_2O$ (Chapter III),[7] $(CO_2)_2OCS$[4, 5] and $(OCS)_2CO_2$,[6] for example. The barrel-like structures in which the three monomer units are roughly parallel maximize the dispersion interactions, while the slipping and twisting of the molecules enhances the attractive electrostatic forces. There is also a planar, cyclic structure for CO_2 trimer[21] which has not been observed for any other homo-molecular

Reproduced with permission of the copyright owner. Further reproduction prohibited without permission.

trimers except $(HCN)_3$[22] and $(HCCH)_3$.[23] The changes in structural parameters that are seen in comparing the OCS dimer structure to the three dimer faces of the trimer are similar to the changes seen in other trimer complexes. In general, one trimer face more closely resembles the known dimer than the other trimer face. Also, the planarity that is common in dimers of linear triatomic molecules is lost in all faces of the trimer. This reflects the fact that the balance between electrostatic, dispersion and repulsive forces in the trimers is different from that in the corresponding dimers. The addition of a third body to the complex leads to a loss of some of the dispersion forces that cause the dimers to have the planar slipped parallel structure. This loss is compensated for by additional favorable electrostatic and dispersion interactions caused by the third body.

Reproduced with permission of the copyright owner. Further reproduction prohibited without permission.

References for Chapter II

[1] J. P. Connelly, A. Bauder, A. Chisholm and B. J. Howard, Mol. Phys. **88**, 915 (1996).

[2] H. S. Gutowsky, J. Chen, P. J. Hajduk and R. S. Ruoff, J. Phys. Chem. **94**, 7774 (1990).

[3] H. S. Gutowsky, P. J. Hajduk, C. Chuang and R. S. Ruoff, J. Chem. Phys. **92**, 862 (1990).

[4] S. A. Peebles and R. L. Kuczkowski, Chem. Phys. Lett. **286**, 421 (1998).

[5] S. A. Peebles and R. L. Kuczkowski, J. Chem. Phys. **109**, 5276 (1998).

[6] S. A. Peebles and R. L. Kuczkowski, J. Phys. Chem. **102**, 8091 (1998).

[7] R. A. Peebles, S. A. Peebles and R. L. Kuczkowski, Mol. Phys. **96**, 1355 (1999).

[8] M. J. Weida and D. J. Nesbitt, J. Chem. Phys. **105**, 10210 (1996).

[9] R. E. Miller and L. Pedersen, L. J. Chem. Phys. **108**, 436 (1998).

[10] J. K. G. Watson, J. Chem. Phys. **48**, 4517 (1968).

[11] Y. Morino and C. Matsumura, Bull. Chem. Soc. Jpn. **40**, 1095 (1967).

[12] A. G. Maki and D. R. Johnson, J. Mol. Spectrosc. **47**, 226 (1973).

[13] Signs of the dihedral angles are consistent with the definition in: E. B. Wilson, J. C. Decius and P. C. Cross, *Molecular Vibrations*; McGraw-Hill: New York (1955).

[14] J. S. Muenter, J. Chem. Phys. **48**, 4544 (1968).

[15] J. M. LoBue, J. K. Rice and S. E. Novick, Chem. Phys. Lett. **112**, 376 (1984).

[16] R. W. Randall, J. M. Wilkie, B. J. Howard and J. S. Muenter, Mol. Phys. **69**, 839 (1990).

[17] S. A. Peebles and R. L. Kuczkowski, Chem. Phys. Lett. **308**, 21 (1999).

[18] S. A. Peebles and R. L. Kuczkowski, J. Chem. Phys. **111**, 10511 (1999).

[19] K. I. Peterson, R. D. Suenram and F. J. Lovas, J. Chem. Phys. **90**, 5964 (1989).

[20] H. S. Gutowsky and C. Chuang, J. Chem. Phys. **93**, 894 (1990).

[21] G. T. Fraser, A. S. Pine, W. J. Lafferty and R. E. Miller, J. Chem. Phys. **87**, 1502 (1987).

Reproduced with permission of the copyright owner. Further reproduction prohibited without permission.

[22] K. W. Jucks and R. E. Miller, J. Chem. Phys. **88**, 2196 (1988).

[23] D. Prichard, J. S. Muenter and B. J. Howard, Chem. Phys. Lett. **135**, 9 (1987).

Reproduced with permission of the copyright owner. Further reproduction prohibited without permission.

CHAPTER III

MICROWAVE SPECTRUM AND STRUCTURE OF THE $(CO_2)_2N_2O$ COMPLEX

Introduction

The OCS trimer,[1, 2] which was discussed in Chapter II, is one of several homo-

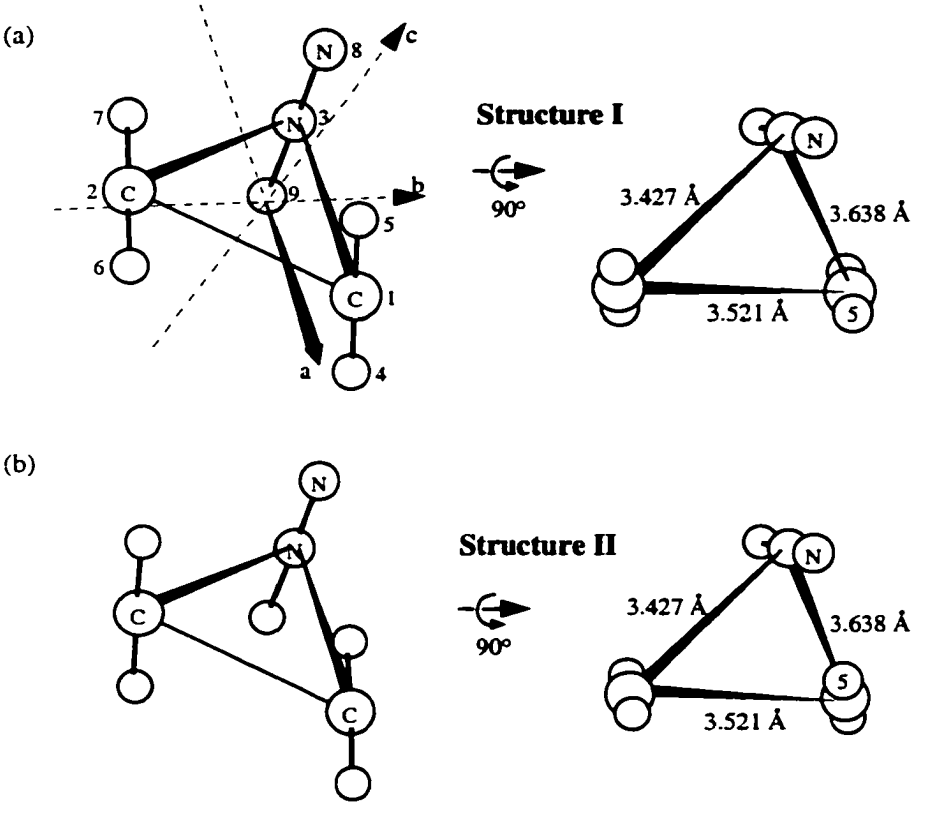


Figure III.1. The two possible structures of $(CO_2)_2N_2O$, (a) Structure I (b) Structure II. In the drawings shown on the left, the N_2O is below the plane of the paper, and the carbon atoms of the CO_2's are in the plane of the paper. A rotation by 90° bringing the nitrogen forward leads to the views shown on the right, where the carbon on the left is slightly in front of the plane and the carbon on the right slightly behind the plane of the paper.

molecular trimers that have been studied by FTMW or infrared spectroscopy. Other

Reproduced with permission of the copyright owner. Further reproduction prohibited without permission.

trimer systems in this category include $(CO_2)_3$,[3,4] $(N_2O)_3$,[5] $(HCCH)_3$[6] and $(HCN)_3$.[7,8] The complexes of OCS, CO_2 and N_2O have the barrel-like structure described in Chapter II, but a planar, pinwheel configuration is also observed for $(CO_2)_3$,[4] $(HCCH)_3$ and $(HCN)_3$.[7] It is estimated that the planar $(CO_2)_3$ structure is higher energy than the barrel-like configuration. The prevalence of these two structure types for homogeneous trimers leads to speculation about the structures of mixed trimers. For instance, would a combination of CO_2 with N_2O or OCS also have a barrel-like structure, and, if so, how would it differ from the homo-molecular species? A third structure type is also indicated by $(HCN)_3$ which has a nearly linear isomer.[8]

The combination of CO_2 and N_2O presents a particularly interesting system, since the two monomers have the same molecular weight and electron configuration. The dimers $(CO_2)_2$,[9,10] $(N_2O)_2$[11] and CO_2-N_2O[12,13] have also been studied, so the effects of a third body on dimer configurations will be readily apparent in a trimer of CO_2 and N_2O. For these reasons, a study of the trimer $(CO_2)_2N_2O$ is reported in this chapter.[14] A structure determination, dipole moment data and comparison with related dimers will be presented. Further discussion relating to the use of a semi-empirical model to predict the $(CO_2)_2N_2O$ structure appears in Chapter VII. The trimers $(CO_2)_2OCS$[15,16] and $(OCS)_2CO_2$[17] have recently been studied in this laboratory, and comparisons will be made between them and the trimer presented here.

Experiment

This work was carried out on the University of Michigan Balle-Flygare type Fourier transform microwave spectrometer described in Chapter I. The spectrometer's autoscan feature was employed to search the 5 – 6 GHz region, as well as smaller areas near 7 and 8 GHz. Most lines were broadened and weakened due to unresolvable quadrupole splitting, leading to a full width at half maximum of about 50 kHz.

Reproduced with permission of the copyright owner. Further reproduction prohibited without permission.

Table III.1. Spectroscopic constants for the seven isotopes of $(CO_2)_2N_2O$.

	$(^{12}CO_2)_2{}^{14}N_2O$	$(^{13}CO_2)_2{}^{14}N_2O$	$^{13}CO_2$-$^{12}CO_2$-$^{14}N_2O$	$^{12}CO_2$-$^{13}CO_2$-$^{14}N_2O$
A/ MHz	1597.4578(29)	1574.9582(31)	1593.5440(26)	1578.7807(30)
B/ MHz	1232.9688(16)	1222.0149(25)	1222.2196(20)	1232.8030(34)
C/ MHz	831.0955(11)	820.3333(14)	825.4715(9)	825.9338(15)
Δ_J/ kHz	2.610(33)	2.602(62)	2.523(53)	2.344(71)
Δ_{JK}/ kHz	−3.63(14)	−3.47(26)	−3.24(24)	−3.23(29)
Δ_K/ kHz	7.30(36)	5.92(35)	2.84(30)	6.75(27)
δ_J/ kHz	0.830(16)	0.848(30)	0.761(25)	0.701(36)
δ_K/ kHz	0.72(10)	0.69(17)	1.03(17)	–
N [a]	43	38	31	34
$\Delta\nu_{rms}$ [b]	11.6	11.8	7.0	11.8

	$(^{12}CO_2)_2{}^{14}N_2{}^{18}O$	$(^{12}CO_2)_2{}^{15}N^{14}NO$	$(^{12}CO_2)_2{}^{15}N_2O$
A/ MHz	1578.4985(71)	1586.7273(10)	1580.9203(5)
B/ MHz	1220.7716(24)	1214.7496(7)	1205.9692(7)
C/ MHz	827.2240(9)	820.5483(4)	815.2210(4)
Δ_J/ kHz	2.338(70)	2.665(21)	2.587(22)
Δ_{JK}/ kHz	−2.00(62)	−3.86(1)	−3.63(9)
Δ_K/ kHz	5.90(33)	6.98(1)	6.942(75)
δ_J/ kHz	0.687(34)	0.870(10)	0.842(10)
δ_K/ kHz	0.90(23)	0.877(52)	0.780(56)
N [a]	24	40	46
$\Delta\nu_{rms}$ [b]	4.3	3.6	3.7

[a] *N* = number of lines in fit

[b] $\Delta\nu_{rms} = [\ \Sigma\ (\nu_{obs} - \nu_{calc})^2 / N\ ]^{1/2}$ in kHz

Reproduced with permission of the copyright owner. Further reproduction prohibited without permission.

Frequencies were reproducible to within 2 kHz for the strongest transitions and about 5kHz for weaker lines with larger splitting. About half the transitions showed several resolvable quadrupole components, although partially resolved Doppler splitting of 10 – 20 kHz was the same magnitude as much of the quadrupole splitting making assignment of the fine structure difficult. An attempt to improve the resolution was made by using a nozzle oriented parallel to the spectrometer cavity, but unidentifiable problems with the nozzle made the transitions so weak that it was impossible to obtain useful data by this method.

All the isotopomers observed were assigned using isotopically enriched samples. $^{13}CO_2$ (99% ^{13}C, Isotec) was used to observe the $(^{13}CO_2)_2N_2O$ spectrum, and a 1:1 mixture of $^{13}CO_2$:$^{12}CO_2$ was used to observe the $^{13}CO_2$-$^{12}CO_2$-N_2O and $^{12}CO_2$-$^{13}CO_2$-N_2O spectra. The $(CO_2)_2{}^{15}N_2O$ isotopomer was observed using $^{15}N_2O$ (99% ^{15}N, Isotec), and the $(CO_2)_2{}^{15}N^{14}NO$ species was observed using $^{15}N^{14}NO$ (98% ^{15}N (terminal), Cambridge). $N_2{}^{18}O$ (48.4% ^{18}O, Prochem/ BOC Ltd.) was used to observe the spectrum of $(CO_2)_2N_2{}^{18}O$. Some lines believed to belong to one or both $C^{18}O_2$-$C^{16}O_2$-N_2O spectra were observed using a 1:1 mixture of $C^{18}O_2$:$C^{16}O_2$ ($C^{18}O_2$: 97.55% ^{18}O, Icon). Only a small amount of $C^{18}O_2$ sample was available, however, and the quantity was not large enough to complete the assignment of either species. Attempts at synthesis of $C^{18}O^{16}O$ by passing $C^{18}O$ over powdered $Cu^{16}O$ at 100° C and about 0.25 atm total pressure in a catalytic reactor were partially successful.[18] This synthesis resulted in a mixture of $C^{18}O_2$, $C^{16}O_2$ and $C^{18}O^{16}O$. A small amount of SO_2 was added to a sample of this CO_2 mixture to probe the relative amounts of each component by examination of the known $1_{01} \rightarrow 2_{02}$ transitions of the CO_2-SO_2 isotopomers.[19] This indicated an intensity ratio of about 2:3:5 for the $C^{18}O_2$, $C^{16}O_2$ and $C^{18}O^{16}O$ isotopomers of the complex; however, a search for one of the four possible $C^{18}O^{16}O$-$C^{16}O_2$-$^{14}N_2O$ isotopomers failed to find any lines, as did a search for $C^{18}O^{16}O$-$C^{16}O_2$-$^{15}N_2O$, and it was concluded that the isotopic enrichment of the sample was not sufficiently high to identify these species. Since ^{18}O

Reproduced with permission of the copyright owner. Further reproduction prohibited without permission.

enriched species of both CO and CO_2 are presently commercially unavailable due to shortage of ^{18}O, no further efforts to obtain $C^{18}O_2$ or $C^{18}O^{16}O$ spectra were possible.

Results

A. Spectra

A search of the region between 5 and 6 GHz revealed fifteen transitions that required CO_2 and/or N_2O. Mixing experiments eliminated nine of these transitions, and the results of Stark effect measurements were used to assign five of the remaining six lines to a trimer containing CO_2 and N_2O. The sixth transition remains unassigned. Despite the fact that the spectrum had been assigned, the identity of the complex remained ambiguous. Since N_2O and CO_2 have the same molecular weight, it was possible that the spectrum could belong to either $(CO_2)_2N_2O$ or $(N_2O)_2CO_2$. This uncertainty was eventually resolved by the assignment of the $(^{13}CO_2)_2N_2O$ isotopomer of the complex, since its spectrum was quite different than that predicted for $(N_2O)_2{}^{13}CO_2$.

a-, *b*-, and *c*-type transitions were observed for all the isotopic species assigned. Estimated center frequencies for the 42 assigned transitions of normal $(CO_2)_2N_2O$ and for the other six isotopomers are listed in Appendix B, as are the residuals for a fit of these lines to a Watson A-reduction Hamiltonian in the I^r representation.[20] The isotopes assigned were $(^{13}CO_2)_2N_2O$, $^{13}CO_2$-$^{12}CO_2$-N_2O, $^{12}CO_2$-$^{13}CO_2$-N_2O, $(CO_2)_2{}^{15}N_2O$, $(CO_2)_2{}^{15}N^{14}NO$, and $(CO_2)_2N_2{}^{18}O$. Fitted spectroscopic constants for all these isotopes including the normal species are listed in Table III.1.

B. Nuclear Quadrupole Hyperfine Structure

Quadrupole splitting was measured for 15 transitions of the normal isotopic species of $(CO_2)_2N_2O$. The nuclear quadrupole coupling constants determined from these

Reproduced with permission of the copyright owner. Further reproduction prohibited without permission.

measurements are within about 25% of the values predicted from N_2O monomer, but it is unclear whether this change is real or an artifact of the large uncertainty in the measurements. Further careful measurements at better resolution will be necessary to determine the quadrupole coupling constants in the trimer accurately. Attempts to improve the spectrometer's resolution by using a nozzle aligned parallel to the axis of microwave propagation were unsuccessful. Resolution of this fine structure is unlikely to change the current spectroscopic results significantly, although it would lead to information about the electric field gradient around the N_2O molecule. This data is not germane to the current structural study, though, and its measurement is perhaps best left to other researchers who are better equipped to perform the precise, very high resolution frequency measurements that are required.

C. Dipole Moment

The dipole moment of the complex was determined by analyzing the Stark effects of 6 transitions (8 components) of the normal species. Unresolved quadrupole splitting due to the two ^{14}N nuclei caused high uncertainty in the normal species measurements, so 5 transitions (9 components) were also analyzed from the $(CO_2)_2{}^{15}N_2O$ isotopomer in which no nuclear quadrupole hyperfine structure was observed since the ^{15}N nuclei are non-quadrupolar. The Stark coefficients and dipole moment components for both isotopomers are listed in Table III.2. Both sets of experimental data show a large induced dipole relative to that predicted by projecting the dipole moment of N_2O (0.16083(2) D[21]) onto the principal axes of the trimer for the structure derived in the next section. The predicted dipole moment components for $(CO_2)_2{}^{14}N_2O$ are $\mu_a = 0.106$ D, $\mu_b = 0.043$ D, and $\mu_c = 0.112$ D, while the observed moments are $\mu_a = 0.16(4)$ D, $\mu_b = 0.14(5)$ D, and $\mu_c = 0.130(2)$ D, with $\mu_{total} = 0.25(4)$ D. The components of the $(CO_2)_2{}^{15}N_2O$ dipole are $\mu_a = 0.1773(6)$ D, $\mu_b = 0.091(8)$ D, and $\mu_c = 0.1248(7)$ D, with $\mu_{total} = 0.235(3)$ D. Both

Reproduced with permission of the copyright owner. Further reproduction prohibited without permission.

Table III.2. Dipole moment data for the normal and $^{15}N_2O$ isotopomers of CO_2-CO_2-N_2O.

Transition	Isotope	$\|M\|$	Observed Stark Coefficient[a]	Obs - Calc[b]
2_{20}-1_{01}	normal	1	0.876	–0.002
2_{20}-1_{10}	normal	1	–0.112	0.053
	$^{15}N_2$	1	–0.082	0.010
3_{03}-2_{02}	normal	1	–0.237	–0.010
		2	–0.801	0.095
	$^{15}N_2$	1	–0.178	0.008
		2	–0.709	0.015
3_{12}-2_{02}	$^{15}N_2$	1	0.242	0.003
		2	0.993	0.014
3_{21}-2_{11}	normal	2	0.100	–0.008
3_{30}-2_{20}	$^{15}N_2$	1	0.315	0.004
		2	1.246	0.013
3_{31}-2_{21}	$^{15}N_2$	1	–0.316	0.002
		2	–1.276	0.014
4_{04}-3_{03}	normal	1	–0.705	0.122
		2	–3.363	–0.058
4_{22}-3_{21}	normal	2	–0.138	–0.043

Normal Dipole (D)		$^{15}N_2$ Dipole (D)	
$\|\mu_a\|$	0.16(4)	$\|\mu_a\|$	0.1773(6)
$\|\mu_b\|$	0.14(5)	$\|\mu_b\|$	0.091(8)
$\|\mu_c\|$	0.130(2)	$\|\mu_c\|$	0.1248(7)
μ_{total}	0.25(4)	μ_{total}	0.235(3)

[a] $\Delta\nu/\varepsilon^2$, units of 10^{-5} MHz/(V cm^{-1})^2
[b] Calculated from the rotational constants in Table III.1 and the dipole components below

Reproduced with permission of the copyright owner. Further reproduction prohibited without permission.

isotopes give a total dipole moment about 50% larger than that of isolated N_2O, with the largest difference from the projected N_2O moment along the *b*-axis of the complex (Figure III.1). The dipole moments of $(CO_2)_2{}^{14}N_2O$ and $(CO_2)_2{}^{15}N_2O$ agree within experimental error, and the slight changes in the dipole moment components that are expected based on rotation of the principal axes upon isotopic substitution are much smaller than the experimental error in the normal species measurements.

Initially, it was hoped that the dipole moment of the normal species would help determine whether the complex assigned was $(CO_2)_2N_2O$ or $(N_2O)_2CO_2$. The information from the dipole moment was ambiguous, however, because the total dipole was approximately halfway between the values expected for one and two N_2O molecules (aligned with reinforcing dipole moments) in the complex. An $(N_2O)_2CO_2$ complex with the monomer moments aligned in opposition to each other would be expected to have a very small total dipole due mainly to induction effects in the complex. As mentioned previously, the ultimate identification of the complex was accomplished by assignment of the $(^{13}CO_2)_2N_2O$ isotope.

D. Structure

Experimental rotational constants for the normal species and six other isotopomers made it possible to do a least-squares fit of the nine structural parameters of the trimer to 21 moments of inertia. The parameters fit were the two C-N distances (C1-N3 and C2-N3), the C1-N3-C2 angle, the angles O7-C2-N3, O4-C1-C2 and N8-N3-C1, and the dihedral angles O7-C2-N3-C1, O4-C1-C2-N3 and N8-N3-C1-C2. See Fig. III.1(a) for the atom numbering and parameters. The fit was run a number of times with different O-C-C-O angles in the initial configuration. Two possible structures that differed only in the location of the oxygens on the carbon dioxide molecules were obtained for the complex (structures I and II in Figures III.1(a) and III.1(b)). The four

Reproduced with permission of the copyright owner. Further reproduction prohibited without permission.

Table III.3. Principal axis coordinates (Å) for the two possible structures of $(CO_2)_2N_2O$.[a]

Atom	*a*		*b*		*c*	
	I	II	I	II	I	II
C1	1.8813		0.8356		0.3372	
	|1.864|		|0.827|		|0.349|
C2	−0.2433		−1.9536		0.0200	
	|−0.233|		|−1.940|		|0.000|
N3	−1.6869		1.1380		−0.3049	
	|−1.670|		|1.124|		|−0.301|
O4	2.6517	2.9697	0.9179	0.7107	−0.5288	−0.0502
O5	1.1109	0.7929	0.7533	0.9605	1.2032	0.7246
O6	0.8451	0.5271	−2.0785	−1.8713	−0.3674	−0.8460
O7	−1.3317	−1.0138	−1.8287	−2.0359	0.4074	0.8860
N8	−2.4316		1.4431		0.4826	
	|−2.418|		|1.429|		|−0.495|
O9	−0.8992		0.8152		−1.1379	
	|−0.884|		|0.804|		|−1.137|
cm (N_2O)	−1.6148		1.1084		−0.3812	
	|−1.598|		|1.095|		|−0.378|

[a] Coordinates obtained by the two inertial fits (structures I and II) are given in columns I and II, respectively, and substitution coordinates are given with absolute value signs.

singly substituted isotopomers that were assigned made a Kraitchman analysis[22] possible

Reproduced with permission of the copyright owner. Further reproduction prohibited without permission.

Table III.4. Parameters for the two trimer structures and ΔI_{rms} from fitting seven isotopic species.

	Structure I	Structure II	Kraitchman
$R(C_1\text{-}N_3)$ / Å	3.638(8)	3.638(8)	3.606
$R(C_2\text{-}N_3)$ / Å	3.427(9)	3.427(9)	3.398
$R(C_1\text{-}C_2)$ / Å	3.521(9)	3.521(9)	3.489
$\theta(C_1\text{-}N_3\text{-}C_2)$ / °	59.7(1)	59.7(1)	
$\theta(O_7\text{-}C_2\text{-}N_3)$ / °	62.6(39)	98.3(45)	
$\theta(O_4\text{-}C_1\text{-}C_2)$ / °	112.9(57)	116.7(57)	
$\theta(N_8\text{-}N_3\text{-}C_1)$ / °	123.2(4)	123.2(4)	
$\tau(O_7\text{-}C_2\text{-}N_3\text{-}C_1)$ / °[a]	146.2(13)	121.0(4)	
$\tau(O_4\text{-}C_1\text{-}C_2\text{-}N_3)$ / °	−113.0(4)	−146.4(10)	
$\tau(N_8\text{-}N_3\text{-}C_1\text{-}C_2)$ / °	104.5(3)	104.5(3)	
ΔI_{rms} / amu•Å^2	0.040	0.040	

[a] Signs of the dihedral angles are consistent with the convention in ref. 23.

for all the atoms in the complex except the oxygen atoms on the CO_2 molecules. The Kraitchman substitution coordinates were in good agreement with the structures obtained in the least-squares fit. The coordinates of the atoms in the principal axis system are given in Table III.3, with the absolute values of the substitution coordinates given below the inertial fit coordinates. The values for the nine fitted coordinates and ΔI_{rms} for the seven isotopic species are given in Table III.4 for structures I and II. The uncertainties in the table are the statistical values from the fitting process. Signs of the dihedral angles are consistent with the convention in Reference 23.

Reproduced with permission of the copyright owner. Further reproduction prohibited without permission.

Isotopic substitution of one or more of the oxygens on the CO_2 molecules is necessary to determine experimentally whether structure I or structure II is correct. An unsuccessful attempt was made to assign some ^{18}O enriched species, but this work was cut short due to limited sample quantities (as described in the Experimental section). However, semi-empirical modeling results using the ORIENT program discussed in Chapter VII point to a definite preference for structure I. This structure also seems more reasonable based on electrostatic arguments, since N8, which is slightly negative, is farther away from O5 which is also slightly negative. Discussion will be limited to structure I in much of the remainder of this chapter. It should be noted that this structure is an average structure in the ground vibrational state (r_0 structure). The equilibrium or r_e structure is expected to be within 0.05 Å for distances and 5° for angles.

Discussion

Figure III.1 shows that the $(CO_2)_2N_2O$ complex has a barrel-like structure similar to those recently observed for $(OCS)_3$,[1, 2] which was discussed in Chapter II, and for $(CO_2)_2OCS$[15, 16] and $(OCS)_2CO_2$.[17] As with $(OCS)_3$, there are several significant differences between the dimer units within the trimer and the isolated dimers. The most noticeable of these is related to the CO_2 dimer portion of the complex which can be compared with both the isolated CO_2 dimer and the $(CO_2)_2$ face of $(CO_2)_2OCS$. The largest change relative to CO_2 dimer is the loss of planarity, with a O-C-C-O dihedral angle of 33.4°. As discussed in Chapter II, this is very similar to the dihedral angles observed in the $(OCS)_2$ portions of OCS trimer and $(OCS)_2CO_2$, but it differs significantly from the O-C-C-O dihedral angle in $(CO_2)_2OCS$.

The C-C distance in $(CO_2)_2N_2O$ decreases from 3.602 Å in the dimer to 3.521 Å in the trimer. This can be compared with an increase to 3.68 Å in the $(CO_2)_2OCS$

Reproduced with permission of the copyright owner. Further reproduction prohibited without permission.

complex, a difference that could be due to the large size of the sulfur atom relative to the small nitrogen atoms. The isolated slipped-parallel CO_2 dimer has a C-C-O angle of 58.0° while in the trimer the corresponding O5-C1-C2 angle is 67.1°, and the O6-C2-C1 angle is 63.3°. Comparison between the CO_2 dimer, the $(CO_2)_2$ face of the trimer, and the $(CO_2)_2$ face of $(CO_2)_2OCS$ is shown in Figure III.2.

Figure III.3 compares the CO_2-N_2O dimer with the two CO_2-N_2O faces of the trimer. The face in Figure III.3(b) has a dihedral angle of 31.8° which is significantly different from the 0° angle necessitated by the planar dimer structure. The face shown in Figure III.3(c) also deviates from planarity, although by about 8° less. In the dimer, the

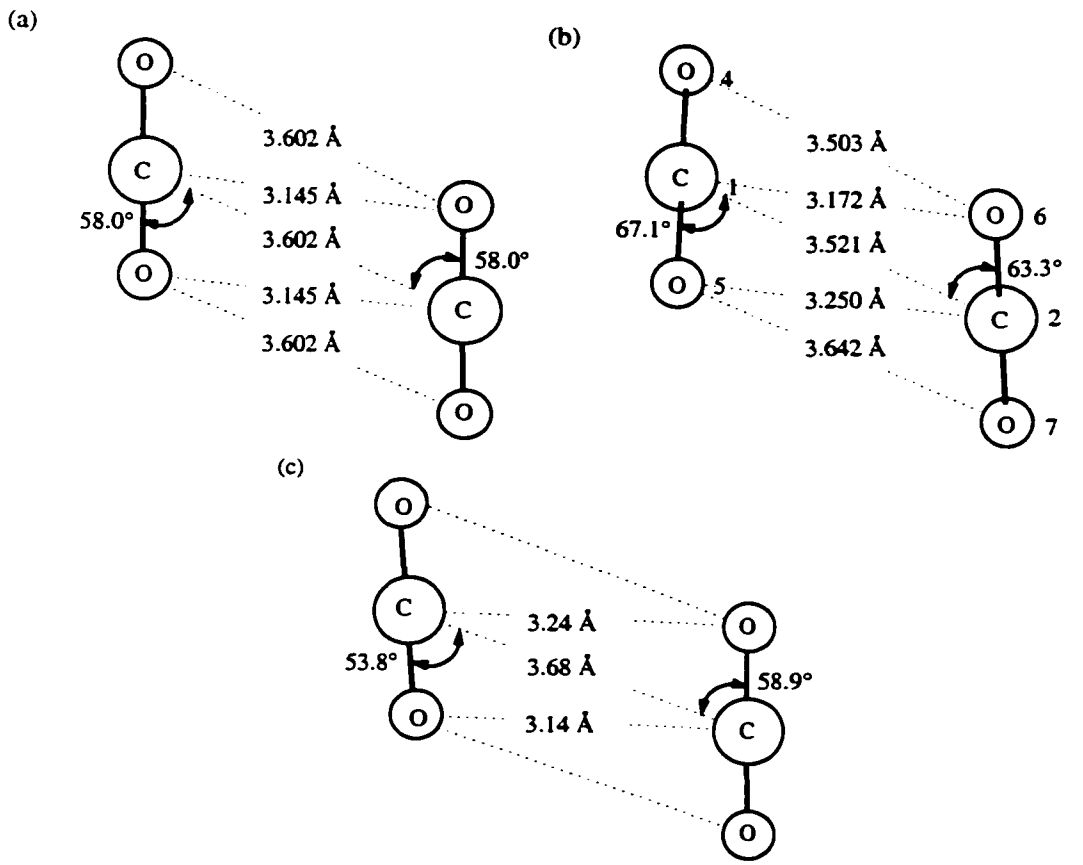


Figure III.2. Experimental structures. (a) CO_2 dimer. (b) The $(CO_2)_2$ face of $(CO_2)_2N_2O$. (c) The $(CO_2)_2$ face of $(CO_2)_2OCS$.

Reproduced with permission of the copyright owner. Further reproduction prohibited without permission.

O-C-N and C-N-O angles are 62.8° and 58.1°, respectively. Figure III.3(b) shows that the

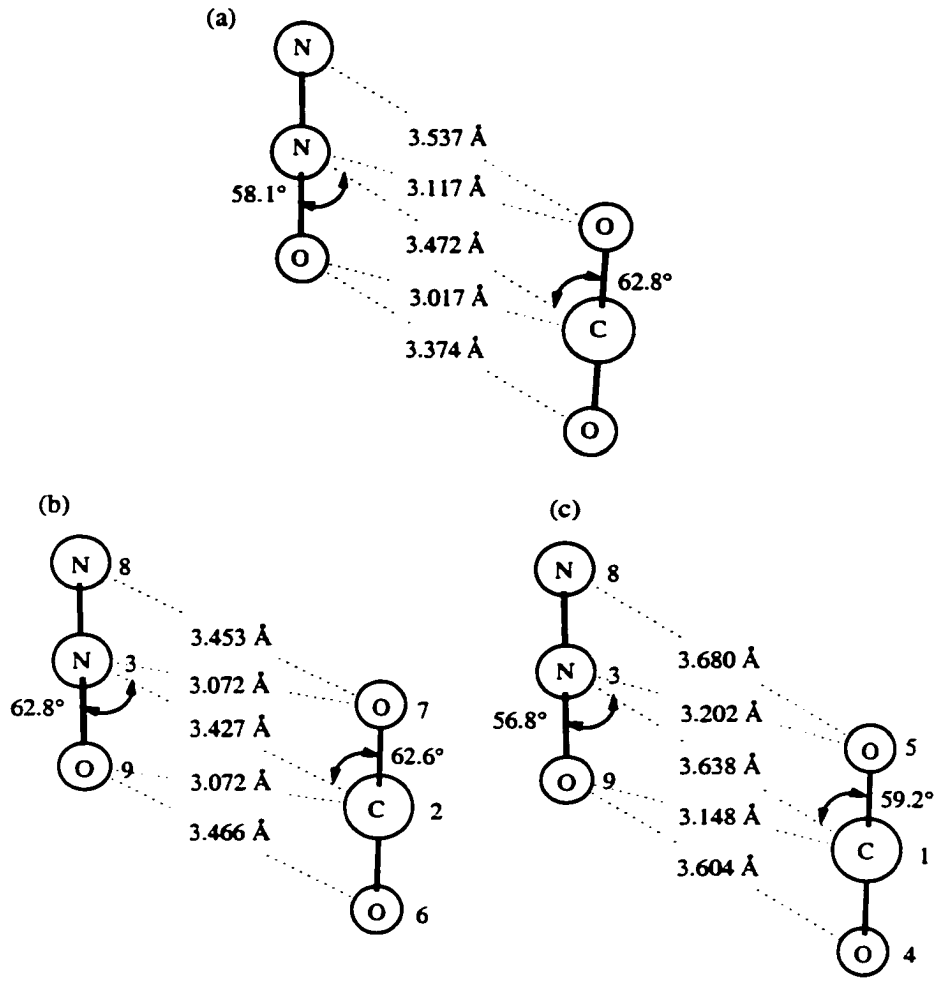


Figure III.3. Experimental structures. (a) CO_2-N_2O. (b) and (c) The two CO_2-N_2O faces of $(CO_2)_2N_2O$.

angles O7-C2-N3 and C2-N3-O9 are 62.6° and 62.8°, while in Figure III.3(c) the angles O5-C1-N3 and C1-N3-O9 are 59.2° and 56.8°. Although the angles in III.3(c) show a slightly larger deviation from the dimer structure than those in III.3(b), the changes are minimal compared to those seen in the $(CO_2)_2OCS$ and $(OCS)_2CO_2$ complexes. In both of those trimers, one face showed 40-50° deviations from the isolated dimer while the other closely resembled the dimer structure. The geometry of those trimers made it impossible for both faces to remain relatively unchanged, but in the current study the

Reproduced with permission of the copyright owner. Further reproduction prohibited without permission.

geometry alters enough to make this possible. When viewed from above (so the $(CO_2)_2$ face is roughly parallel to the page), the N_2O and OCS tilt in opposite directions relative to the CO_2 dimer face of the complexes. It is this difference that makes it possible to preserve the dimer-like structures on two faces of $(CO_2)_2N_2O$ but only one face of $(CO_2)_2OCS$. In the $(OCS)_2CO_2$ complex, preservation of the dimer on both faces is not possible because the OCS molecules are anti-parallel to each other. This means that when one face resembles the dimer, the other face has the OCS rotated approximately 180° from a dimer-like configuration.

The C-N distances on the two faces of the $(CO_2)_2N_2O$ complex are 3.427 Å (C2-N3) and 3.638 Å (C1-N3), while the distance in the isolated dimer is 3.472 Å. Although the C2-N3 distance changes little from the dimer structure (–0.045 Å), the C1-N3 distance changes by 0.166 Å, a relatively large amount. These changes in distance are comparable to the changes that were seen in the two CO_2/OCS trimers, where the distance on one face showed a small change from the dimer, and a significant change in the opposite sense was seen on the second face. In OCS trimer the difference from the isolated dimer is also much larger on one face than the other, although in that case both trimer faces are longer than the isolated dimer. It is also interesting to note that the C-C distance in CO_2 dimer is about 0.13 Å longer than the C-N(central) distance in CO_2-N_2O. While a similar change is seen between the $(CO_2)_2$ face of the trimer and III.3(b), the longer face (fig. III.3(c)) has an equally large change in the opposite direction. Also, N_2O dimer has a central N-N distance of 3.421 Å, a value that is comparable to the C-N distances of CO_2-N_2O and $(CO_2)_2N_2O$.

Conclusion

The $(CO_2)_2N_2O$ complex has been found to have a barrel-like structure that resembles those seen in several similar systems.[1 - 3, 5, 15 - 17] This configuration, in which

Reproduced with permission of the copyright owner. Further reproduction prohibited without permission.

the three monomer units are roughly parallel, maximizes the dispersion interactions while the slipping and twisting of the sticks enhances the attractive electrostatic forces. This slipping and twisting is exaggerated compared to the $(OCS)_3$ structure of Chapter II, an effect which is explained by the facts that $(CO_2)_2N_2O$ is a hetero-molecular complex and the two CO_2 molecules in the cluster have symmetry which is not present in OCS. The two mixed trimers involving CO_2 and OCS that have been studied in this lab have a similar asymmetric barrel-like structure which also resembles that observed for a variety of homogeneous trimers including $(CO_2)_3$ and $(N_2O)_3$.[3, 5] CO_2 trimer also exhibits a second planar, pinwheel isomer with C_{3h} symmetry which is estimated to be higher in energy.[4] Although the equivalent planar configuration of $(N_2O)_3$ has not been observed, it is interesting to speculate whether a planar form of $(CO_2)_2N_2O$ could also exist. This possibility could be the origin of the one unassigned transition that remains from the initial search for the $(CO_2)_2N_2O$ spectrum.

Reproduced with permission of the copyright owner. Further reproduction prohibited without permission.

References for Chapter III

[1] J. P. Connelly, A. Bauder, A. Chisholm and B. J. Howard, Mol. Phys. **88**, 915 (1996).

[2] R. A. Peebles and R. L. Kuczkowski, J. Phys. Chem. **103**, 6344 (1999).

[3] M. J. Weida and D. J. Nesbitt, J. Chem. Phys. **105**, 10210 (1996).

[4] G. T. Fraser, A. S. Pine, W. J. Lafferty and R. E. Miller, J. Chem. Phys. **87**, 1502 (1987).

[5] R. E. Miller and L. Pedersen, J. Chem. Phys. **108**, 436 (1998).

[6] D. Prichard, J. S. Muenter and B. J. Howard, Chem. Phys. Lett. **135**, 9 (1987).

[7] K. W. Jucks and R. E. Miller, J. Chem. Phys. **88**, 2196 (1988).

[8] R. S. Ruoff, T. Emilsson, T. D. Klots, C. Chuang and H. S. Gutowsky, J. Chem. Phys. **89**, 138 (1988).

[9] M. A. Walsh, T. H. England, T. R. Dyke and B. J. Howard, Chem. Phys. Lett. **142**, 265 (1987).

[10] K. W. Jucks, Z. S. Huang, R. E. Miller, G. T. Fraser, A. S. Pine and W. J. Lafferty, J. Chem. Phys. **88**, 2185 (1988).

[11] Z. S. Huang and R. E. Miller, J. Chem. Phys. **89**, 5408 (1988).

[12] C. Dutton, A. Sazonov and R. A. Beaudet, J. Phys. Chem. **100**, 17772 (1996).

[13] H. O. Leung, J. Chem. Phys. **108**, 3955 (1998).

[14] R. A. Peebles, S. A. Peebles and R. L. Kuczkowski, Mol. Phys. **96**, 1355 (1999).

[15] S. A. Peebles and R. L. Kuczkowski, Chem. Phys. Lett. **286**, 421 (1998).

[16] S. A. Peebles and R. L. Kuczkowski, J. Chem. Phys. **109**, 5276 (1998).

[17] S. A. Peebles and R. L. Kuczkowski, J. Phys. Chem. **102**, 8091 (1998).

[18] H. A. Jones and H. S. Taylor, J. Chem. Phys. **27**, 623 (1923).

[19] L. H. Sun, I. I. Ioannou and R. L. Kuczkowski, R. L., Mol. Phys. **88**, 255 (1996).

[20] J. K. G. Watson, J. Chem. Phys. **48**, 4517 (1968).

[21] L. H. Scharper, J. S. Muenter and V. W. Laurie, J. Chem. Phys. **53**, 2513 (1970).

Reproduced with permission of the copyright owner. Further reproduction prohibited without permission.

[22] J. Kraitchman, Am. J. Phys. **21**, 17 (1953).

[23] E. B. Wilson, Jr., J. C. Decius and P. C. Cross, *Molecular Vibrations*; New York: McGraw Hill (1955).

Reproduced with permission of the copyright owner. Further reproduction prohibited without permission.

CHAPTER IV

MICROWAVE SPECTRA, DIPOLE MOMENT, AND STRUCTURAL ANALYSIS OF N_2O-SO_2

Introduction

The previous two chapters focused on two trimers of linear triatomic molecules. These trimers showed a characteristic barrel-like structure where the three monomers were roughly parallel with their centers of mass forming a triangle. The relatively complex trimer systems are simplified by the use of linear monomers which reduce the number of structural parameters to be determined. The observed structures have been easily rationalized by comparison with related dimers.

A logical step beyond the study of trimers of linear monomers is a trimer with two linear monomers and one bent monomer. The $(N_2O)_2$•SO_2 trimer, described in Chapter V, is a complex of this type. In order to make a useful comparison between this trimer system and its component dimers, it will be necessary to know the structure of the isolated N_2O-SO_2 dimer. This dimer system is also interesting in comparison to a series of related complexes, and it will be discussed in this chapter.

The 1:1 dimer of SO_2 and N_2O is the continuation of a series of SO_2-X dimers, where X is a linear triatomic (CO_2,[1] OCS[2] or CS_2[3]). The previous members of this series have a plane of symmetry, with the sulfur end of the SO_2 tilted toward the oxygen end of the OCS or one of the carbons of the CS_2 (Figure IV.1). The CO_2 complex has C_{2v} symmetry with the sulfur above the carbon atom and the plane of the SO_2 perpendicular to the CO_2 axis. Since N_2O and CO_2 are isoelectronic, comparison between CO_2-SO_2 and

Reproduced with permission of the copyright owner. Further reproduction prohibited without permission.

N_2O-SO_2 will be particularly interesting. In previously studied dimers, N_2O and CO_2 have been shown to behave slightly differently when combined with the same molecule because of the dipolar nature of N_2O. For instance, CO_2-H_2O has a T-shaped structure where the oxygen of the water molecule points toward the carbon of the CO_2.[4] While the structure of N_2O-H_2O is similar, with the oxygen of the water forming a T with the N_2O, one of the hydrogens on the water twists toward the oxygen of the N_2O so that the symmetry observed in the CO_2 complex is lost.[5,6]

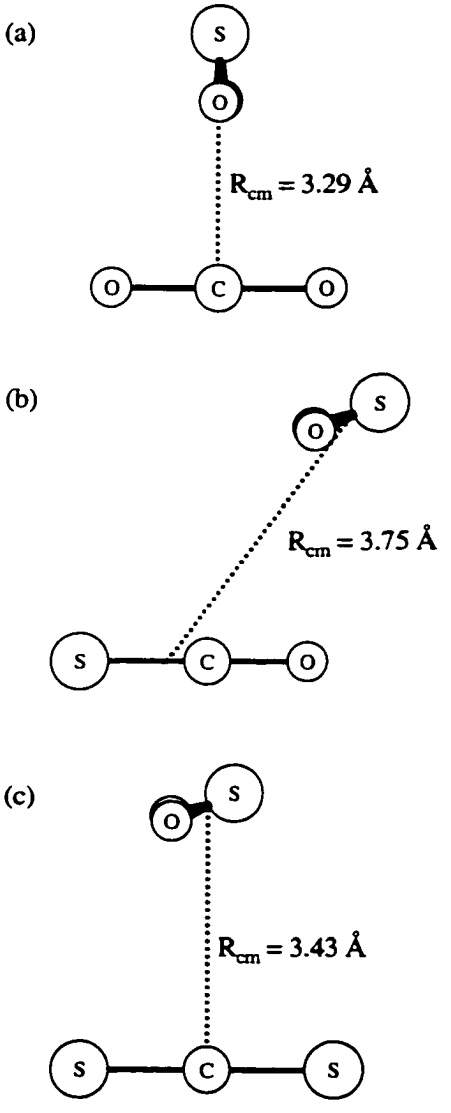


Figure IV.1. The structures of (a) CO_2-SO_2, (b) OCS-SO_2, and (c) CS_2-SO_2. See text for references.

Reproduced with permission of the copyright owner. Further reproduction prohibited without permission.

Experiment

An initial range of about 1 GHz was searched using the FT-MW spectrometers at the University of Michigan, and the experimental techniques described in Chapter I.[7] Many transitions were observed, and mixing experiments in which one component at a time was removed from the sample were used to eliminate those lines that did not require both components. While the strongest transitions had a signal-to-noise ratio in excess of 20 after ten gas pulses, the weaker lines required several thousand gas pulses to reach a reasonable intensity.

All the isotopic species were measured with enriched samples, although the strongest $^{34}SO_2$ transitions were visible in natural abundance. The isotopically enriched species that were assigned are $^{15}N_2O$-SO_2, $^{15}N_2O$-$^{34}SO_2$, $^{15}N_2O$-$S^{18}O_2$ and $N_2{}^{18}O$-SO_2. The $^{15}N_2O$ (99% ^{15}N) was obtained from Isotec; the $S^{18}O_2$ (97% ^{18}O) and $^{34}SO_2$ (90% ^{34}S) were obtained from Icon, and the $N_2{}^{18}O$ (48.4% ^{18}O) was obtained from BOC Labs.

Results

A. Spectra

The spectrum of N_2O-SO_2 was observed in the 5.5 – 14.5 GHz region. Transitions were split into doublets by 90 to 200 MHz. Although dipole moment measurements indicate that all three selection rules operated, only *a*-dipole and a few *c*-dipole transitions were assigned. The splitting of the spectrum caused transition frequencies to be perturbed, and line intensities showed unusual patterns, as well. These and other aspects of the assignment process are discussed in Appendix C.

For the normal isotopomer 11 *a*-type and 3 *c*-type transitions were measured for the higher frequency component, and 10 *a*-type transitions were measured for the lower frequency component. The combination of frequency fits and Stark splitting

Reproduced with permission of the copyright owner. Further reproduction prohibited without permission.

Reproduced with permission of the copyright owner. Further reproduction prohibited without permission.

measurements for the stronger *a*- and *c*-dipole transitions was sufficient to confirm these assignments. Spectroscopic constants for all the assigned isotopes are given in Tables

Table IV.1. Spectroscopic constants for N_2O-SO_2 and isotopomers with isotopic substitution in N_2O.

	N_2O-SO_2		$^{15}N_2O$-SO_2		$N_2{}^{18}O$-SO_2	
	lower	upper	lower	upper	lower	upper
A / MHz	5500[a]	6126.9781(15)	5500[a]	6070.7640(18)	5500[a]	5942.1522(63)
B / MHz	1463.483(23)	1494.537(37)	1418.535(24)	1446.280(48)	1427.895(61)	1462.01(13)
C / MHz	1420.953(23)	1435.474(36)	1379.852(18)	1397.165(48)	1404.170(26)	1418.24(13)
D_J / kHz	72.2(79)	68.23(3)	64.91(27)	69.58(6)	28.39(94)	69.48(13)
D_{JK} / MHz	−1.381(6)	2.232(19)	−2.320(5)	1.530(25)	−2.320[b]	1.414(66)
d_1 / kHz	2.32(62)	–	5.37(30)	–	5.37[b]	–
d_2 / kHz	–	15.7(22)	–	40.0(16)	–	50.3(43)
H_J / kHz	−0.188(15)	−0.167(2)	−0.188[b]	−0.1323(6)	−0.188[b]	−0.142(3)
N[c]	7	10	7	10	4	11
$\Delta\nu_{rms}$ / kHz[d]	26.25	1.15	42.84	1.21	97.77	4.11

[a] fixed, not fitted
[b] fixed at value from normal or $^{15}N_2O$•SO_2 species
[c] number of lines in fit
[d] see Table II.1 for definition of $\Delta\nu_{rms}$

assignments. Spectroscopic constants for all the assigned isotopes are given in Tables

IV.1 and IV.2, and transition frequencies are listed in Appendix C. The spectra have

Table IV.2. Spectroscopic constants for isotopomers of $^{15}N_2O$-SO_2 with isotopic substitution of SO_2.

	$^{15}N_2O$-$S^{18}O_2$		$^{15}N_2O$-$^{34}SO_2$	
	lower	upper	lower	upper
A / MHz	5500 [a]	5656.5695(99)	5500 [a]	6079.7059(53)
B / MHz	1394.46(16)	1426.507(79)	1389.906(20)	1421.64(11)
C / MHz	1333.54(11)	1351.694(78)	1358.757(20)	1376.37(11)
D_J / kHz	64.9 [b]	74.26(13)	39.86(60)	68.09(11)
D_{JK} / MHz	−2.320 [b]	2.958(41)	−2.671(9)	1.088(56)
d_1 / kHz	5.37 [b]	–	5.37 [b]	–
d_2 / kHz	–	29.9(26)	–	54.0(36)
H_J / kHz	−0.188 [b]	−0.195(2)	−0.188 [b]	−0.131(2)
N [c]	3	10	6	11
$\Delta\nu_{rms}$ / kHz [d]	1011	4.18	53.55	3.46

[a] fixed, not fitted
[b] fixed at value from normal or $^{15}N_2O$•SO_2 species
[c] number of lines in fit
[d] see Table II.1 for definition of $\Delta\nu_{rms}$

been fit to Watson's S-reduction Hamiltonian in the I^r representation.[8] It was necessary to include one P^6 term in order to obtain a fit of reasonable quality. D_K and d_1 for the upper set of transitions and D_K and d_2 for the lower set of transitions were poorly determined and thus fixed at zero. It should be noted that for the upper tunneling component there was a very high correlation (1.000 in most cases) between B, C and D_{JK}.

Reproduced with permission of the copyright owner. Further reproduction prohibited without permission.

For many of the lower tunneling component fits it was necessary to fix some of the spectroscopic constants at the values from the normal or $^{15}N_2O$-SO_2 species because of the small number of transitions in the fit. The *A* rotational constant for the lower tunneling component was also fixed, because the lack of *c*-type transitions prevented determination of this constant. Due to the very small dependence of the *a*-type transitions in this near prolate top ($\kappa = (2B - A - C)/(A - C) = -0.97$) on the *A* rotational constant, the value at which *A* was fixed had little effect on the quality of the fit and the values of the other constants. The inability to identify *c*-type transitions for the lower tunneling doublet spectra is probably due to these transitions being much weaker than the corresponding higher frequency lines. The only evidence of quadrupole splitting in the spectra was in the *c*-type transitions which had two or three strong components. An estimated center frequency was used in the spectral fitting process. The splitting caused a decrease in signal intensity which probably added to the difficulty of observing the lower tunneling doublet *c*-type transitions.

Since each tunneling component could be fit separately without a tunneling splitting correction, it is believed that the *a*- and *c*-dipole transitions are not tunneling-rotation transitions but are pure rotational transitions perturbed by the interaction between tunneling and rotation (Coriolis interactions). The large value of D_{JK} and the reversed sign for the two tunneling states is typical of such perturbed fits using the Watson Hamiltonian.[9]

Tunneling motions in structures with C_s symmetry can be eliminated by the observation of all the expected $K_a = 0$ and $K_a = 1$ *a*-dipole transitions for the normal isotope. This type of structure would exchange symmetry equivalent oxygen atoms (for instance, by rotation of SO_2 about its C_2 axis) leading to missing levels because of the nuclear spin of zero for ^{16}O. The doublet pattern observed is more indicative of tunneling between mirror image structures with non-equivalent oxygens on the SO_2 and therefore

Reproduced with permission of the copyright owner. Further reproduction prohibited without permission.

an asymmetric structure. This asymmetry is confirmed by the observation of all three dipole moment components discussed next.

B. Dipole Moment

The dipole moment of the normal isotopomer of N_2O-SO_2 was measured by quantitatively examining the Stark effects of 12 *M* components from the higher frequency tunneling doublets of 7 transitions. Values of μ_a = 0.6102(8) D, μ_b = 0.668(31) D and μ_c = 0.806(28) D were determined, giving a total dipole moment of 1.212(25) D. The relatively good fit for the three dipole components using the constants in Table IV.1 and second order perturbation theory suggests that any tunneling contribution to the *b*-dipole component is less than about 10%. The dipole moment components are reported in Table IV.3 along with predicted values obtained by projecting monomer dipole moments onto the principal axes of four possible experimental structures consistent with the moments of inertia. Stark coefficients for the measured transitions are given in Table IV.4. A discussion of the four structures in Table IV.3 in relation to the experimental dipole

Table IV.3. Experimental and predicted[a] dipole moment components for N_2O-SO_2 (in D).

	Experiment	Structure I Projections	Structure II Projections	Structure III Projections	Structure IV Projections
μ_a	0.6102(8)	1.456	1.458	1.450	1.441
μ_b	0.668(31)	0.333	0.265	0.356	0.210
μ_c	0.806(28)	0.314	0.381	0.641	0.722
μ_{total}	1.212(25)	1.526	1.529	1.625	1.625

[a] obtained by projecting the dipole moments of N_2O and SO_2 on the principal axes.

Reproduced with permission of the copyright owner. Further reproduction prohibited without permission.

moment will be given later in this chapter. The presence of all three dipole components indicates a non-symmetric structure.

Table IV.4. Stark coefficients for the N_2O-SO_2 upper tunneling doublet.

$J'_{Ka'Kc'} - J''_{Ka''Kc''}$	M	$\Delta\nu/E^{2\,a}$	Obs. – Calc.[a]
2_{02}-1_{01}	1	0.2713	0.0078
2_{11}-1_{10}	1	–3.7708	0.0007
3_{03}-2_{02}	0	–0.0938	0.0031
	1	–0.0353	0.0009
	2	0.1445	–0.0016
3_{12}-2_{11}	1	–0.1372	–0.0030
	2	–0.5305	–0.0061
4_{04}-3_{03}	0	–0.0193	–0.0012
	3	0.1038	–0.0070
4_{13}-3_{12}	2	–0.0861	–0.0015
	3	–0.1510	0.0076
5_{05}-4_{04}	4	0.0854	–0.0054

[a] units of 10^{-4} MHz cm^2/V^2. Calculated Stark coefficients were obtained using the constants in Table IV.1 and the experimental dipole components in Table IV.3.

Reproduced with permission of the copyright owner. Further reproduction prohibited without permission.

C. Structure

As indicated above, the presence of all three dipole components and all the K_a =

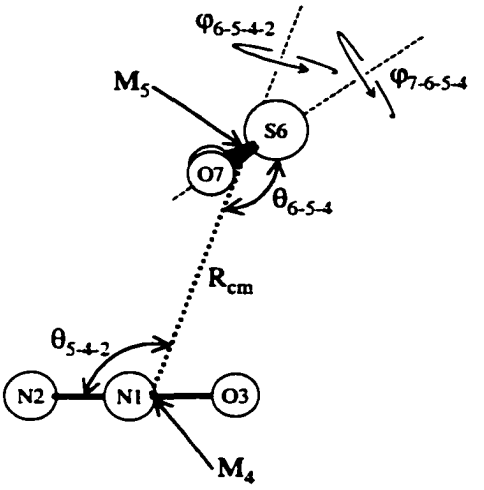


Figure IV.2. The parameters used to define the structure of N_2O-SO_2. M4 and M5 are the centers of mass of N_2O and SO_2, respectively.

Table IV.5. Structural parameters for the four inertial fits. See Figure IV.2 for atom numbering scheme.

	Structure I	Structure II	Structure III	Structure IV
R_{cm} / Å	3.3306(6)	3.3306(6)	3.3306(7)	3.3306(7)
$\theta_{5\text{-}4\text{-}2}$ / °	111.2(10)	111.1(10)	111.6(12)	111.7(12)
$\theta_{6\text{-}5\text{-}4}$ / °	156.6(51)	156.9(49)	161.3(54)	160.3(58)
$\varphi_{6\text{-}5\text{-}4\text{-}2}$ / °[a]	−158.3(57)	153.2(66)	−26.2(96)	−30.0(99)
$\varphi_{7\text{-}6\text{-}5\text{-}4}$ / °[a]	−115.0(59)	−65.2(57)	119.5(97)	119.1(87)
s.d.[b]	0.274	0.267	0.294	0.296

[a] The signs of the dihedral angles are consistent with the definition in Reference 11.
[b] standard deviation of the fit in amu Å^2.

Reproduced with permission of the copyright owner. Further reproduction prohibited without permission.

Reproduced with permission of the copyright owner. Further reproduction prohibited without permission.

0,1 *a*-dipole transitions for both tunneling components is consistent with a structure which lacks a symmetry plane. Before more detailed structure information can be

Table IV.6. Principal axis coordinates (in Å) for Structures I - IV of N_2O-SO_2. Absolute values of Kraitchman substitution coordinates are given in brackets.

	a				*b*				*c*			
	I	II	III	IV	I	II	III	IV	I	II	III	IV
N1	−1.9989	−1.9989	−2.0000	−2.0002	0.0438	−0.0612	0.0536	0.0478	0.0609	0.0482	0.0137	0.0230
N2	−2.4693	−2.4702	−2.4606	−2.4603	0.2235	0.1061	−0.0716	0.2069	−0.9484	−0.9635	−1.0083	−0.9945
O3	−1.5047	−1.5033	−1.5161	−1.5168	−0.1449	−0.2322	0.1851	−0.1194	1.1213	1.1110	1.0874	1.0920
		[1.525]				[0][a]				[1.210]		
M4	−1.9690	−1.9687	−1.9707	−1.9709	0.0324	−0.0715	0.0615	0.0376	0.1252	0.1126	0.0788	0.0878
M5	1.3545	1.3543	1.3557	1.3558	−0.0223	0.0492	−0.0423	−0.0259	−0.0861	−0.0774	−0.0542	−0.0604
S6	1.6922	1.6923	1.6917	1.6898	−0.1018	0.1028	−0.1174	−0.0775	0.0153	0.0388	−0.1641	−0.1885
	[1.680]		[1.686]			[0][a]			[0.359]	[0.360]	[0.349]	[0.349]
O7	1.2540	0.7776	1.2478	1.2528	1.2596	1.1994	1.2399	1.2337	−0.0335	−0.0538	−0.0716	0.1823
O8	0.7801	1.2554	0.7919	0.7913	−1.1452	−1.2081	−1.1746	−1.1823	−0.3414	−0.3334	0.1830	−0.0469

[a] These are set at zero; Kraitchman's equations gave imaginary values.

derived, it is necessary to consider whether the rotational constants obtained from fitting the spectra are useful or whether they are affected too strongly by tunneling motions to be helpful. It appears that they are useful although sufficiently affected by rotation-tunneling interaction effects to obscure a precise or unique structural determination.

Using only constants from the upper tunneling component, 14 moments of inertia are available for determining a structure. (I_c from $^{15}N_2O$-$S^{18}O_2$ was eliminated, because it fit poorly compared to the other moments of inertia.) Five parameters are required to define the structure for an asymmetric dimer involving a linear molecule, assuming the monomer structures are unchanged upon complexation (R_{N-O} = 1.185 Å, R_{N-N} = 1.128 Å, R_{S-O} = 1.431 Å, and θ_{O-S-O} = 119.3°[10]). The parameters chosen (Figure IV.2) comprise the distance between the centers of mass of the two monomers (R_{cm}), the angle between R_{cm} and the N_2O axis (θ_{5-4-2}), and the angle between the symmetry axis of SO_2 and R_{cm} (θ_{6-5-4}). Rotation of the S6-M5 axis out of the M5-M4-N2 plane is given by $\varphi_{6-5-4-2}$, and rotation of the SO_2 plane relative to the S6-M5-M4 plane is given by $\varphi_{7-6-5-4}$. The signs of the dihedral angles are consistent with the convention in Reference 11.

Least-squares fitting of the moments of inertia led to four possible dimer configurations which are illustrated in Figure IV.3. The structural parameters are given in Table IV.5. Structures I and II are quite similar, with the sulfur end of the SO_2 above the oxygen end of the N_2O. The sulfur atom is rotated slightly out of the M5-M4-N2 plane, and the plane of the SO_2 molecule is tilted so one oxygen points slightly down toward the N_2O and the other tips up away from it. Structures III and IV have a similar tilting and twisting of the SO_2 molecule, but the overall alignment tips the sulfur end of SO_2 farther away from the oxygen end of N_2O. The standard deviations of the inertial fits favor Structure II slightly over Structure I. Structures III and IV seem a little less likely both because of slightly poorer inertial fits and the seemingly less favorable electrostatic interactions when the oxygens of SO_2 point more toward the oxygen end of N_2O.

Reproduced with permission of the copyright owner. Further reproduction prohibited without permission.

Four inertial fits of similar quality arise because the signs of the atom coordinates

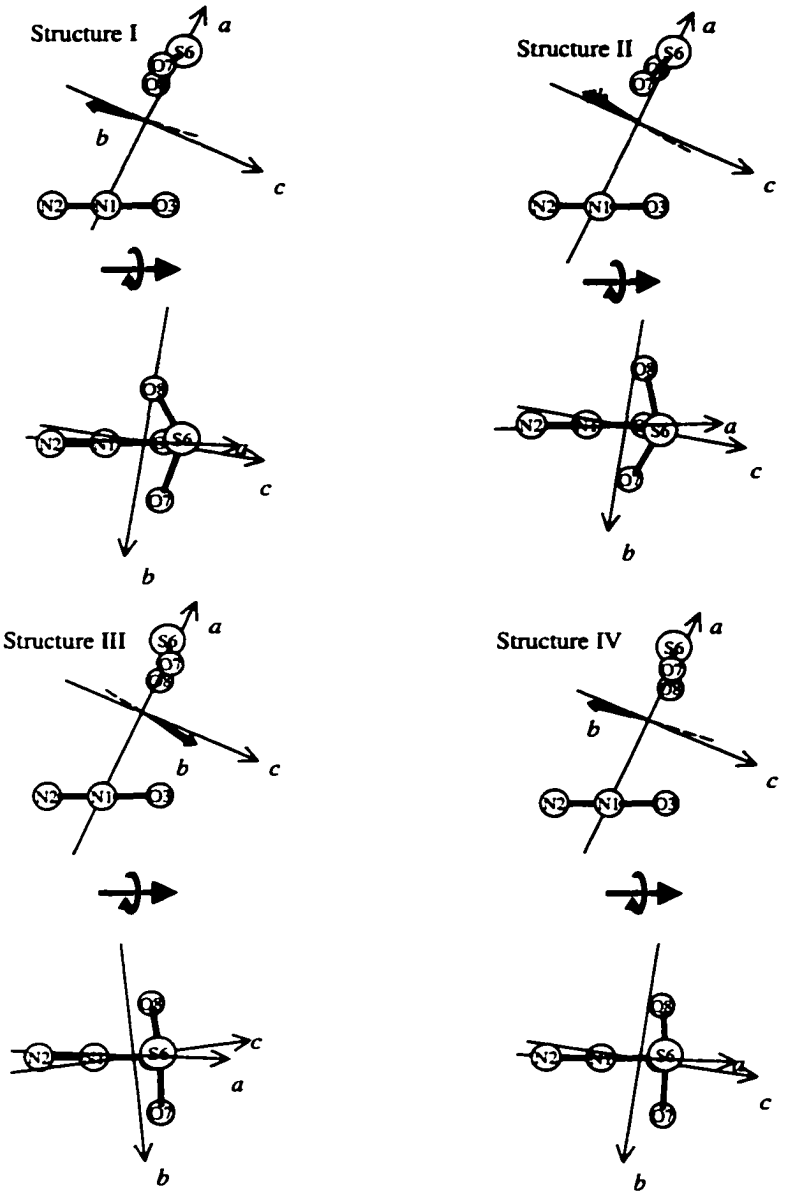


Figure IV.3. The four structures for N_2O-SO_2 obtained from least-squares fitting of the moments of inertia. In the top view, a plane containing N2 and the centers of mass of both monomers is parallel to the plane of the page. A rotation of 90° about the arrow gives the bottom view in which the N2-M4-M5 plane is perpendicular to the plane of the page.

are ambiguous due to their quadratic dependence on the moments of inertia. This ambiguity along with uncertainty in the moments due to the tunneling motion and other large amplitude vibrations allows for shifts of atoms across axes (sign changes) with

Reproduced with permission of the copyright owner. Further reproduction prohibited without permission.

other compensating adjustments in the monomer position resulting in multiple least-squares inertial fits of similar quality. One can often eliminate some of these structures by comparing their coordinates with a more direct calculation using Kraitchman's substitution equations.[12] This normally reduces vibrational effects. A partial Kraitchman substitution structure could be obtained due to the assignment of the $N_2{}^{18}O\text{-}SO_2$ and $^{15}N_2O\text{-}^{34}SO_2$ (and $^{15}N_2O\text{-}^{32}SO_2$) species. Unfortunately, the calculation led to imaginary values for the *b*-coordinates of both O3 and S6. This complication, presumably due to the large amplitude vibrational motions in the dimer, made a comparison with the four inertial fit structures inconclusive. The absolute values of the substitution coordinates are given in Table IV.6 along with the principal axis coordinates for the four inertial fit structures. The S6 Kraitchman coordinates vary from structure to structure because they were determined by using the $^{15}N_2O\text{-}^{32}SO_2$ species as the parent molecule and then transformed into the principal axis system of $^{14}N_2O\text{-}^{32}SO_2$. The transformation matrix that carries out this axis system conversion varies slightly depending on the dimer structure used to calculate it. The *a*-coordinates for both atoms are in good agreement with the four inertial fit structures, with the closest agreement for Structure IV when considering both atoms. The *c*-coordinate of O3 from the Kraitchman calculation agrees relatively well with all four configurations, with Structures I and II having the closest value, but agreement for S6 is fairly poor. Only Structures III and IV agree at all well with the S6 *c*-coordinate, and Structures I and II have very poor agreement with this value. Given the large amplitude motions present in the complex, the poor agreement between inertial and substitution coordinates is not surprising.

The dipole moment components predicted for the four structures by projecting the dipole moments of the monomers onto the inertial axes of the complex are given in Table IV.4. The comparison with the experimental values is poor for all the components except μ_c for Structures III and IV. The dipole data, like the Kraitchman calculations and inertial fits, is inconclusive in distinguishing between the four inertial structures. A

Reproduced with permission of the copyright owner. Further reproduction prohibited without permission.

combination of polarization effects and vibrational averaging effects on both the dipole components and the inertial structure determinations is the likely origin of the ambiguous results.[2]

Discussion

A. Structure Inferences

The unambiguous structural conclusion is that N_2O-SO_2 lacks a plane of symmetry. Its configuration resembles the SO_2 complexes with CO_2, OCS and CS_2 with the SO_2 straddling the N_2O axis but, in this case, in an asymmetric fashion. Whether the equilibrium structure is similar to I – IV, where the asymmetry is slight, or is more asymmetric, as predicted by a semi-empirical model (Chapter VII), cannot be clearly ascertained from the data presented here. The amount of isotopic data available in this study would normally be sufficient to determine reasonably reliable quantitative parameters; however, poor agreement between the Kraitchman substitution coordinates and the four fitted structures and between the dipole moment projections and the measured dipole components cautions against accepting any of the structures too literally. Perturbations in the moments of inertia due to the tunneling motion are at the heart of the problem. It is beyond the scope of this study to calculate corrections to the moments due to the large amplitude motion, and high quality semi-empirical or *ab initio* modeling of N_2O-SO_2 is also out of reach. The latter is likely to be the most productive way to advance the understanding of this system at the present time. Lower level semi-empirical and *ab initio* calculations will be discussed in Chapter VII.

Reproduced with permission of the copyright owner. Further reproduction prohibited without permission.

B. Structure Comparisons

Comparison of the structural parameters of N_2O-SO_2 with those for the SO_2 complexes with CO_2, OCS and CS_2 leads to some interesting observations. The most obvious of these is the asymmetry of the N_2O complex. Because the complex is isoelectronic with CO_2, one expects a structure with C_s symmetry, since the lack of symmetry in the N_2O monomer makes the C_{2v} arrangement observed for CO_2-SO_2 unlikely. The twisted structure of N_2O-SO_2 makes a comparison of intermolecular distances more meaningful than a comparison of angles. Structure I will be used for comparison purposes. R_{cm} in CO_2-SO_2 is 3.29 Å, while in N_2O-SO_2 it is about 3.33 Å. This distance and some other atom-atom distances are apparently similar.

The twisting of SO_2 is consistent with the differences seen between CO_2-HCCH[13] and N_2O-HCCH[14] (Chapter VI) and between CO_2-H_2O[4] and N_2O-H_2O.[5] Both of the CO_2 complexes have a symmetric planar structure with the center of the second molecule in line with the carbon of the CO_2. In CO_2-HCCH the monomers are parallel, and in CO_2-H_2O the hydrogen atoms point away from CO_2 giving a roughly T-shaped geometry. In the N_2O complexes, however, one hydrogen atom from the acetylene or water molecule tilts toward the oxygen of the N_2O. This leads to a non-parallel structure for N_2O-HCCH and a distorted T-shaped structure for N_2O-H_2O. The asymmetric structure in N_2O-SO_2, when compared to CO_2-SO_2, shows perhaps more complex changes than observed in the other CO_2 and N_2O systems discussed. Aside from the twisting away from C_s symmetry it is quite similar to the structure observed for OCS-SO_2. It is also possible that the observed C_{2v} configuration for CO_2-SO_2 is an average structure and that the equilibrium structure has C_s symmetry. The discussion in Chapter VII will indicate that this is the prediction of a semi-empirical model and *ab initio* calculations.[2]

The diversity of structural forms for dimers of SO_2 can be further extended to its dimers with other linear molecules such as HCCH,[15, 16] HF,[17, 18] HCl,[17] N_2,[19] and HCN,[20]

Reproduced with permission of the copyright owner. Further reproduction prohibited without permission.

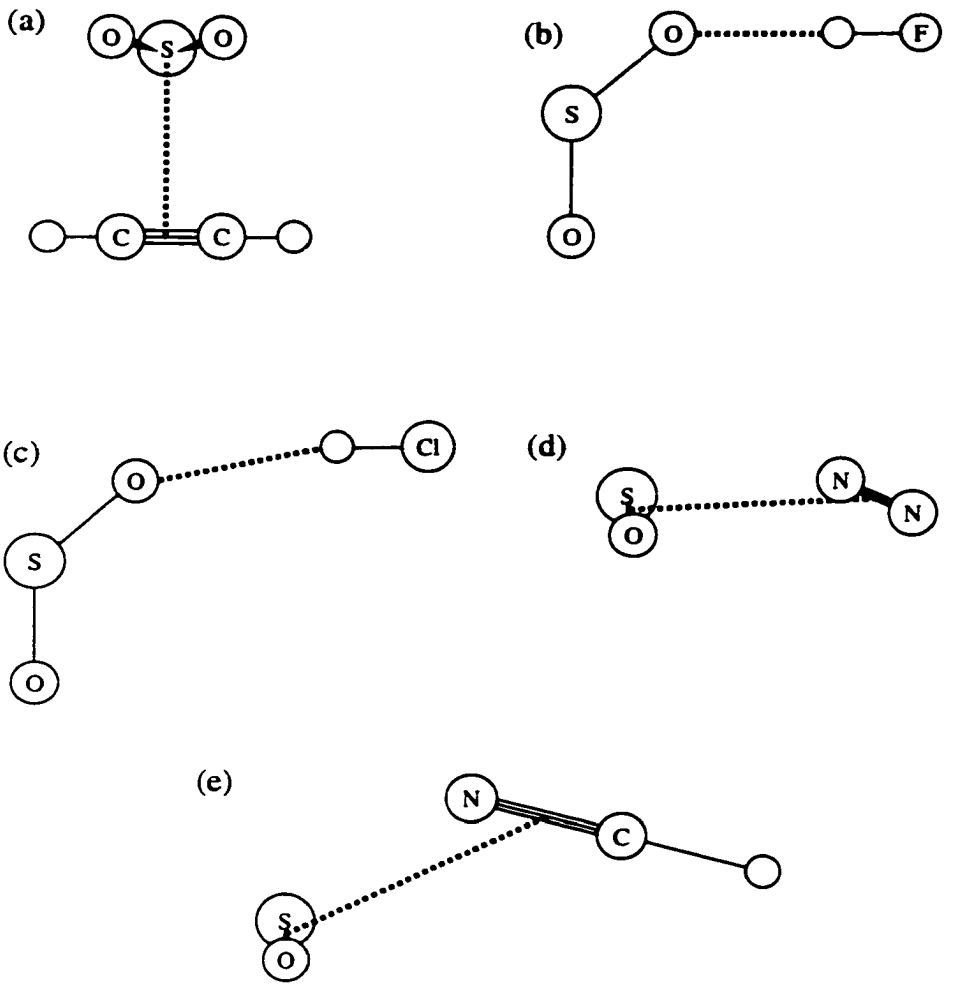


Figure IV.4. Dimers of SO_2 with linear molecules. a) HCCH-SO_2, b) HF-SO_2, c) HCl-SO_2, d) N_2-SO_2, e) HCN-SO_2. See text for references.

illustrated in Figure IV.4. It is apparent that the competition between attractive forces (electrostatic, dispersion, polarization) and repulsive forces is subtle and complex. SO_2 is a delicate probe of these interactions. These are challenging systems to model, and certainly an interesting set to test state-of-the-art calculations.

Summary

The structure of the N_2O-SO_2 dimer is asymmetric, unlike the structures of the similar complexes, CO_2-SO_2,[1] OCS-SO_2[2] and CS_2-SO_2.[3] A tunneling motion is present in

Reproduced with permission of the copyright owner. Further reproduction prohibited without permission.

the complex. The asymmetry of the structure indicates that the motion involved is equivalent to moving the SO_2 through a C_s structure, similar to that observed for OCS-SO_2, to a mirror image conformation. The fit of the structural parameters to moments of inertia of the isotopic species gives four possible configurations for the complex. Dipole moment arguments, the quality of the fits, and comparison with Kraitchman coordinates are inconclusive in identifying a clear preference among the four fitted structures. Comparison with other complexes in the series is not straightforward due to the asymmetry, but R_{cm} and atom-atom distances are similar in going from CO_2-SO_2 to the isoelectronic N_2O-SO_2. This is consistent with the observed structures of CO_2-H_2O, N_2O-H_2O, CO_2-HCCH and N_2O-HCCH, where center-of-mass distances remain virtually unchanged between the corresponding CO_2 and N_2O complexes despite very definite changes in angular geometry. It will be interesting to observe how the N_2O-SO_2 structure changes when another N_2O molecule is added to the system. The next chapter will discuss these changes by describing a study of the $(N_2O)_2$•SO_2 complex. It will be of particular interest to see whether the barrel-like configuration seen in $(OCS)_3$[21, 22] and $(CO_2)_2N_2O$[23] is present in the more complicated trimer or if addition of a bent molecule to the system leads to a more complex structural form.

Reproduced with permission of the copyright owner. Further reproduction prohibited without permission.

References for Chapter IV

[1] L. H. Sun, I. I. Ioannou and R. L. Kuczkowski, Mol. Phys. **88**, 255 (1996).

[2] S. A. Peebles, L. H. Sun, I. I. Ioannou and R. L. Kuczkowski, J. Mol. Struct. **485-486**, 211 (1999).

[3] S. A. Peebles, L. H. Sun and R. L. Kuczkowski, J. Chem. Phys. **110**, 6804 (1999).

[4] P. A. Block, M. D. Marshall, L. G. Pedersen and R. E. Miller, J. Chem. Phys. **96**, 7321 (1992).

[5] K. I. Peterson and W. Klemperer, J. Chem. Phys. **80**, 2439 (1984).

[6] D. Zolandz, D. Yaron, K. I. Peterson and W. Klemperer, J. Chem. Phys. **97**, 2861 (1992).

[7] K. W. Hillig, II, J. Matos, A. Scioly and R. L. Kuczkowski, Chem. Phys. Lett. **133**, 359 (1987).

[8] W. Gordy and R. L. Cook, *Microwave Molecular Spectra, Third Edition*; New York: John Wiley & Sons (1984), Chapter 8 and references therein.

[9] A. M. Andrews, A. Taleb-Bendiab, M. S. LaBarge, K. W. Hillig, II and R. L. Kuczkowski, J. Chem. Phys. **93**, 7030 (1990).

[10] M. D. Harmony, V. W. Laurie, R. L. Kuczkowski, R. H. Schwendeman, D. A. Ramsay, F. J. Lovas, W. J. Lafferty and A. G. Maki, J. Phys. Chem. Ref. Data **8**, 619 (1979).

[11] E. B. Wilson, J. C. Decius and P. C. Cross, *Molecular Vibrations*; New York: McGraw-Hill (1955).

[12] J. Kraitchman, Am. J. Phys. **21**, 17 (1953).

[13] J. S. Muenter, J. Chem. Phys. **90**, 4048 (1989).

[14] R. A. Peebles, S. A. Peebles, R. L. Kuczkowski and H. O. Leung, J. Phys. Chem. A **103**, 10813 (1999).

[15] J. S. Muenter, R. L. DeLeon and A. Tokozeki, Faraday Discuss. Chem. Soc. **73**, 63 (1982).

[16] A. M. Andrews, K. W. Hillig, II, R. L. Kuczkowski, A. C. Legon and N. W. Howard, J. Chem. Phys. **94**, 6947 (1991).

[17] A. J. Fillery-Travis and A. C. Legon, Chem. Phys. Lett. **123**, 4 (1986).

Reproduced with permission of the copyright owner. Further reproduction prohibited without permission.

[18] A. J. Fillery-Travis and A. C. Legon, J. Chem. Phys. **85**, 3180 (1986).

[19] Y. D. Juang, M. A. Walsh, A. K. Lawin and T. R. Dyke, J. Chem. Phys. **97**, 832 (1992).

[20] E. J. Goodwin and A. C. Legon, J. Chem. Phys. **85**, 6826 (1986).

[21] R. A. Peebles and R. L. Kuczkowski J. Phys. Chem. **103**, 6344 (1999).

[22] J. P. Connelly, A. Bauder, A. Chisholm and B. J. Howard, Mol. Phys. **88**, 915 (1996).

[23] R. A. Peebles, S. A. Peebles and R. L. Kuczkowski Mol. Phys. **96**, 1355 (1999).

Reproduced with permission of the copyright owner. Further reproduction prohibited without permission.

CHAPTER V

$(N_2O)_2$•SO_2: ROTATIONAL SPECTRUM AND STRUCTURE OF THE FIRST VAN DER WAALS TRIMER CONTAINING SULFUR DIOXIDE

Introduction

The first two experimental chapters of this thesis focused on trimers of linear triatomic molecules. The homo-molecular complex $(OCS)_3$[1, 2] was examined first, followed by an examination of $(CO_2)_2N_2O$.[3] The use of linear monomers aided structure determination by minimizing the number of parameters needed to describe the trimer's configuration; however, good understanding of intermolecular forces in trimer systems requires the study of more complex clusters. This chapter, which presents a determination and discussion of the structure of the $(N_2O)_2$•SO_2 complex,[4] is a first step toward the understanding of trimeric systems involving non-linear monomers. By including the bent SO_2 molecule, $(N_2O)_2$•SO_2 has one more structural parameter than the previously discussed trimers. The intermolecular interactions may be more complex than in trimers of only linear molecules, and assignment of the N_2O•SO_2 dimer,[5] discussed in Chapter IV, will allow an examination of these interactions and how they change between the dimer and the trimer. Comparisons with $(N_2O)_3$[6] and $(N_2O)_2$[7] will also be interesting. The dimer assumes the slipped-parallel configuration that is common in complexes between two linear monomers, and the trimer has the familiar barrel-like structure discussed previously. It will be interesting to see if $(N_2O)_2$•SO_2 mimics these arrangements. Although addition of an SO_2 molecule to a roughly slipped-parallel N_2O

Reproduced with permission of the copyright owner. Further reproduction prohibited without permission.

dimer fragment would seem logical, a more cyclic configuration, where the N_2O molecules resemble a portion of the planar isomer of $(CO_2)_3$[8] would also be possible.

Experiment

The rotational spectrum of $(N_2O)_2$•SO_2 was measured in the 5.5 – 9.5 GHz region. This very wide search range resulted in a large number of transitions that required both sample components. Many transitions remained after the assignment of the spectrum of N_2O•SO_2 (Chapter IV),[5] and it was possible to assign most of these to a species that was assumed to be a trimer containing both N_2O and SO_2. The rotational constants of the assigned spectrum were consistent with various model structures for either $(N_2O)_2$•SO_2 or $(SO_2)_2$•N_2O that were obtained using the semi-empirical program described in Chapter VII.[9] Preliminary assignment of the fully ^{15}N substituted isotopomer of the complex was accomplished using unassigned transitions from searches for $^{15}N_2O$•SO_2. The rotational constants for this species were still consistent with either of the possible N_2O/SO_2 trimer combinations; however, they showed a small preference for models that contained two N_2O molecules and one SO_2. Isotope shifts were used to predict the spectra of $^{15}N_2O$•$^{14}N_2O$•SO_2 and $^{14}N_2O$•$^{15}N_2O$•SO_2, and the assignment of both isotopomers close to these predictions confirmed that the carrier of the spectrum was $(N_2O)_2$•SO_2.

The spectrum showed no evidence of splitting due to the four quadrupolar ^{14}N nuclei in the complex, although the transitions of the isotopomers containing $^{14}N_2O$ were considerably weaker than those containing only $^{15}N_2O$. Transitions of the mixed $^{15}N_2O/^{14}N_2O$ isotopomers were also not visibly split.

The spectra of four isotopomers of $(N_2O)_2$•SO_2 were measured in addition to the normal species. For the measurement of $(^{15}N_2O)_2$•SO_2, $^{15}N_2O$•$^{14}N_2O$•SO_2, $^{14}N_2O$•$^{15}N_2O$•SO_2, and $(^{15}N_2O)_2$•$^{34}SO_2$, enriched $^{15}N_2O$ (99% ^{15}N, Isotec) was used, and

Reproduced with permission of the copyright owner. Further reproduction prohibited without permission.

for the assignment of $(^{15}N_2O)_2{\bullet}^{34}SO_2$, enriched $^{34}SO_2$ (90% ^{34}S, Icon) was also used. A 50:50 mixture of $^{15}N_2O$ and $^{14}N_2O$ was used to assign the mixed N_2O isotopic species.

Results

A. Spectra

Both *a*- and *b*-type transitions were observed for the five isotopomers. Transition

Table V.1. Spectroscopic constants for $(N_2O)_2{\bullet}SO_2$. (*A*, *B* and *C* in MHz, distortion constants in kHz.)

	$(^{14}N_2O)_2{\bullet}SO_2$	$(^{15}N_2O)_2{\bullet}SO_2$	$^{15}N_2O{\bullet}^{14}N_2O{\bullet}SO_2$ [a]	$^{14}N_2O{\bullet}^{15}N_2O{\bullet}SO_2$ [b]	$(^{15}N_2O)_2{\bullet}^{34}SO_2$
A	1369.1014(11)	1337.1700(3)	1363.4695(10)	1344.1393(23)	1315.6368(6)
B	1115.5816(11)	1070.4026(2)	1085.5748(10)	1098.8989(18)	1068.6156(6)
C	730.5790(4)	703.7046(2)	717.1382(4)	716.7940(8)	696.9613(3)
Δ_J	1.389(24)	1.347(4)	1.294(20)	1.482(53)	1.289(14)
Δ_{JK}	0.743(89)	–0.066(19)	0.618(79)	0.618 [e]	0.230(52)
Δ_K	1.104(65)	1.969(2)	1.224(59)	1.076(90)	1.587(37)
δ_J	0.399(12)	0.392(2)	0.349(9)	0.460(26)	0.376(6)
δ_K	1.318 (45)	0.892(11)	1.035(53)	1.73(18)	0.952(29)
N [c]	46	49	41	21	33
$\Delta\nu_{rms}$ [d]	5.4	1.8	5.3	6.3	2.6

[a] N_1 and N_2 substituted
[b] N_5 and N_6 substituted
[c] number of lines in fit
[d] in kHz, see Table II.1 for definition of $\Delta\nu_{rms}$
[e] fixed at value from $^{15}N_2O{\bullet}^{14}N_2O{\bullet}SO_2$

Reproduced with permission of the copyright owner. Further reproduction prohibited without permission.

frequencies and the residuals from a fit of these lines to a Watson A-reduction Hamiltonian in the I^r representation[10] are listed in Appendix D. The spectroscopic constants for the assigned species [$(^{14}N_2O)_2{\bullet}SO_2$, $(^{15}N_2O)_2{\bullet}SO_2$, $^{15}N_2O{\bullet}^{14}N_2O{\bullet}SO_2$, $^{14}N_2O{\bullet}^{15}N_2O{\bullet}SO_2$, and $(^{15}N_2O)_2{\bullet}^{34}SO_2$] are given in Table V.1. The fairly large differences between the normal species centrifugal distortion constants and those for the $(^{15}N_2O)_2{\bullet}SO_2$ and $(^{15}N_2O)_2{\bullet}^{34}SO_2$ species can be explained by a high correlation between the Δ_{JK} and Δ_K constants and a smaller correlation between these constants and δ_K. When one of these constants was fixed for fits of the $(^{15}N_2O)_2{\bullet}SO_2$ species, the others converged to values similar to those of the normal isotopomer, but the quality of the fit was lower. This was probably because the fixed constant had a fairly large contribution to the transition frequency. A fit using the Watson S-reduction Hamiltonian[11] was of similar quality to the A-reduction fit and also showed high correlation between D_{JK} and D_K.

Attempts at assigning the $(^{15}N_2O)_2{\bullet}S^{18}O_2$ species using 97% ^{18}O enriched SO_2 were unsuccessful. Lines belonging to the $^{15}N_2O{\bullet}S^{18}O_2$ dimer were about a factor of ten weaker than the normal dimer. Since the normal trimer lines are about two orders of magnitude weaker than the strongest dimer lines, the $S^{18}O_2$ lines may have been too weak to observe. The cause of these problems involving $S^{18}O_2$ is unknown. ^{18}O and ^{16}O may exchange readily from water, which is ubiquitous in the sample manifold, or some other process may have lowered the stated enrichment.

Reproduced with permission of the copyright owner. Further reproduction prohibited without permission.

B. Dipole Moment

Stark effects for a total of fourteen *M* components from four transitions of

Table V.2. Stark coefficients for the transitions used to calculate the dipole moment of $(^{15}N_2O)_2$•SO_2.

$J'_{K_aK_c'}$	$J''_{K_aK_c''}$	$\|M\|$	$\Delta\nu / E^2$ [a]	Obs. – Calc. [a]
4_{31}	3_{22}	0	–0.151	0.001
		1	0.865	–0.031
		2	4.024	–0.018
		3	9.286	0.003
3_{21}	2_{12}	0	–0.981	0.029
		2	7.346	0.006
4_{23}	3_{12}	0	0.257	–0.005
		1	0.942	–0.028
		2	3.053	–0.038
		3	6.666	0.040
5_{33}	4_{22}	1	0.259	–0.007
		2	0.509	–0.014
		3	0.936	–0.018
		4	1.537	–0.020

[a] units of 10^{-5} MHz•cm^2/V^2. The calculated coefficients were obtained with the rotational constants in Table V.1 and the $(^{15}N_2O)_2$•SO_2 dipole moment components in Table V.3.

$(^{15}N_2O)_2$•SO_2 were measured. The observed Stark coefficients are listed in Table V.2. They give the dipole moment components in Table V.3 of μ_a = 0.561(1) D, μ_b = 1.276(2)

Reproduced with permission of the copyright owner. Further reproduction prohibited without permission.

Table V.3. Dipole moment components for $(N_2O)_2 \cdot SO_2$ and the projections of monomer moments for the two possible structures.

	Experiment [a]	Structure I	Structure II
μ_a / D	0.561(1)	0.573	0.278
μ_b / D	1.276(2)	1.316	0.995
μ_c / D	0.064(2)	0.152	1.091
μ_{total} / D	1.396(2)	1.443	1.503

[a] μ_a, μ_b and μ_c components transformed from the principal axes of $(^{15}N_2O)_2 \cdot SO_2$ to the principal axes of $(^{14}N_2O)_2 \cdot SO_2$. $(^{15}N_2O)_2 \cdot SO_2$ principal axis components are $\mu_a = 0.606$ D, $\mu_b = 1.256$ D, $\mu_c = 0.058$ D.

D, $\mu_c = 0.064(2)$ D, and $\mu_{total} = 1.396(2)$ D in the $(^{14}N_2O)_2 \cdot SO_2$ principal axis system. The largest Stark shifts were in the range of 600 – 800 kHz for several components, and the greatest μ_c contributions were about 30 – 50 kHz. Although μ_c-type transitions might be observable, none were detected after lengthy averaging. They were about 1000 times weaker than the μ_b-type transitions and below the sensitivity of the spectrometer.

C. Structure

The ten parameters required to define the structure of the trimer are illustrated in Figure V.1. They include two distances and an angle that define the locations of the centers of mass of the three monomers, an angle and a dihedral angle defining the orientation of each of the N_2O molecules relative to the plane containing the three centers of mass, and an angle and two dihedral angles defining the orientation of the SO_2 molecule relative to the plane with the three centers of mass.[12]

Assignment of four isotopomers and the normal species provided 15 moments of inertia with which to determine the 10 parameters, assuming that the monomer structures

Reproduced with permission of the copyright owner. Further reproduction prohibited without permission.

remain unchanged (R_{N-O} = 1.185 Å, R_{N-N} = 1.128 Å; R_{S-O} = 1.431 Å, θ_{O-S-O} = 119.3°[13]). Least-squares fitting of these 10 parameters to the moments of inertia led to two

Table V.4. Structural parameters for the two possible $(N_2O)_2 \bullet SO_2$ configurations.

	Structure I[a]	Structure II
R_{4-8} / Å	3.8558(23)	3.7885(65)
R_{4-12} / Å	3.5316(13)	3.591(14)
θ_{12-4-8} / °	52.494(26)	52.50(36)
θ_{1-4-8} / °	83.330(85)	86.0(15)
$\phi_{1-4-8-12}$ / °	−129.99(10)	−121.4(20)
θ_{5-8-12} / °	97.672(95)	107.0(15)
$\phi_{5-8-12-4}$ / °[b]	−151.19(21)	137.5(22)
θ_{9-12-4} / °	90.75(14)	93.8(17)
$\phi_{9-12-4-8}$ / °	163.83(84)	137.7(29)
$\phi_{10-9-12-4}$ / °	−118.66(36)	−112.8(32)
s.d.[c]	0.0036	0.0529

[a] Structure I is preferred.
[b] The signs of the dihedral angles are consistent with the definition in Reference 12.
[c] standard deviation of the inertial fit in amu•Å^2.

structures (Table V.4) that are consistent with the inertial data. Assignment of the $(^{15}N_2O)_2 \bullet {}^{32}SO_2$ and $(^{15}N_2O)_2 \bullet {}^{34}SO_2$ isotopomers also allowed the determination of Kraitchman coordinates[14] for the sulfur atom of the SO_2. Since the Kraitchman calculation determined the sulfur coordinates in the principal axis system of

Reproduced with permission of the copyright owner. Further reproduction prohibited without permission.

$(^{15}N_2O)_2 \cdot SO_2$, it was necessary to transform the coordinates to the normal isotopomer axis system before comparisons could be made with the inertial fit results.

As seen in Table V.4, comparing the least-squares fitting of the experimental moments of inertia, Structure I has a lower standard deviation than Structure II. (See

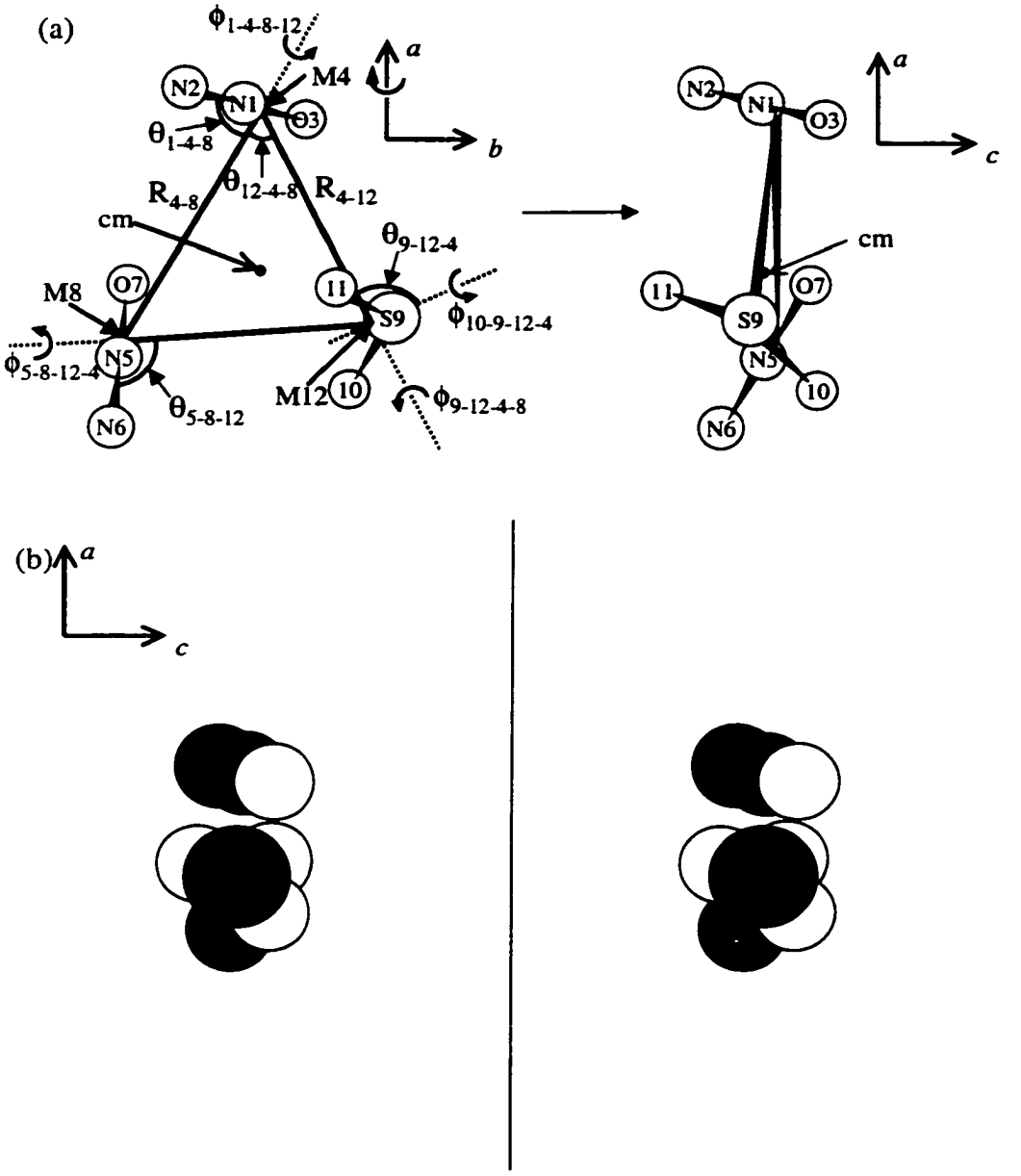


Figure V.1. Structure I from the inertial fit of $(N_2O)_2SO_2$ showing the ten parameters used to define the structure. (a) The *ab* plane is parallel to the page in the left hand view, and the *ac* plane is parallel to the page in the right hand view. (b) Stereo image of Structure I of $(N_2O)_2SO_2$ in the *ac* plane.

Reproduced with permission of the copyright owner. Further reproduction prohibited without permission.

Figures V.1 and V.2.[15]) This gives a preliminary indication that Structure I is the actual configuration of the complex. Comparison of the experimental dipole moment components and the projections of the monomer dipole moments onto the principal axes

Table V.5. Principal axis coordinates (in Å) for Structures I and II for $(N_2O)_2 \cdot SO_2$.[a]

	a		*b*		*c*	
	I	II	I	II	I	II
N1	2.3445	2.3146	–0.2415	–0.3957	0.0376	0.2595
N2	2.5604	2.5868	–1.0233	–0.9857	–0.7464	–0.6626
O3	2.1177	2.0287	0.5798	0.2241	0.8611	1.2281
M4	2.3307	2.2973	–0.1916	–0.3580	0.0876	0.3183
N5	–1.2133	–1.2465	–1.8536	–1.7886	0.0996	–0.0896
N6	–2.1867	–2.1652	–1.9537	–2.0110	–0.4616	0.5261
O7	–0.1908	–0.2815	–1.7484	–1.5550	0.6892	–0.7363
M8	–1.1512	–1.1879	–1.8472	–1.7744	0.1354	–0.1289
S9	–0.6603	–0.6811	1.7223	1.7134	–0.0771	0.1215
	[0.659][b]	[0.655]	[1.723]		[0.079]	[0.086]
O10	–1.6608	–1.7622	1.1715	0.7991	0.7852	0.3291
O11	–0.2637	–0.0723	0.9948	1.6428	–1.2438	–1.0930
M12	–0.8115	–0.7631	1.4023	1.4668	–0.1533	–0.1305

[a] See Figure V.1 for atom numbering. Structure I is preferred.
[b] Absolute values of Kraitchman coordinates are in brackets below the corresponding coordinates. The values vary slightly for the two structures, because they were calculated in the $(^{15}N_2O)_2 \cdot SO_2$ principal axis system and then transformed to the $(^{14}N_2O)_2 \cdot SO_2$ principal axes.

Reproduced with permission of the copyright owner. Further reproduction prohibited without permission.

for both structures (Table V.3) leads to stronger evidence that Structure II is unlikely. Its dipole moment projection has a significant μ_c component which contradicts experimental evidence. The difference is too large to be accounted for by possible induced dipole

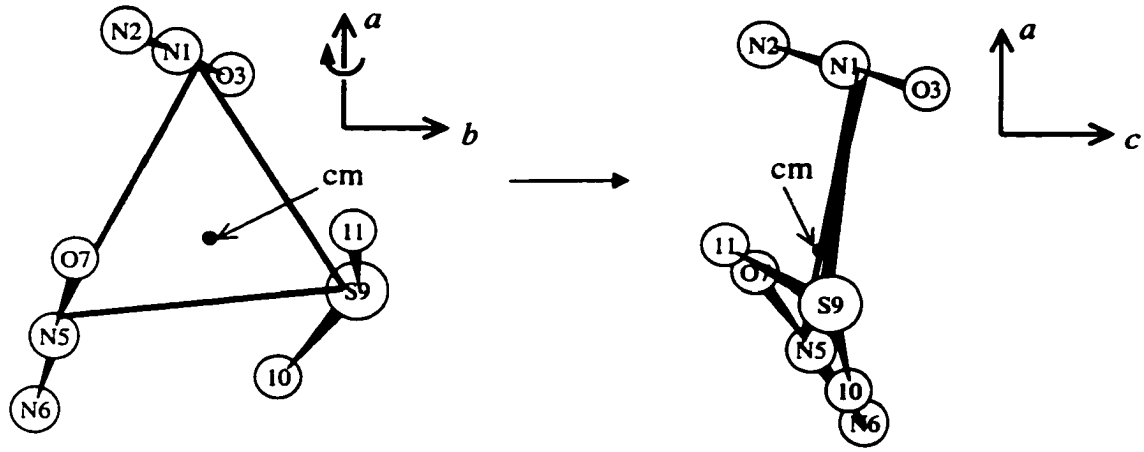


Figure V.2. Views of Structure II of $(N_2O)_2SO_2$ in the *ab* and *ac* planes.

moment components. Furthermore, the projected dipole components for Structure I are quite similar to the observed dipole moment components. The principal axis coordinates are given for both configurations in Table V.5.

Although Structure II can be eliminated based on the dipole moment data, its appearance as a plausible inertial fit deserves comment. It arises from coordinate sign ambiguities in the moments of inertia. This can be perceived by comparing Figure V.1(a) with Figure V.2. One N_2O is approximately reflected across the *ab* plane. The equilibrium structure of I is probably within ±0.05 Å and ±5° of the N_2O related parameters in Table V.4 (first seven rows) while the parameters associated with SO_2 (next three rows) are less certain, probably within ±10°. Structure I also resembles a prediction from a semi-empirical model which will be discussed in Chapter VII.

Reproduced with permission of the copyright owner. Further reproduction prohibited without permission.

Discussion

Studies over the past few years have indicated that many trimers involving only linear molecules tend to have a barrel-shaped or triangular structure, where the three monomers align themselves roughly parallel to each other with their centers of mass forming a triangle that is approximately perpendicular to the axes of the molecules.[1, 3, 16-20] This arrangement presumably maximizes the dispersion interaction while the twisting and turning away from three parallel sticks further balances the electrostatic and repulsive interactions. When the current work began, it was unknown whether a roughly triangular structure with the N_2O molecules approximately parallel to each other would still occur or whether a different structural form would take shape. The results show that the $(N_2O)_2$•SO_2 configuration is very different from the barrel-like structure observed previously in other systems.

Comparison of the trimer with the recently studied N_2O•SO_2 dimer is interesting, although qualified, since the dimer structure may not be very accurate (Chapter IV).[5] The N_2O•SO_2 spectrum is split into doublets due to a tunneling motion; no consideration of this contribution to the moments of inertia was given when determining the structure. Figure V.3(a) illustrates a configuration for the dimer consistent with the experimental data. While structural details may be less certain, it is clear that the SO_2 straddles the N_2O axis asymmetrically, as illustrated. The equilibrium configuration may be even more asymmetric than suggested by Figure V.3(a). In fact, the ORIENT semi-empirical model predicts a considerably more asymmetric structure with one of the S-O bonds nearly parallel to the N-N-O axis (Chapter VII).[9]

One face of the trimer [Figure V.3(b)] bears a strong resemblance to the N_2O•SO_2 dimer in Figure V.3(a). In fact, the trimer might be described as the N_2O•SO_2 dimer to which another N_2O nestles such that its central N (slightly positive) is attracted to the terminal O (slightly negative) of the neighboring N_2O, while its terminal oxygen (slightly

Reproduced with permission of the copyright owner. Further reproduction prohibited without permission.

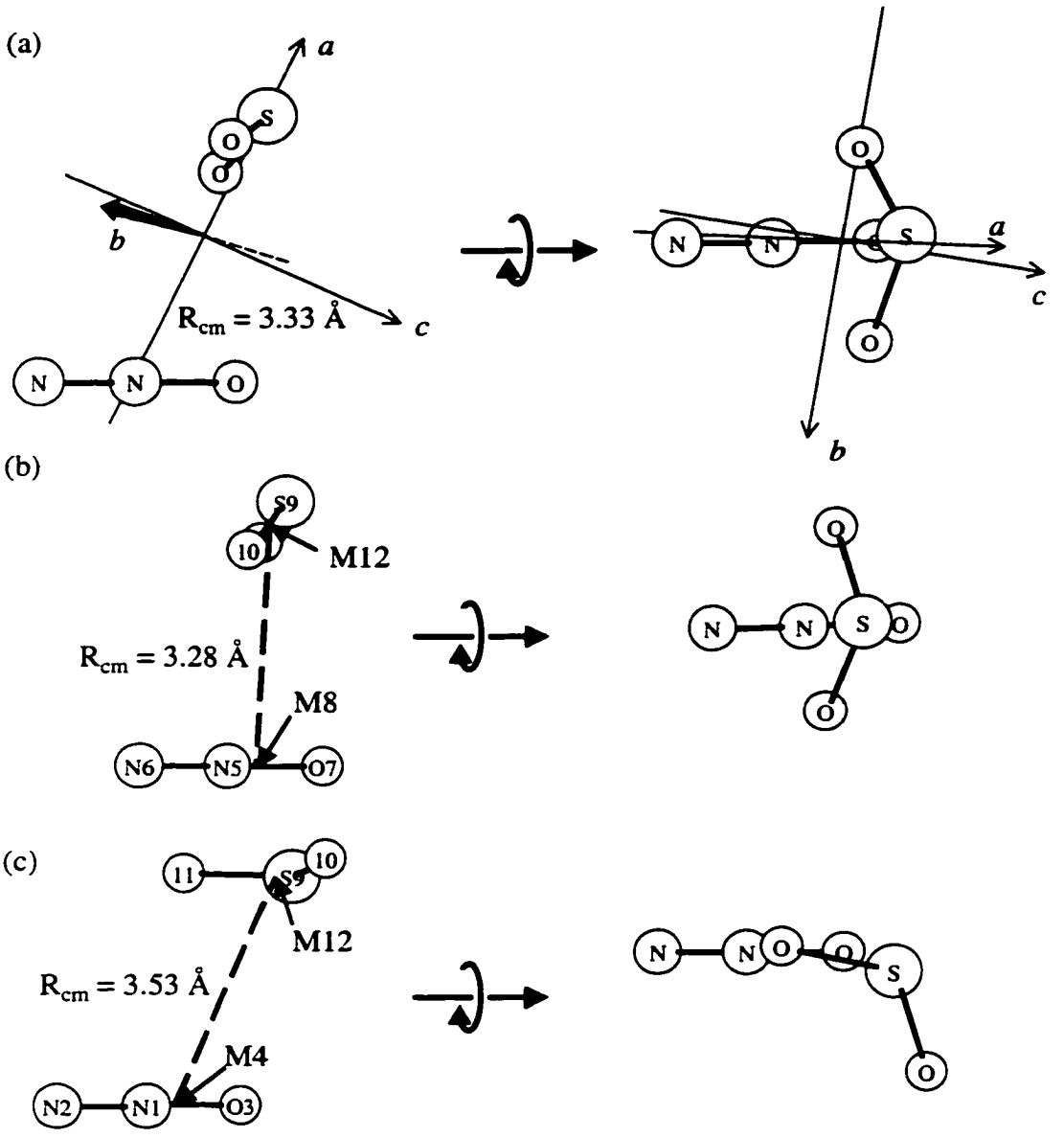


Figure V.3. Experimental structure of N_2O-SO_2 dimer (a) and the two N_2O-SO_2 faces of $(N_2O)_2SO_2$ (b and c). The views on the left side of the figure place the plane containing the N_2O and two centers-of-mass parallel to the page. The views on the right align this plane perpendicular to the page.

negative) is attracted to the sulfur (positive). The center-of-mass separation ($M_{12} - M_8$ = 3.28 Å) and the $S_9 - N_5$ distance of 3.62 Å in V.3(b) are both in good agreement with the dimer, showing deviations of only 0.05 Å – 0.07 Å from the $N_2O{\bullet}SO_2$ values. The S_9-M_{12}-M_8-O_7 angle of V.3(b) is 10.9° compared to the dimer value of 21.7°. Although

Reproduced with permission of the copyright owner. Further reproduction prohibited without permission.

these numbers seem close, the difference is significant. The S_9-M_{12}-M_8 angle of 154.2°, however, is very similar to the dimer angle of 156.6°.

It is interesting that the other N_2O•SO_2 face of the trimer (Figure V.3(c)) resembles more strongly the semi-empirical dimer orientation mentioned above, with nearly parallel N-O and S-O bonds. The center-of-mass distance, $M_{12} - M_4$, for this portion of the trimer is 3.53 Å. This compares with a distance of 3.33 Å in the isolated dimer. The $S_9 - N_1$ distance for the trimer face is 3.59 Å. In the dimer the comparable distance is 3.69 Å. It is interesting that the center-of-mass distance is longer in the trimer, while the distance between the nitrogen and sulfur atoms gets slightly shorter. Perhaps comparison of the angles that orient the SO_2 relative to the N_2O will help elucidate these differences.

In N_2O•SO_2 the S-M_{SO_2}-M_{N_2O}-O dihedral angle is 21.7° (Structure I in Chapter IV). The S-M-M-O angle in Figure V.3(c) is $\phi_{9\text{-}12\text{-}4\text{-}3} = 41.6°$, a difference of about 20° from the dimer value. Also, the S-M-M angle in the dimer is 156.6°, while the trimer face has an angle, $\theta_{9\text{-}12\text{-}4}$, of 90.8°. This decrease in the angle between the dimer and the trimer allows the S-N distance to get shorter, while the center-of-mass distance can lengthen slightly.

The orientation of the two N_2O monomers relative to each other in the trimer is intermediate between a T-shaped and crossed structure. This alignment is very different from the experimental N_2O dimer configuration where the monomers are parallel to each other with opposing dipole moments (slipped parallel structure).[7] It appears that a quadrupole-quadrupole like interaction must dominate the arrangement of these two molecules, with the slightly negative oxygen end of one pointing roughly toward the slightly positive central nitrogen of the other. A comparison with HCCH dimer is interesting. The dimer of acetylene is T-shaped and undergoes a geared internal rotation, passing through a slipped-parallel intermediate.[21, 22] In the $(HCCH)_2$•OCS trimer the HCCH molecules appear to be intermediate between T-shaped and parallel relative to

Reproduced with permission of the copyright owner. Further reproduction prohibited without permission.

each other (but non-planar), and it was proposed that an intermediate configuration in the tunneling process of the dimer was "trapped" in the trimer.[23] The N_2O-N_2O configuration in $(N_2O)_2$•SO_2 resembles the HCCH-HCCH arrangement in $(HCCH)_2$•OCS. This raises the question of whether a T-shaped isomer of $(N_2O)_2$ is possible, although there has been no experimental evidence for this type of structure, yet. Indeed, the observation of this intermediate N_2O-N_2O configuration in the trimer brings to mind the isoelectronic CO_2 dimer. Although it has now been proven that $(CO_2)_2$ has a slipped-parallel geometry, it was widely believed for some time that the structure was T-shaped.[24, 25]

Summary

The structure of the trimer $(N_2O)_2$•SO_2 has been determined by microwave spectroscopy. The complex is the first trimer containing the bent molecule SO_2 to be studied by this technique, although many SO_2 containing dimers have been studied,[5, 26 - 31] as have many trimers containing only linear molecules or combinations of linear molecules with rare gas atoms or occasionally water.[1, 17, 18, 20, 32 - 35]

Comparison of the trimer structure with the structure of N_2O•SO_2 has shown that one N_2O-SO_2 face of the trimer is quite different from the isolated dimer, while the other N_2O-SO_2 face is quite similar to it. In order to preserve the favorable configuration in one N_2O-SO_2 unit, it was necessary to twist the other unit away from the dimer structure. The N_2O-N_2O face of the trimer does not resemble the isolated N_2O dimer. This suggests that the two sets of N_2O-SO_2 interactions are strong enough to force the N_2O molecules from the slipped parallel arrangement which they have in the isolated dimer to a higher energy T-shaped orientation. Theoretical techniques are used to explore this idea further in Chapter VII.

Reproduced with permission of the copyright owner. Further reproduction prohibited without permission.

It will be interesting to see if other trimers of two linear molecules with SO_2 have a structure similar to that observed for $(N_2O)_2 \cdot SO_2$ or if they will conform more to the barrel-shaped triangular structure that is common for most linear molecule trimers. Since the dimers of CO_2,[27] OCS[26] and CS_2[28] with SO_2 all have a plane of symmetry, which $N_2O \cdot SO_2$ lacks, these trimers may tend toward more symmetric triangular configurations.

Reproduced with permission of the copyright owner. Further reproduction prohibited without permission.

References for Chapter V

[1] R. A. Peebles and R. L. Kuczkowski, J. Phys. Chem. A. **103**, 6344 (1999).

[2] J. P. Connelly, A. Bauder, A. Chisholm and B. J. Howard, Mol. Phys. **88**, 915 (1996)

[3] R. A. Peebles, S. A. Peebles and R. L. Kuczkowski, Mol. Phys. **96**, 1355 (1999).

[4] R. A. Peebles and R. L. Kuczkowski, J. Chem. Phys. **112**, 8839 (2000).

[5] R. A. Peebles and R. L. Kuczkowski, J. Phys. Chem. A., **104**, 4968 (2000).

[6] R. E. Miller and L. Pedersen, L. J. Chem. Phys. **108**, 436 (1998).

[7] Z. S. Huang and R. E. Miller, J. Chem. Phys. **89**, 5408 (1988).

[8] G. T. Fraser, A. S. Pine, W. J. Lafferty and R. E. Miller, J. Chem. Phys. **87**, 1502 (1987).

[9] A. J. Stone, A. Dullweber, M. P. Hodges, P. L. A. Popelier and D. J. Wales, *ORIENT: A program for studying interactions between molecules*, Version 3.2, University of Cambridge (1995).

[10] J. K. G. Watson, J. Chem. Phys. **48**, 4517 (1968).

[11] W. Gordy and R. L. Cook, *Microwave Molecular Spectra, Third Edition*; New York: John Wiley & Sons (1984), Chapter 8 and references therein.

[12] The signs of the dihedral angles are consistent with the following: E. B. Wilson, J. C. Decius and P. C. Cross, *Molecular Vibrations* (McGraw-Hill, New York, 1955).

[13] M. D. Harmony, V. W. Laurie, R. L. Kuczkowski, R. H. Schwendeman, D. A. Ramsay, F. J. Lovas, W. J. Lafferty and A. G. Maki, J. Phys. Chem. Ref. Data **8**, 619 (1979).

[14] J. Kraitchman, Am. J. Phys. **21**, 17 (1953).

[15] From the plotting program MolWin, Version 2.3, P. V. Ganelin, Dept. of Chemistry, The Catholic University of America (1994).

[16] S. A. Peebles and R. L. Kuczkowski, Chem. Phys. Lett. **286**, 421 (1998).

[17] S. A. Peebles and R. L. Kuczkowski, J. Chem. Phys. **109**, 5276 (1998).

[18] S. A. Peebles and R. L. Kuczkowski, J. Phys. Chem. **102**, 8091 (1998).

[19] S. A. Peebles and R. L. Kuczkowski, Chem. Phys. Lett. **308**, 21 (1999).

Reproduced with permission of the copyright owner. Further reproduction prohibited without permission.

[20] S. A. Peebles and R. L. Kuczkowski, J. Chem. Phys. **111**, 10511 (1999).

[21] D. G. Prichard, R. N. Nandi and J. S. Muenter, J. Chem. Phys. **89**, 115 (1988).

[22] G. T. Fraser, R. D. Suenram, F. J. Lovas, A. S. Pine, J. T. Hougen, W. J. Lafferty and J. S. Muenter, J. Chem. Phys. **89**, 6028 (1988).

[23] S. A. Peebles and R. L. Kuczkowski, J. Mol. Struct., accepted for publication.

[24] M. A. Walsh, T. H. England, T. R. Dyke and B. J. Howard, Chem. Phys. Lett. **142**, 265 (1987).

[25] K. W. Jucks, Z. S. Huang, R. E. Miller, G. T. Fraser, A. S. Pine and W. J. Lafferty, J. Chem. Phys. **88**, 2185 (1988).

[26] S. A. Peebles, L. H. Sun, I. I. Ioannou and R. L. Kuczkowski, J. Mol. Struct. **485-486**, 211 (1999).

[27] L. H. Sun, I. I. Ioannou and R. L. Kuczkowski, Mol. Phys. **88**, 211 (1996).

[28] S. A. Peebles, L. H. Sun and R. L. Kuczkowski, J. Chem. Phys. **110**, 6804 (1999).

[29] L. H. Sun, X.Q. Tan, J. J. Oh and R. L. Kuczkowski, J. Chem. Phys. **103**, 6440 (1995).

[30] A. Taleb-Bendiab, K. W. Hillig, II and R. L. Kuczkowski, J. Chem. Phys. **98**, 3627 (1993).

[31] R. L. Kuczkowski and A. Taleb-Bendiab in *Structures and Conformations of Nonrigid Molecules*, J. Laane, et al, eds. (Kluwer Academic Publishers, The Netherlands, 1993).

[32] M. S. Ngari and W. Jager, J. Chem. Phys. **111**, 3919 (1999).

[33] H. S. Gutowsky and C. Chuang, J. Chem. Phys. **93**, 894 (1990).

[34] E. Arunan, T. Emilsson and H. S. Gutowsky, J. Chem. Phys. **101**, 861 (1994).

[35] Z. Kisiel, E. Białkowska-Jaworska, L. Pszczółkowski, A. Milet, C. Struniewicz, R. Moszynski and J. Sadlej, J. Chem. Phys. **112**, 5767 (2000).

Reproduced with permission of the copyright owner. Further reproduction prohibited without permission.

CHAPTER VI

ISOTOPIC STUDIES, STRUCTURE AND MODELING OF THE NITROUS OXIDE•ACETYLENE COMPLEX

Introduction

The previous chapters of this thesis have concentrated on an extension of microwave spectroscopy to larger, more complex systems than those previously studied. Trimers of linear and bent molecules have been a focus, with the particular goal of determining how dimers change upon addition of a third body to the system. It has also been indicated throughout this work that the application of semi-empirical and *ab initio* models to the complexes studied will be discussed in detail in the final chapter. In the current chapter the HCCH•N_2O dimer is presented as an example of a relatively simple system with some interesting aspects related to the results of semi-empirical modeling. This complex has previously been studied experimentally by several groups,[1-3] who also used a semi-empirical interaction model to investigate its structure.[1,4] The initial studies proposed a parallel arrangement with a line perpendicular to the two monomers joining their centers of mass. The available data from one isotopic species was insensitive to detecting small deviations from a parallel configuration. The proposed structure was similar to that of the isoelectronic HCCH•CO_2 complex, which has been studied experimentally and with the same interaction model that was applied to HCCH•N_2O.[4-6] The interaction model described in Chapter VII has recently been helpful in modeling the three trimers described in Chapters II, III and V[7-9] as well as HCCH•OCS[10] and $HCCH(OCS)_2$.[11] It was noted in the HCCH•OCS study that this model predicted that the

Reproduced with permission of the copyright owner. Further reproduction prohibited without permission.

oxygen end of the N_2O would tip about 10 –15 degrees toward the acetylene molecule in the HCCH•N_2O complex.[10] Other complexes involving N_2O have shown similar decreases in symmetry when compared to the corresponding CO_2 complexes. For example, H_2O•CO_2 has C_{2v} symmetry, with the oxygen of H_2O pointing toward the carbon of CO_2 in a T-shaped configuration.[12, 13] H_2O•N_2O also has a T-shaped structure, but the oxygen of the N_2O is drawn toward one of the H_2O hydrogens, causing a distortion of the T.[14]

The current work investigates the discrepancy between the two sets of HCCH•N_2O calculations by studying various isotopomers of the complex. This allows a complete structural determination which was not possible with the previous data from only one isotope.

Experiment

The spectra of six isotopomers of HCCH•N_2O were measured in the 5.5 – 18.5 GHz range on the Balle-Flygare Fourier transform microwave spectrometers[15] at Mount Holyoke College and the University of Michigan.[2, 16, 17] The $H^{12}C^{12}CH$•$^{14}N_2O$ and $H^{12}C^{12}CH$•$^{15}N^{14}NO$ isotopomers were measured at Mount Holyoke by Professor Helen Leung who had already begun studies on this system. She expanded a mixture of 1% HCCH and 2% N_2O in argon through a General Valve Series 9 nozzle at a backing pressure of 4 – 5 atm. Measurement of the $H^{12}C^{12}CH$•$^{14}N_2O$ spectrum has been reported previously.[2] Spectra of the remaining four isotopomers, $H^{12}C^{12}CH$•$^{15}N_2O$, $H^{13}C^{12}CH$•$^{15}N_2O$, $H^{12}C^{13}CH$•$^{15}N_2O$ and $H^{12}C^{12}CD$•$^{15}N_2O$ were measured at the University of Michigan under the conditions described in Chapter I. All the isotopic species were measured using enriched samples. $^{15}N_2O$ (99% ^{15}N) was obtained from Isotec; $H^{12}C^{13}CH$ (99.2% ^{13}C) was obtained from CDN Isotopes; HCCD (98.9% D) was

Reproduced with permission of the copyright owner. Further reproduction prohibited without permission.

Table VI.1. Spectroscopic constants for $HCCH{\bullet}N_2O$ and the five assigned isotopomers (in MHz unless otherwise noted).

	$H^{12}C^{12}CH{\bullet}^{14}N_2O$ [a]	$H^{12}C^{12}CH{\bullet}^{15}N_2O$	$H^{13}C^{12}CH{\bullet}^{15}N_2O$
A	9394.26826(22)	9153.3378(12)	9097.5293(37)
B	2831.85640(8)	2786.8284(7)	2718.3913(18)
C	2168.07804(7)	2128.7172(6)	2089.6146(14)
D_J	0.012290(3)	0.011778(17)	0.011450(51)
D_{JK}	0.056768(40)	0.05545(14)	0.05217(45)
D_K	—[b]	—[b]	—[b]
d_1	–0.003365(2)	–0.003232(24)	–0.003135(36)
d_2	–0.000727(10)	–0.00060(10)	–0.000727[e]
N[c]	15	12	11
$\Delta\nu_{rms}$ / kHz[d]	0.832	1.00	3.24

	$H^{12}C^{13}CH{\bullet}^{15}N_2O$	$H^{12}C^{12}CH{\bullet}^{15}N^{14}NO$[f]	$H^{12}C^{12}CD{\bullet}^{15}N_2O$[g]
A	9095.9382(42)	9153.47455(15)	8739.4775(32)
B	2725.1120(20)	2808.76903(6)	2734.3984(15)
C	2089.4814(16)	2141.50685(5)	2075.3275(12)
D_J	0.011325(58)	0.0120267(15)	0.011133(80)
D_{JK}	0.05448(51)	0.0558972(76)	0.05672(42)
D_K	—[b]	–0.060972(39)	—[b]
d_1	–0.003041(40)	–0.0033240(6)	–0.003092(12)
d_2	–0.000727[e]	–0.0007028(5)	–0.000727[e]
N[c]	11	22	11
$\Delta\nu_{rms}$ / kHz[d]	3.68	0.227	2.81

[a] Data from Reference 2. Fit of 121 hyperfine components from 15 rotational transitions.
[b] D_K was fixed at zero, because it was not well determined.
[c] N = number of rotational transitions in the fit.
[d] see Table II.1 for definition of $\Delta\nu_{rms}$.
[e] Fixed at value from normal isotopomer.
[f] Fit of center frequencies of 22 rotational transitions.
[g] Fit of center frequencies of 11 rotational transitions.

obtained from CDN, and $^{15}N^{14}NO$ (98% ^{15}N) was obtained from Cambridge Isotopes.

Reproduced with permission of the copyright owner. Further reproduction prohibited without permission.

The Mount Holyoke nozzle was aligned parallel to the direction of microwave propagation, while the Michigan nozzle was perpendicular to the spectrometer cavity, except for the HCCD•$^{15}N_2O$ isotopomer, for which a parallel arrangement was used. This alignment improved the spectral resolution, facilitating the assignment of nuclear quadrupole hyperfine structure due to the deuterium nucleus. Line widths from the parallel nozzle were 6 – 7 kHz full width at half maximum (FWHM), while the perpendicular nozzle gave FWHM values of about 30 kHz. A typical transition of the normal isotopomer required 10,000 gas pulses to obtain a reasonable signal-to-noise ratio (S/N). Transitions of the $^{15}N_2O$ isotopomers were much stronger due to the lack of hyperfine structure from the quadrupolar ^{14}N nuclei. 200 shots were required to give a S/N of about 20 for the *b*-type transitions of the $H^{12}C^{12}CH•^{15}N_2O$ isotopomer. Since two isotopic species were present in the $H^{12}C^{13}CH$ sample mixture ($H^{13}C^{12}CH•^{15}N_2O$ and $H^{12}C^{13}CH•^{15}N_2O$), there was a decrease in signal intensity. The $H^{12}C^{13}CH$ transitions required about 1000 gas pulses to obtain a S/N of around 5, and the HCCD transitions had similar intensity. The HCCD•$^{15}N_2O$ isotopomer with D close to the oxygen was assigned. The isotopomer with the D at the nitrogen end of the N_2O was weaker, presumably due to an isotope effect, and not assigned. The *a*-type transitions of all species were considerably weaker due to the very small *a*-component of the dipole moment.

Results

A. Spectra

Spectral data for the HCCH•N_2O complex and results based on an analysis of the nuclear quadrupole hyperfine structure of the normal species have been published previously.[2, 3] For the normal isotopomer, 6 *a*-type and 9 *b*-type transitions were

Reproduced with permission of the copyright owner. Further reproduction prohibited without permission.

measured, while 4 *a*-type and 8 *b*-type transitions were measured for HCCH•$^{15}N_2O$, and 4 *a*-type and 7 *b*-type transitions were measured for each of the $H^{12}C^{13}CH$ isotopomers and the HCCD isotopomer. 9 *a*-type and 13 *b*-type transitions were measured for HCCH•$^{15}N^{14}NO$. The spectra were fit to Watson's S-reduction Hamiltonian in the I^r representation.[18] The spectroscopic constants for all the isotopomers are given in Table VII.1. For most of the isotopes, D_K was not well determined, so it was fixed at a value of zero. For the $H^{13}C^{12}CH$ species and HCCD species, d_2 was not well determined, and it was fixed at the value of d_2 from the normal isotope. The nuclear quadrupole hyperfine structure of the normal species has been analyzed previously,[2] and the hyperfine structure of $H^{12}C^{12}CH$•$^{15}N^{14}NO$ and $H^{12}C^{12}CD$•$^{15}N_2O$ will be treated in future work from the Mount Holyoke group. For the current study, center frequencies after preliminary analysis of the quadrupole splittings of the $H^{12}C^{12}CH$•$^{15}N^{14}NO$ and $H^{12}C^{12}CD$•$^{15}N_2O$ transitions were fit to obtain rotational constants. The frequencies of all the transitions measured in the current study, including unsplit center frequencies for $H^{12}C^{12}CH$•$^{15}N^{14}NO$ and $H^{12}C^{12}CD$•$^{15}N_2O$ are listed in Appendix E. The transition frequencies of the normal isotopomer are given in Reference 2.

B. Dipole Moment

The dipole moment of the HCCH•$^{15}N_2O$ isotopomer was measured. The small dipole moment components and small Stark coefficients combined to give very small shifts in the transition frequencies. At the largest fields, the shifts were 200 – 300 kHz. Data were obtained on 1 component each from 7 transitions, and a least-squares fit of the measured Stark coefficients led to dipole moment components of $\mu_a = 0.0915(7)$ D and $\mu_b = 0.1503(19)$ D, with $\mu_{tot} = 0.1759(16)$ D. The dipole moment data are summarized in Tables VI.2 and VI.3. Projection of the N_2O dipole moment (0.16083 D[19]) onto the principal axes of the complex predicts a pure *b*-type spectrum for HCCH•N_2O (Table

Reproduced with permission of the copyright owner. Further reproduction prohibited without permission.

Table VI.2. Observed and calculated Stark coefficients for $HCCH\bullet{}^{15}N_2O$.

$J'_{Ka'Kc'}$	$J''_{Ka''Kc''}$	$\|M\|$	Observed[a]	Calculated[a]
2_{11}	2_{02}	2	0.585	0.569
3_{12}	3_{03}	3	0.394	0.409
2_{11}	1_{10}	1	–0.901	–0.889
2_{12}	1_{11}	1	0.900	0.906
2_{02}	1_{01}	1	0.317	0.304
1_{10}	1_{01}	1	1.247	1.252
1_{11}	0_{00}	0	0.250	0.272

[a] Units of 10^{-6} MHz•cm^2•V^{-2}. The calculated coefficients were obtained with the constants in Table VI.1 and dipole components in Table VI.3.

VI.3, column 2), since the μ_a projection is too small to cause observable transitions. Hence, the presence of *a*-type transitions in the measured spectrum indicates an induced dipole along the *a*-axis. Measurement of both *a*- and *b*-components of the dipole moment confirms this. These results for $HCCH\bullet N_2O$ are consistent with the results for the isoelectronic complex $HCCH\bullet CO_2$, where the dipole moment of 0.161 D is due entirely to induction effects.[5] Calculations using the semi-empirical model described in Chapter VII predict only the *b*-component of the dipole moment of $HCCH\bullet N_2O$ when induction is omitted from the calculation, but when distributed polarizabilities are included an *a*-component close to the experimental value is predicted. These dipole moment results are summarized in Table VI.3 for comparison with experiment and will be analyzed further in the Discussion.

Reproduced with permission of the copyright owner. Further reproduction prohibited without permission.

Table VI.3. Dipole moment components for HCCH•N_2O from experiment and semi-empirical modeling (in D).

	Expt [a]	Expt. Proj. [b]	ORIENT (no induction, K = 1.225 mE_h)	ORIENT (induction K = 1.35 mE_h) [c]	ORIENT (Dist. Pol., K = 1.28 mE_h) [d]
μ_a	0.0915(7)	0.01	0.01	0.29	0.09
μ_b	0.150(2)	0.16	0.69	0.70	0.66
μ_{tot}	0.176(2)	0.16	0.69	0.76	0.67

[a] Measured dipole moment components for HCCH•$^{15}N_2O$.
[a] Projection of monomer dipole moment onto principal axes of experimental structure.
[b] Induction included in calculation via monomer polarizabilities.
[c] Induction included in calculation via distributed polarizabilities.

C. Structure

The spectra of the six assigned isotopic species provided 18 moments of inertia with which to determine three structural parameters. These parameters are the N2-M4-M9 and M4-M9-C7 angles and the M4-M9 (center of mass) distance, using the numbering scheme shown in Figure VI.1. The moments of inertia of the normal species lead to a planar moment ($P_{cc} = 0.5(I_a + I_b - I_c)$) of –0.421 amu•Å^2. This small negative number indicates that the complex is planar and relatively rigid. A fit of the structural parameters to all the moments of inertia leads to a large standard deviation because of the inertial defect ($\Delta = I_c - I_a - I_b = -1/2(P_{cc})$). This parameter should be zero, since $I_c = I_a + I_b$, but in practice it has a small positive value due to out-of-plane motions in the complex. For this reason, only I_a and I_b for each isotope were included in the inertial fit.

Reproduced with permission of the copyright owner. Further reproduction prohibited without permission.

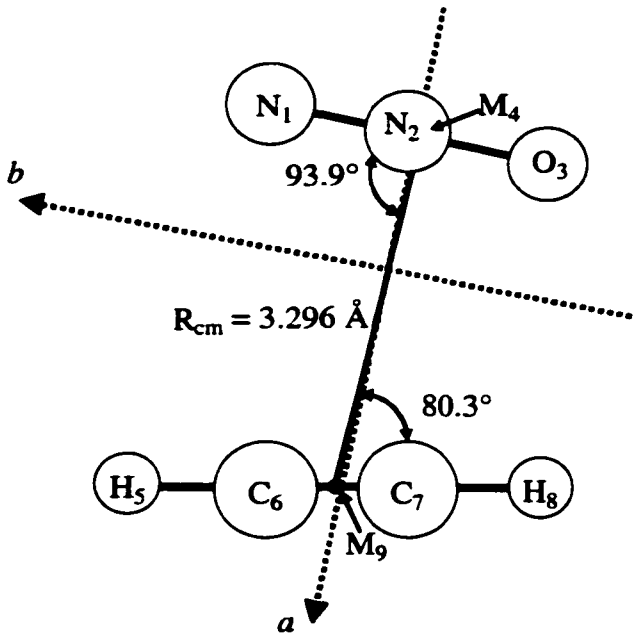


Figure VI.1. Structure of HCCH-N_2O showing fitted angles and atom numbering scheme. M_4 and M_9 are the centers of mass of the two monomers.

This led to a structure determination with a ΔI_{rms} of 0.107 amu•Å^2 and with $\theta_{N2\text{-}M4\text{-}M9}$ = 93.9(5)°, $\theta_{M4\text{-}M9\text{-}C7}$ = 80.3(8)° and R_{cm} = 3.2961(8) Å.* As in the previous chapters, this is an effective ground state structure, and R_{cm} should be within 0.05 Å and the angles within 5° of the equilibrium values. The structural parameters are summarized in Table VI.4. It was assumed that the monomer structures would remain unchanged from their uncomplexed values ($R_{N\text{-}O}$ = 1.191 Å, $R_{N\text{-}N}$ = 1.126 Å[20] and $R_{C\text{-}H}$ = 1.061 Å, $R_{C\text{-}C}$ = 1.203 Å[21]).

The assignment of the new isotopic species allowed the determination of Kraitchman substitution coordinates for both of the nitrogen atoms, both of the carbon atoms and one hydrogen atom in the complex.[22] The absolute values of the Kraitchman

---

* Fits of I_a and I_c gave comparable ΔI_{rms} and $\theta_{N2\text{-}M4\text{-}M9}$ = 94.3(6)°, $\theta_{M4\text{-}M9\text{-}C7}$ = 80.9(9)° and R_{cm} = 3.3033(6) Å. The values from the fit of I_a and I_b are slightly preferred since ΔI_{rms} is marginally smaller. Fits of I_b and I_c would not converge.

Reproduced with permission of the copyright owner. Further reproduction prohibited without permission.

coordinates are given in Table VI.5 which also shows the principal axis coordinates of the structure obtained from the inertial fit. The coordinates of atoms H8, C6, C7 and N2 were obtained by treating the $H^{13}C^{12}CH\bullet^{15}N_2O$, $H^{12}C^{13}CH\bullet^{15}N_2O$, $H^{12}C^{12}CH\bullet^{15}N^{14}NO$ and $H^{12}C^{12}CD\bullet^{15}N_2O$ species as single substitutions of the $H^{12}C^{12}CH\bullet^{15}N_2O$ isotope. The coordinates of atom N1 were determined from $H^{12}C^{12}CH\bullet^{15}N^{14}NO$ and the normal isotopomer. The substitution coordinates are obtained in the principal axis system of the parent species, so it was necessary to transform the coordinates of atoms N2, C6, C7 and H8 to the principal axis system of normal $HCCH\bullet N_2O$ before comparisons could be made. The transformed coordinates are shown in Table VI.5. The only coordinate that differs significantly from the inertial fit value is *a* for atom N1. The substitution and inertial fit structures disagree by 0.094 Å for this coordinate.

A two parameter fit holding the HCCH and N_2O units parallel was also explored.

Table VI.4. Structural parameters for the $HCCH\bullet N_2O$ complex. See Figure VI.1 for the atom numbers.

	Expt [a]	Previous Experimental Structure [b]	Muenter Model [c]
M_4-M_9/Å	3.2961(8)	3.305	3.31
N_2-M_4-M_9/°	93.9(5)	90.0	91
M_4-M_9-C_7/°	80.3(8)	90.0	90
A/MHz	9394.2683	9281.2	9387(1)
B/MHz	2831.8564	2829.9	2829.6(3)
C/MHz	2168.0780	2168.7	2166.6(2)

[a] The quality of the fit was $\Delta I_{rms} = 0.107$ amu•Å^2 where $\Delta I_x = I_x$ (obs) $- I_x$ (calc).
[b] Reference 2. The distance is an average distance while the angles are taken to be equilibrium values. Rotational constants were calculated from structural parameters with monomer structures from refs. 20 and 21.
[c] References 1 and 4.

Reproduced with permission of the copyright owner. Further reproduction prohibited without permission.

R_{cm} and $\theta_{N2\text{-}M4\text{-}M9}$ were varied while holding $\theta_{M4\text{-}M9\text{-}C7}$ equal to $\theta_{N2\text{-}M4\text{-}M9}$ (see Figure

Table VI.5. Principal axis coordinates for $HCCH{\bullet}N_2O$ for tilted structure (I) and parallel structure (II).[a] Kraitchman coordinates[b] are given in brackets.

	a / Å		*b* / Å	
	I	II	I	II
N_1	−1.311	−1.056	1.194	1.241
	[1.217]		[1.209]	
N_2	−1.230	−1.214	0.071	0.126
	[1.218]		[0.065]	
O_3	−1.145	−1.382	−1.117	−1.053
M_4	−1.225	−1.225	−0.004	0.052
H_5	2.346	2.306	1.646	1.557
C_6	2.171	2.156	0.600	0.507
	[2.117]		[0.586]	
C_7	1.972	1.987	−0.587	−0.684
	[1.992]		[0.612]	
H_8	1.796	1.837	−1.633	−1.734
	[1.798]		[1.653]	
M_9	2.071	2.071	0.006	−0.089

[a] Structures I and II were obtained from least squares fitting I_a and I_b for the six isotopes. See text.
[b] Coordinates calculated using Kraitchman equations (ref. 22).

VI.1). The best least-squares fit to I_a and I_b for the six isotopic species gave R_{cm} =

Reproduced with permission of the copyright owner. Further reproduction prohibited without permission.

3.29924(66) Å and $\theta_{N2\text{-}M4\text{-}M9}$ = 84.35(23)°. The quality of the fit (ΔI_{rms} = 0.132 amu•Å^2) was poorer than for the tilted structure fits. A comparison of the Cartesian coordinates from this fit and the Kraitchman coordinates is given in Table VI.5. Although ΔI_{rms} is not substantially different for this structure, the Cartesian coordinates are in overall poorer agreement with the Kraitchman calculated values compared to the tilted configuration. This leads to a preference for the tilted structure as the best fit to the isotopic shift data; however, the overall comparisons of ΔI_{rms} and the Kraitchman coordinates are not unequivocally compelling, so the parallel structure cannot be definitively eliminated. Large amplitude vibrational effects on the moments of inertia contribute a residual ambiguity in the interpretation of the isotope shift data.

The substitution coordinates can be used to calculate the N-N and C-C distances and the C7-H8 distance in N_2O and HCCH. This calculation gives an N-N distance of 1.144 Å, a C-C distance of 1.205 Å and a C7-H8 distance of 1.059 Å. These differ by about 0.02 Å, 0.002 Å and 0.002 Å, respectively, from the monomer values. This is reasonable agreement given that large amplitude effects on the rotational constants have not been taken into account.

Discussion

The data from six isotopomers of HCCH•N_2O have allowed a full determination of the structure of the complex. The inertial fit, supported by substitution coordinates for five atoms, indicates that the two molecules deviate from a parallel configuration by 13.6°. The oxygen of the N_2O inclines towards the acetylene molecule. Semi-empirical modeling using the ORIENT program[23] described in the next chapter gives structures in good agreement with these results[10] which are in contrast to earlier studies of HCCH•N_2O which proposed a parallel or nearly parallel structure.[1-3] These studies used a different semi-empirical model, developed by Muenter, to model the HCCH•N_2O system.[1,4] This

Reproduced with permission of the copyright owner. Further reproduction prohibited without permission.

model was in agreement with the parallel structure that had been proposed. The two semi-empirical models differ in the form of the dispersion-repulsion terms that are used and also in the distributed multipole moments which were employed. These differences and the results from theoretical calculations will be discussed further in Chapter VII.

Results from the current work indicate that the addition of induction to a calculation has little effect on the predicted structures, but the inclusion of induction does become important in the prediction of dipole moment components. Examination of Table VI.3 shows that the projection of the N_2O dipole moment onto the principal axes of the complex leads to a very small μ_a (~0.01 D). The experimentally determined dipole moment gave $\mu_a = 0.09$ D, however, indicating that there is an induced dipole along the *a*-axis of the complex. This axis, as shown in Figure VI.1, connects the slightly positive central nitrogen of N_2O to the π-system of the acetylene triple bond and a fair amount of induction from this quadrupole-quadrupole interaction is not surprising. Semi-empirical predictions reflect this induced moment. Comparison of dipole moment predictions for different calculations should be made with some caution, though. It has been shown that the dipole moment of N_2O is very sensitive to the level of calculation used to compute it,[24] and examination of changes in dipole moment components, indicating the direction in which induced moments occur, is presumably more reliable than examination of the magnitude of the dipole moment components. The semi-empirical calculation that neglected induction led to a very small μ_a component, just as was predicted by projection of the N_2O dipole onto the experimental structure, but when induction was added to the calculation, μ_a was predicted to be significant. While the calculation that used point polarizabilities over estimated the size of the induced dipole ($\mu_a \sim 0.29$ D), the distributed polarizability calculation predicted a value ($\mu_a \sim 0.09$ D) very close to the experimental one. This quantitative agreement is probably fortuitous, since *ab initio* dipole moment calculations usually differ significantly from experimental ones, and μ_b and the dipole moment of N_2O are both over estimated by a large amount in the present calculations.

Reproduced with permission of the copyright owner. Further reproduction prohibited without permission.

Summary

The structure and dipole moment of the acetylene-nitrous oxide complex have been determined. The addition of isotopic data to the existing microwave data on the normal species allowed a fit of the three structural parameters to 12 moments of inertia, and substitution coordinates for five atoms were also obtained. Both the inertial fit data and the substitution coordinates indicate a structure in which the oxygen of the N_2O inclines toward the acetylene with an angle between the monomers of 13.6°. This structure agrees well with that predicted using the semi-empirical model described in the next chapter. The change in the predicted μ_a dipole moment upon addition of induction to the calculation was in the direction expected based on the experimental results.

The slightly tilted N_2O structure determined in this work differs from the prediction from an interaction model described by Muenter and previously used on the $(HCCH)_2$, $HCCH{\bullet}CO_2$ and $(CO_2)_2$ complexes.[1,4] Semi-empirical and *ab initio* calculations will be described further in Chapter VII.

The ORIENT semi-empirical model and the Muenter model are quite simplistic, and close agreement (or disagreement) with experimental details should not be considered profoundly significant. Furthermore, the difference between the parallel and tilted structures is quite small and subtle. Given the non-rigidity of such complexes, a rigorous determination of the equilibrium structure must await further experimental and theoretical developments. Equilibrium configurations much closer to parallel cannot be completely eliminated with the present data.

Reproduced with permission of the copyright owner. Further reproduction prohibited without permission.

References for Chapter VI

[1] T. A. Hu, L. H. Sun and J. S. Muenter, J. Chem. Phys. **95**, 1537 (1991).

[2] H. O. Leung, J. Chem. Phys. **107**, 2232 (1997).

[3] H. O. Leung, Chem. Comm. **22**, 2525 (1996).

[4] J. S. Muenter, J. Chem. Phys. **94**, 2781 (1991).

[5] J. S. Muenter, J. Chem. Phys. **90**, 4048 (1989).

[6] D. G. Prichard, R. N. Nandi, J. S. Muenter and B. J. Howard, J. Chem. Phys. **89**, 1245 (1988).

[7] R. A. Peebles and R. L. Kuczkowski, J. Phys. Chem. **103**, 6344 (1999).

[8] R. A. Peebles, S. A. Peebles and R. L. Kuczkowski, Mol. Phys. **96**, 1355 (1999).

[9] R. A. Peebles and R. L. Kuczkowski, J. Chem. Phys. **112**, 8839 (2000).

[10] S. A. Peebles and R. L. Kuczkowski, J. Phys. Chem. **103**, 3884 (1999).

[11] S. A. Peebles and R. L. Kuczkowski, Chem. Phys. Lett. **308**, 21 (1999).

[12] P. A. Block, M. D. Marshall, L. G. Pedersen and R. E. Miller, J. Chem. Phys. **96**, 7321 (1992).

[13] K. I. Peterson and W. J. Klemperer, J. Chem. Phys. **80**, 2439 (1984).

[14] D. Zolandz, D. Yaron, K. I. Peterson and W. Klemperer, J. Chem Phys. **97**, 2861 (1992).

[15] T. J. Balle and W. H. Flygare, Rev. Sci. Instrum. **52**, 33 (1981).

[16] H. O. Leung, D. Gangwani and J.-U. Grabow, J. Mol. Spectrosc. **184**, 106 (1997).

[17] K. W. Hillig, II, J. Matos, A. Scioly and R. L. Kuczkowski, Chem. Phys. Lett. **133**, 359 (1987).

[18] W. Gordy and R. L. Cook, *Microwave Molecular Spectra, Third Edition*; New York: John Wiley & Sons (1984), Chapter 8 and references therein.

[19] L. H. Scharper, J. S. Muenter and V. W. Laurie, J. Chem. Phys. **53**, 2513 (1970).

[20] D. K. Coles, E. S. Elyash and U. J. G. Gorman, Phys. Rev. **72**, 9732 (1947).

Reproduced with permission of the copyright owner. Further reproduction prohibited without permission.

[21] M. D. Harmony, V. W. Laurie, R. L. Kuczkowski, R. H. Schwendeman, D. A. Ramsay, F. J. Lovas, W. J. Lafferty and A. G. Maki, J. Phys. Chem. Ref. Data **8**, 619 (1979).

[22] J. Kraitchman, Am. J. Phys. **21**, 17 (1953).

[23] A. J. Stone, A. Dullweber, M. P. Hodges, P. L. A. Popelier and D. J. Wales, *ORIENT: A program for studying interactions between molecules, Version 3.2*, University of Cambridge (1995).

[24] K. Mogi, T. Komine and K. Hirao, J. Chem. Phys. **95**, 8999 (1991).

Reproduced with permission of the copyright owner. Further reproduction prohibited without permission.

CHAPTER VII

SEMI-EMPIRICAL AND *AB INITIO* MODELING OF WEAKLY BOUND DIMERS AND TRIMERS

Introduction

The preceding chapters describe the use of microwave spectroscopy to determine the structures of several small weakly bound complexes. Dimer and trimer species are of interest for several reasons, including their atmospheric significance, the insight that they can give about reaction mechanisms,[1,2] and as models for biological systems. The most important and directly applicable reason to study these complexes, though, is to gain a better understanding of intermolecular forces on a basic level. Comprehension of how the forces between molecules balance in the stable structural forms of van der Waals complexes comes in several ways. Direct examination of experimental structures combined with a certain amount of chemical intuition often makes it possible to recognize what type of force governs a particular interaction. Examination of a series of related complexes can then lead to further insight into how intermolecular forces vary in relation to certain molecular properties. Experimental structures can also be used as a means to test and develop theoretical interaction models. This is the aspect of the study of van der Waals molecules which will be discussed in this chapter. A theoretical model which consistently predicts experimental structures closely is likely to be useful on many different systems, but if a certain type of system is consistently predicted incorrectly, there is a flaw in the model. This indicates an incomplete understanding of the intermolecular forces present and the need for modifications. This chapter will examine

Reproduced with permission of the copyright owner. Further reproduction prohibited without permission.

the complexes that were discussed in Chapters II – VI by comparing experimental configurations with those predicted by a semi-empirical interaction model. Some *ab initio* calculations will also be examined. It is hoped that this will lead to insight into the general strengths and weaknesses of the models employed.

Theoretical Methods

A. Semi-empirical Calculations Using the ORIENT Model

This chapter will present extensive results from the semi-empirical model that is implemented in the ORIENT program.[3] A description of the program, which has the capability to represent electrostatic, dispersion, repulsion and induction interactions by combining *ab initio* and experimental results, is given below. A more detailed explanation of the different aspects of the interaction model can be found in a recent book by Stone.[4]

The model represents the electrostatic interactions in a complex with distributed multipole moments (DMMs). These series of point multipoles (charge, dipole, ...) are placed on each atom and sometimes at bond centers or other locations in a monomer. They are calculated using the CADPAC suite of *ab initio* programs[5] with a TZ2P basis set at the SCF level. The moments are calculated through hexadecapoles, and the monomer is fixed at its experimental structure. A sum of the interactions of the point multipoles on each atom with those on each atom on the other monomers then gives the electrostatic interaction energy for the complex.

The atom-atom dispersion and repulsion terms originate with experimental results. The form of the interaction is given by Equation (VII.1)

$$U_{\exp-6} = \sum_{i,j} K \exp\left[-\alpha_{ij}\left(R_{ij} - \rho_{ij}\right)\right] - \frac{C_6^{ij}}{R_{ij}^6} \qquad \text{(VII.1)}$$

Reproduced with permission of the copyright owner. Further reproduction prohibited without permission.

The α, ρ and C_6 terms have been determined by Mirsky,[6] and are listed in Table 11.2 of Reference 4. The pre-exponential factor K is a convenient energy unit which is adjusted to give good reproduction of intermolecular distances. The default value is 0.001 E_h (219.474 cm^{-1}), which frequently underestimates intermolecular distances slightly. The term α describes the hardness of the repulsion. A very large value of α (~25 a_0^{-1}) gives an essentially hard sphere repulsion; typical values are closer to 5 a_0^{-1}. The term ρ is related to the size of the atom, and C_6 is a constant related to the dispersion interaction. These parameters have also been determined by Spackman,[7] but his tabulation is less successful than the Mirsky parameters when used with the ORIENT model.[8]

The contribution of induction to the intermolecular interaction energy can be modeled in two ways. In the simpler method, experimental molecular polarizabilities are placed at the center of mass of each monomer. Then an iterative procedure is carried out, where the induced dipole on one monomer due to the electrostatic charge distribution of the other is calculated and vice versa until convergence is achieved. The more complex method uses a similar iterative procedure, but instead of point polarizabilities it uses distributed polarizabilities. These are similar to the DMMs that are used for the electrostatic charge distribution in that they place point polarizabilities at atom centers and occasionally bond centers, and a similar sum over the atoms in the complex is necessary. Distributed polarizabilities are computed with the CADPAC program at the same level of calculation as the DMMs.

B. *Ab initio* Calculations

Ab initio calculations use purely theoretical data to examine the interactions within and between molecules. Groups of mathematical functions called basis sets are used to model molecules by representing the electron orbitals. Molecular properties are then determined by performing further calculations. In the case of the complexes

Reproduced with permission of the copyright owner. Further reproduction prohibited without permission.

discussed here, the positions of the monomers were varied until a minimum energy configuration was attained. Several different levels of calculation were carried out. The simplest computations are at the Hartree-Fock (HF) level (also referred to as Self-consistent field or SCF). This type of calculation assumes that there is no correlation between the electrons' positions; however, this is frequently a poor assumption for van der Waals complexes, since their structures can depend heavily (via dispersion interactions) on electron correlation. More complicated calculations use second order Möller-Plessett perturbation theory (MP2 calculations) to account for electron correlation. These computations are much larger than simple SCF ones, so they can be very time consuming. A method that can give results fairly close in quality to MP2 calculations, but with much shorter computation times, is density functional theory (DFT). This relatively new method uses functionals (functions of functions) in a calculation to include information on electron correlation and other properties. The Gaussian 94 *ab initio* program was used for all of the computations.[9]

Most calculations were performed with the medium sized 6-31G* basis set which limits them to a reasonable length but also accounts for polarization in the molecules. As with electron correlation, polarization can be important for obtaining accurate structural predictions. Addition of diffuse functions to the basis set lengthened calculation times considerably while lending no improvement to the results. Larger basis sets, such as cc-pVDZ which is designed for problems where electron correlation is significant, led to little improvement over the 6-31G* results, while extending computation times considerably.

Many previous *ab initio* studies of van der Waals complexes exist, but these tend to focus on very large calculations that are beyond the capabilities of a mainly experimental researcher. These "professional" calculations typically use MP2, MP4 or coupled cluster methods and cc-PVDZ or larger basis sets with many polarization functions. The results are typically relatively accurate.[10, 11, 12] In this work, the goal was

Reproduced with permission of the copyright owner. Further reproduction prohibited without permission.

to determine whether reasonable results are available from smaller, more accessible calculations. Many researchers have used smaller calculations for rationalization purposes, but are they suitable for structure prediction, as well?

OCS Trimer Calculations

The OCS trimer is an example of a homo-molecular trimer of linear triatomic

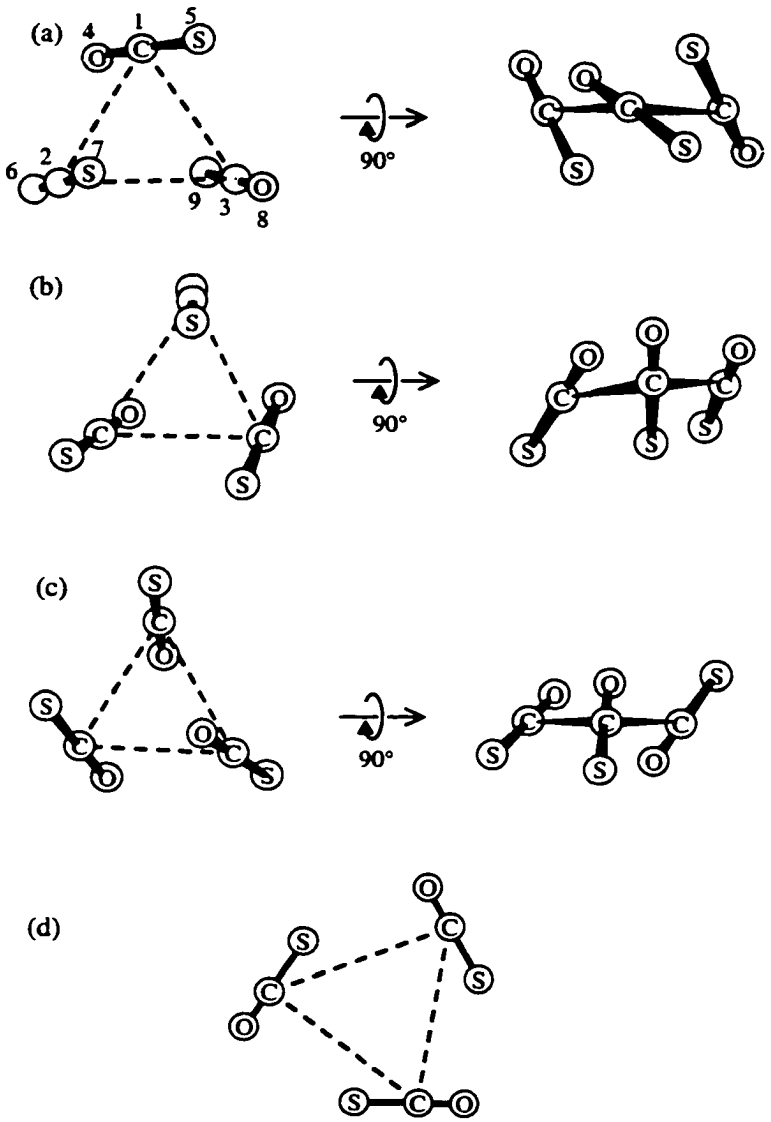


Figure VII.1. The four OCS trimer structures obtained with the ORIENT modeling program using the default value of K and distributed multipole moments only at atom centers. (a) E = –0.00760 E_h, (b) E = –0.00712 E_h, (c) E = –0.00689 E_h, (d) E = –0.00517 E_h. The same comments as in Figure II.1 apply to the viewing perspectives except that the three OCS molecules are no longer nearly parallel to the plane of the page in the right side view.

Reproduced with permission of the copyright owner. Further reproduction prohibited without permission.

monomers. The system was studied because of its relative simplicity and to resolve the structural ambiguity in the results of the original study by Connelly and coworkers.[13] Their study examined the rotational spectrum of only the normal isotopomer, and two structures were proposed that were consistent with the spectroscopic data (similar to Figs. VII.1 (a) and (b)). The semi-empirical model of Muenter, described later in this chapter, was used to determine these structures which will be referred to as parallel, (b), and antiparallel, (a). The experimental work described in Chapter II aimed to distinguish between the two structural forms, and the first step in the process was to perform semi-empirical calculations similar to Connelly's but using the ORIENT model. The previous report[1] predicted that the anti-parallel configuration was of lower energy and, thus, the more likely of the two possibilities. Calculations with ORIENT also favored the anti-parallel configuration, although they gave slightly different structural parameters.

Initially, DMMs were calculated only at the atom centers in the OCS molecule (Appendix F), and structure optimizations using these DMMs led to four minima (Figure VII.1). The lowest energy structure (VII.1(a)) corresponds to the anti-parallel arrangement of molecules that has been confirmed experimentally (E = –0.00760 E_h). The next lowest energy structure (VII.1(b)) has a parallel barrel-shaped arrangement (E = –0.00712 E_h) which roughly agrees with the parallel structure also proposed by Connelly, *et al.* The next higher energy structure (VII.1(c)) again has an anti-parallel arrangement of monomers (E = –0.00689 E_h), but in this structure the oxygen atom of one OCS is opposite the carbon atom of the second OCS. The fourth structure has the highest energy (E = –0.00517 E_h) and is a planar cyclic configuration (VII.1(d)) with the carbon atoms arranged in an equilateral triangle.

To test the sensitivity of the calculations to the DMMs, a new set of DMMs that included additional multipoles located at the bond centers of the OCS molecules was calculated (Appendix F). Again, four structures were found, and they differed little from those predicted without bond centers. The structural parameters of the minimum energy

Reproduced with permission of the copyright owner. Further reproduction prohibited without permission.

anti-parallel arrangement of molecules are given for the calculations with and without

Table VII.1. Comparison of predicted structural parameters (units of Å or degree) for $(OCS)_3$ [Structure in Fig. VII.1(a)].

	DMMs at Atom Centers [a]	DMMs at Atom and Bond Centers [a]	DMMs Ref [13] [b]	DMMs Atom Centers, K = 0.00083 E_h [a]	Muenter Model [c]
C1-C2 [d]	3.653	3.658	3.685	3.544	3.816
C1-C3	3.731	3.694	3.692	3.621	3.778
C2-C3	3.908	3.853	3.811	3.802	3.891
C1-C2-C3	59.0	58.9	59.0	59.0	58.7
C2-C3-C1	57.1	57.9	58.8	57.0	59.7
C3-C1-C2	63.9	63.2	62.2	64.1	61.6
S5-C1-C3	70.8	71.0	73.7	70.3	74.8
S7-C2-C1	71.3	70.5	72.7	70.8	72.7
O8-C3-C2	116.0	115.4	111.3	116.6	110.2
S5-C1-C3-C2	139.9	138.0	133.3	140.6	133.9
S7-C2-C1-C3	72.0	73.5	76.1	71.4	77.5
O8-C3-C2-C1	97.5	97.3	96.4	97.8	96.0
S5-C1-C3-S9	−148.9	−150.7	−152.2	−148.6	−151.0
S7-C2-C1-S5	27.2	27.3	24.5	27.5	25.7
S9-C3-C2-S7	−164.7	−163.5	−165.2	−164.2	−165.1

[a] DMM = distributed multipole moments in Appendix F. $K = 0.001$ in equation (VII.1) unless otherwise noted.
[b] DMMs (with bond centers) from Reference 13, used through hexadecapoles.
[c] DMMs and model from Reference 13.
[d] Atom numbering as in Figure VII.1.

Reproduced with permission of the copyright owner. Further reproduction prohibited without permission.

bond centers in Table VII.1, columns 1 and 2.

A third set of calculations used the DMMs (truncated at the hexadecapole level) that were calculated by Connelly, *et al* and used in their structural predictions.[13] These DMMs also included bond centers. Again, similar minimum energy structures were found, but one of the barrel-like configurations showed noticeable changes from the structure obtained in the first set of calculations. This configuration is comparable to Figure VII.1(c), but the central OCS in the view on the right is shifted up the page to put the sulfur atom between the carbons of the other two OCS molecules. Table VII.1 lists both the Connelly, *et al* lowest energy structural parameters (Muenter model) and those from ORIENT using their DMMs (column 3).

Finally, the sensitivity of the calculation to the pre-exponential factor K was tested. Modeling of OCS dimer with $K = 0.00083\ E_h$ reproduced the experimental C-C distance to within 0.001 Å[14] (see Figure II.2). The OCS trimer optimizations were repeated with this value of K in the hope that a better reproduction of the experimental OCS trimer structure would result. This did not occur, though; the new calculations gave bond lengths considerably shorter than those observed experimentally for the OCS trimer. Again, four minimum energy structures were found which were similar to the configurations observed in the previous calculations, although the C-C distances were much shorter than those obtained with the default value of K (see Table VII.1, column 4). A parallel, polar form of OCS dimer was also predicted with $K = 0.00083\ E_h$. This isomer, which is 0.393 kJ/mol less stable than the known anti-parallel form, is shown in Figure II.2(c). Although the spectrum of the polar OCS dimer has not been assigned in the microwave region, there has been evidence of its existence in other work.[15]

In summary, Table VII.1 indicates a small variance in structural details for the lowest energy conformer of $(OCS)_3$ depending on the DMMs and pre-exponential factor that are used. It is pleasing that all the calculations suggest the same low energy form. Given the simplicity of the model, including the absence of anisotropic effects in the

Reproduced with permission of the copyright owner. Further reproduction prohibited without permission.

dispersion and repulsion terms, and the neglect of polarization, the variation in details is not surprising.

$(CO_2)_2N_2O$ Calculations

Assignment of the $(CO_2)_2N_2O$ spectrum was made significantly less difficult by predicting the structure using the ORIENT model before experimental work began. This approach was previously successful in the assignment of the $(OCS)_2CO_2$ complex.[16] The

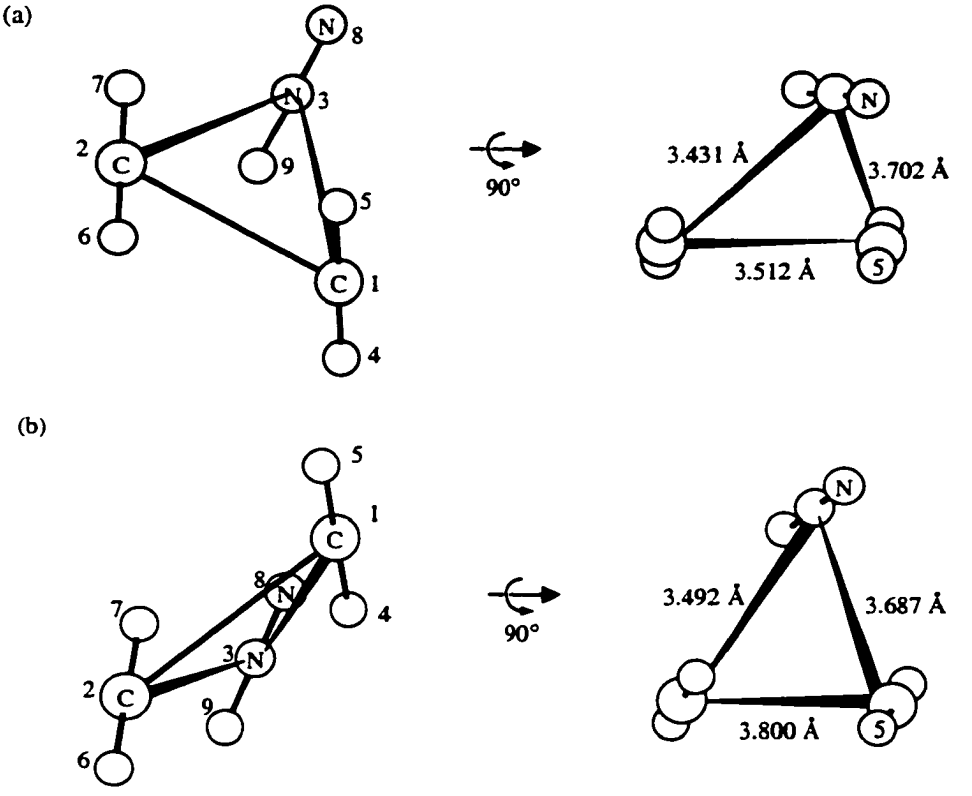


Figure VII.2. Two semi-empirical structures for $(CO_2)_2N_2O$. Structure (a) closely resembles the experimental structure in Fig. III.1(a). See Table VII.2 for energies.

minimum energy structure that emerged from the semi-empirical calculations is shown in Figure VII.2(a), and a slightly higher energy structure is given in VII.2(b). The first configuration clearly resembles the experimental structure [Fig. III.1(a)] very closely.

Reproduced with permission of the copyright owner. Further reproduction prohibited without permission.

The DMMs that were used for the calculation are given in Appendix F. The rotational constants and structural parameters from the predicted configuration are compared with the experimental values in Table VII.2. The similarity is remarkable and much more quantitative than has been observed in similar systems.[16, 17, 18] Only one angle differs from the experiment by greater than 5°. A second configuration for $(CO_2)_2N_2O$ was also predicted with the semi-empirical model. Its parameters are listed in the third column of Table VII.2, and it is shown in Figure VII.2(b). This structure is about 1.27 mE_h less stable than the minimum energy configuration. The major difference between the two structures is a shifting of the N_2O from a position where the oxygen is between the CO_2 carbons in VII.2(a) to a configuration where the central nitrogen of N_2O is between the carbons in VII.2(b). Comparison of the predicted rotational constants for the two structures shows that, while *B* and *C* for the lower energy configuration are very close to the experimental values, *A* is better reproduced by the less favorable structure. The other rotational constants for this second structure are not in such close agreement with experiment, though, and this can be used as further evidence that the configuration is not a good reproduction of the experimental structure.

Ab initio calculations were also used to model $(CO_2)_2N_2O$. Computations were carried out at the HF level and using density functional theory (DFT). A 6-31G* basis set was used. Attempts at fixing the monomer structures at their experimental geometries in this and the following sections led to difficulty obtaining converged structures, so these were full optimizations; however, the changes in the monomer structures were small, so comparisons with experiment should remain valid. The resulting structural parameters are given in the last two columns of Table VII.2. Both the HF and DFT calculations are in reasonable agreement with experiment, with the DFT results appearing to be slightly preferable. The most noticeable problem with the predictions is the relatively large over-estimation of the intermolecular distances. Both levels of computation give values that are 0.1 – 0.3 Å longer than the experimental values, while the angles are in good

Reproduced with permission of the copyright owner. Further reproduction prohibited without permission.

agreement with both the experimental and semi-empirical results. The large errors in the distances lead to a relatively large discrepancy between the predicted and experimental rotational constants, making the *ab initio* results less likely to be a useful tool for assigning unknown spectra.

These *ab initio* structure optimizations were started from a geometry similar to the experimental structure, and an extensive search for other local minima on the potential

Table VII.2. Structural parameters and rotational constants for the experimental and two semi-empirical structures of $(CO_2)_2N_2O$ (in Å and degrees).

	Expt.	ORIENT -8.0500 mE_h	ORIENT -6.7845 mE_h	SCF/ 6-31G*	B3LYP/ 6-31G*
$R(C_1\text{-}N_3)$	3.638(8)	3.702	3.687	3.908	3.892
$R(C_2\text{-}N_3)$	3.427(9)	3.431	3.492	3.553	3.554
$R(C_1\text{-}C_2)$	3.521(9)	3.512	3.800	3.678	3.601
$\theta(C_1\text{-}N_3\text{-}C_2)$	59.7(1)	58.9	63.9	58.8	57.6
$\theta(O_7\text{-}C_2\text{-}N_3)$	62.6(39)	62.2	61.1	63.1	62.5
$\theta(O_4\text{-}C_1\text{-}C_2)$	112.9(57)	121.7	61.8	120.4	120.1
$\theta(N_8\text{-}N_3\text{-}C_1)$	123.2(4)	126.9	71.9	128.7	126.4
$\tau(O_7\text{-}C_2\text{-}N_3\text{-}C_1)$	146.2(13)	148.1	52.3	143.4	145.3
$\tau(O_4\text{-}C_1\text{-}C_2\text{-}N_3)$	−113.0(4)	−114.5	−58.4	−108.9	−116.1
$\tau(N_8\text{-}N_3\text{-}C_1\text{-}C_2)$	104.5(3)	107.5	147.6	106.1	105.7
A / MHz	1597.4615	1654.0	1563.1	1540.8	1573.4
B / MHz	1232.9736	1211.5	1153.6	1128.7	1120.5
C / MHz	831.0952	812.3	756.4	758.1	760.8

Reproduced with permission of the copyright owner. Further reproduction prohibited without permission.

energy surface was not performed. The possibility of a planar cyclic configuration was investigated, though, and local minima with this structure were found at both the SCF and DFT levels of calculation. The DFT calculation indicates that the planar configuration is 0.640 mE_h (133 cm^{-1}) less stable than the observed barrel-like structure. It would be interesting to do more comprehensive theoretical calculations on the $(CO_2)_2N_2O$ system to determine what other configurations could be relatively stable; however, these calculations would be quite time consuming and are beyond the scope of the current study.

N_2O•SO_2 Dimer

Theoretical calculations on the N_2O•SO_2 dimer should be particularly interesting because of the experimental difficulties that the tunneling motion in the complex caused. As seen in Chapter IV, this complex has an asymmetric structure, in contrast to the configurations observed for the three similar complexes of CO_2,[19] OCS[20] and CS_2[21] with SO_2. In previous studies, the model in the ORIENT program has had difficulty predicting the structures of other SO_2 complexes,[8] although the dimers with OCS and CS_2 were relatively well reproduced after some adjustments to the default parameters were made.[20]

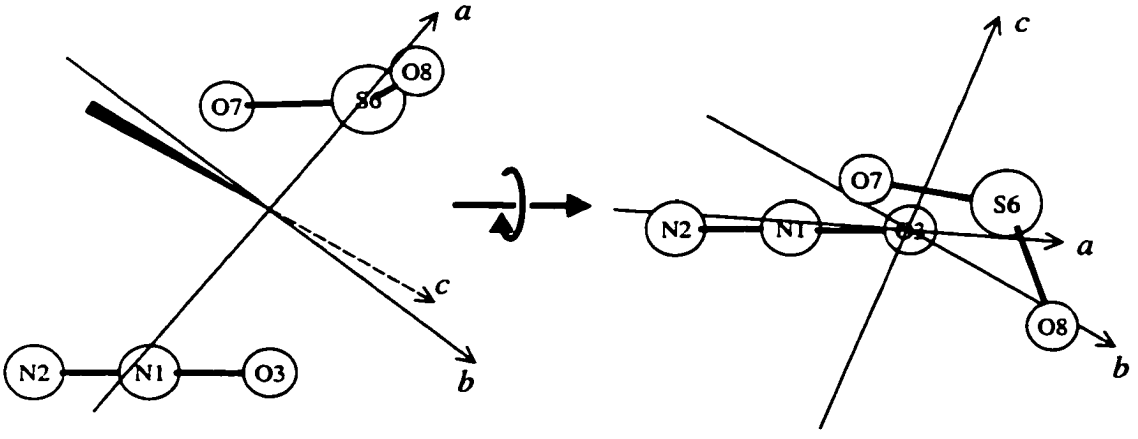


Figure VII.3. The structure predicted by a semi-empirical model for N_2O-SO_2. See Figure IV.3 for an explanation of the orientation of the complex.

Reproduced with permission of the copyright owner. Further reproduction prohibited without permission.

[21] For CO_2-SO_2 the experimental C_{2v} structure could not be reproduced with the ORIENT program.[19] It will be interesting to see how well the N_2O•SO_2 structure is predicted by the semi-empirical model. The DMMs that were used for the calculations are given in Appendix F.

Although a structure with C_1 symmetry was predicted for each of the three other SO_2 complexes, C_s structures were also predicted for each of them. Except in the case of CO_2, the experimental data was consistent with the predicted structures of higher

Table VII.3. Experimental, semi-empirical and *ab initio* structural parameters for N_2O•SO_2.

	Structure I	ORIENT	SCF/ 6-31G*	B3LYP/ 6-31G*	MP2/ 6-31G*	TS (B3LYP)
R_{cm} / Å	3.3306(6)	3.618	3.586	3.621	3.499	3.414
$\theta_{5\text{-}4\text{-}2}$ / °	111.2(10)	118.6	119.9	118.4	114.2	113.1
$\theta_{6\text{-}5\text{-}4}$ / °	156.6(51)	101.3	92.7	91.5	104.3	139.8
$\varphi_{6\text{-}5\text{-}4\text{-}2}$ / °	−158.3(57)	131.4	131.7	129.3	122.4	180.0
$\varphi_{7\text{-}6\text{-}5\text{-}4}$ / °	−115.0(59)	122.8	122.5	125.8	123.8	−90.0

symmetry (Fig. IV.1). The highly symmetric C_{2v} structure consistent with the spectrum for CO_2-SO_2 could not be reproduced with the ORIENT program, except as a transition state. The CO_2-SO_2 spectrum is also consistent with effective C_{2v} symmetry, however, with the complex having a C_s equilibrium structure and large amplitude motions moving the SO_2 over or through a low barrier at the crossed configuration. When the model was applied to the N_2O-SO_2 system, the only structure that could be obtained was one with C_1 symmetry (see Figure VII.3), similar to those obtained for the previous three complexes. The C_s structure was found only as a "solution of wrong index" (a saddle point or

Reproduced with permission of the copyright owner. Further reproduction prohibited without permission.

transition state on the potential energy surface), when it appeared that the structure optimization was converging, but the program stepped away from the structure, since it was not a minimum on the potential energy surface. This second structure was 0.0002 E_h (44 cm^{-1}) higher in energy than the global minimum.

Of the four structures whose parameters are given in Table IV.3, Structures I and II most closely resemble the results of the ORIENT calculation. It should be noted, however, that the similarity is purely qualitative. While the computation predicts that one S-O bond will be nearly parallel to the N-O bond (Figure VII.3), the experimental results give a structure where the SO_2 symmetry axis is more nearly parallel to N_2O. Structural parameters resulting from the semi-empirical calculation are given in Table VII.3 for comparison. The semi-empirical calculations on the SO_2 complexes with CO_2, OCS and CS_2 also did not agree well with experiment in quantitative details.

The experimental N-S distance in $N_2O{\bullet}SO_2$ of 3.69 Å shows an impressive agreement with the ORIENT value of 3.64 Å. The experimental R_{cm} distance is 3.33 Å, though, compared to a semi-empirical distance of 3.62 Å. It is interesting that the model has reproduced one distance well while differing by nearly 0.3 Å in the other. It appears upon examination of the two structures that this is due to a tipping of the SO_2 plane downwards (toward N1) in the experimental structure while leaving the sulfur atom in roughly the same position as predicted by ORIENT.

The structures obtained from *ab initio* calculations on $N_2O{\bullet}SO_2$ are similar to the semi-empirical results. Several calculations were performed at the SCF, DFT and MP2 levels of approximation. The results of the three computations differ only by a few degrees in most angles. There is a slightly wider range of values for the angle between R_{cm} and the SO_2 symmetry axis, with the MP2 calculation having a value about 10° larger than the other calculations. As with $(CO_2)_2N_2O$, the *ab initio* calculations seem to greatly over-estimate the intermolecular distances. In this case the difference is consistent with the semi-empirical calculation, though, since the $S\text{-}N_{central}$ distance is in good agreement

Reproduced with permission of the copyright owner. Further reproduction prohibited without permission.

with experiment, and only R_{cm} is overestimated. The N-S distances from the *ab initio* calculations range from 3.64 to 3.69 Å, all similar to the experimental value of 3.69 Å.

A calculation was performed with the dimer constrained to C_s symmetry. This gave a transition state at a structure similar to that observed for SO_2-OCS and predicted by ORIENT for SO_2-CO_2. The structural parameters for this configuration are given in the last column of Table VII.3. Although the *ab initio* prediction for the global minimum is quite different from the experimental results, the existence of a transition state at this structure provides evidence that the proposed tunneling motion between two asymmetric configurations is feasible. The transition state is about 126 cm^{-1} higher in energy than the global minimum. This barrier may be low enough to support the suggestion that tunneling occurs between two mirror image conformations as proposed in Chapter IV.

As with the $(CO_2)_2N_2O$ calculations, the computations on N_2O•SO_2 were done with only the 6-31G* basis set and did not explore many different geometrical configurations. It is possible, and indeed probable, that exploration of more complex calculations and other regions of the potential energy surface would lead to different local minima.

$(N_2O)_2$•SO_2 Calculations

As with the $(CO_2)_2N_2O$ trimer, semi-empirical modeling was an important part of the spectral assignment process in the study of $(N_2O)_2$•SO_2. Three structures were obtained from the ORIENT program, and the global minimum structure for the complex deviated significantly from the expected barrel-like geometry (see Appendix F for DMMs).

The previously described problems modeling N_2O•SO_2 with ORIENT and the difference in the predicted structure from trimers of only linear triatomics led to skepticism about the validity of the model; however, experiment showed that the lowest

Reproduced with permission of the copyright owner. Further reproduction prohibited without permission.

energy structure (E = –0.01041 E_h, Table VII.4) does resemble experimental Structure I (Figure V.1). It aligns the N_2O molecules in a non-planar conformation that is intermediate between T-shaped and crossed. The oxygen end of one N_2O points toward

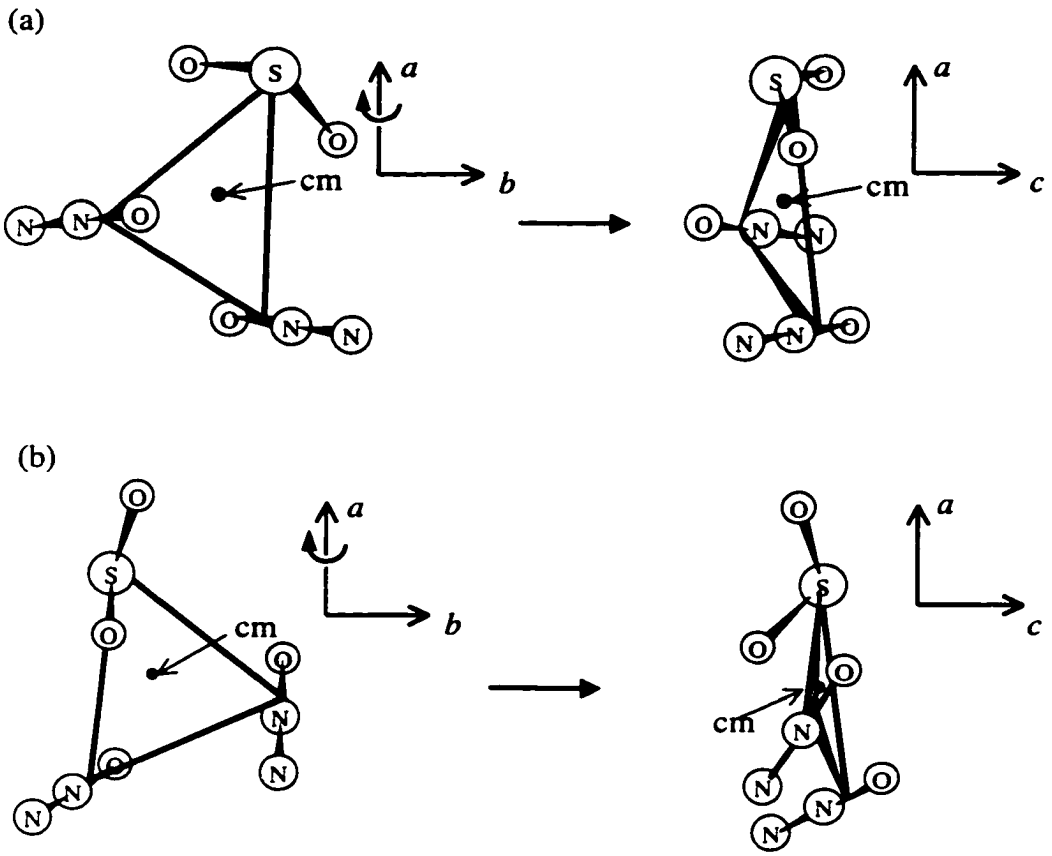


Figure VII.4. The second (a) and third (b) highest energy structures predicted by the ORIENT program for $(N_2O)_2SO_2$. The lowest energy structure resembles Structure I, shown in Fig. V.1. See Table VII.4 for the energies of the three configurations.

the central nitrogen of the other N_2O. The SO_2 molecule is positioned so the oxygen atoms roughly straddle both N_2O molecules. This structure roughly resembles the pinwheel, planar C_3 structure of one of the two observed CO_2 trimers,[22, 23] where each CO_2 dimer fragment is more T-shaped than slipped-parallel. Two other configurations were found which have the N_2O molecules aligned roughly parallel to each other (Figure VII.4). In these structures, the sulfur atom of the SO_2 and the centers of mass of the N_2O

Reproduced with permission of the copyright owner. Further reproduction prohibited without permission.

molecules form a triangle which is roughly perpendicular to the N_2O axes. In the lower energy of these two structures (E = –0.00968 E_h) the N_2O molecules are aligned with

Table VII.4. Comparison of experimental, *ab initio* and semi-empirical structural parameters for $(N_2O)_2 \cdot SO_2$ (in Å and degrees).

	Expt. Structure I	SCF/ 6-31G*	–0.01041 E_h (–2285 cm^{-1})	–0.00968 E_h (–2125 cm^{-1})	–0.00960 E_h (–2107 cm^{-1})
R_{4-8}	3.8558	4.011	3.749	3.423	3.498
R_{4-12}	3.5316	3.616	3.580	3.393	3.841
θ_{12-4-8}	52.494	52.0	51.62	66.11	57.78
θ_{1-4-8}	83.330	87.7	83.49	117.23	125.49
$\phi_{1-4-8-12}$	–129.99	–136.8	–135.32	112.86	–97.42
θ_{5-8-12}	97.672	102.5	107.63	99.52	123.68
$\phi_{5-8-12-4}$	–151.19	–154.7	–139.20	–127.27	–48.39
θ_{9-12-4}	90.75	88.1	88.91	119.87	69.33
$\phi_{9-12-4-8}$	163.83	164.0	162.09	–123.47	105.69
$\phi_{10-9-12-4}$	–118.66	–118.8	–128.12	115.03	–174.40
A / MHz	1369.1014	1346.0	1415.5	1355.4	1547.2
B / MHz	1115.5816	1071.6	1135.9	1164.7	965.4
C / MHz	730.5790	689.1	739.6	716.8	672.2

their dipoles opposing each other (anti-parallel), and in the higher energy conformation (E = –0.00960 E_h) the dipole moments are aligned roughly parallel to each other. While the second conformation (Fig. VII.4(a)) appears to optimize the interactions between the

Reproduced with permission of the copyright owner. Further reproduction prohibited without permission.

N_2O molecules, the first and third configurations seem to optimize interactions between SO_2 and N_2O. Since the energy difference between these structures is only about 18 cm^{-1}, one cannot say definitely that the energy ordering is accurate. The 160 cm^{-1} difference between these two configurations and the global minimum, however, is probably sufficient to confirm that it is the most favorable configuration.

Examination of the two faces of the lowest energy structure that contain one SO_2 and one N_2O shows that one face has a structure similar to that predicted for the N_2O•SO_2 dimer (Figure VII.3). On the other face the SO_2 straddles the N_2O molecule more symmetrically. Since this structure seems to optimize the interaction between two pairs of monomers while avoiding the unfavorable parallel alignment of the N_2O dipoles, it is sensible that it is lowest in energy. Nevertheless, it is very different from most previously observed trimer structures, and the rotational constants of all three configurations are similar to those found for the normal isotopomer (Table VII.4).

Analysis of the data from five isotopomers and determination of the dipole moment of the complex (Chapter V) led to the conclusion that the experimental structure does resemble the lowest energy theoretical structure. Examination of Table VII.4 shows that the distances for Structure I are within about 0.1 Å of the semi-empirical predictions, and most angles are within 5°. A few of the angles are 10° – 15° from the prediction, but the qualitative agreement is still quite good.

The S-M-M-O angle in Figure V.3(c) (one N_2O-SO_2 face of the experimental structure) is $\phi_{9\text{-}12\text{-}4\text{-}3} = 41.6°$, while the S-M-M angle is 90.8°. This strongly resembles the ORIENT prediction for the dimer, where the dihedral angle is 48.6° and the S-M-M angle is 101.3°. Both parameters are within 10° of those on the trimer face. It is interesting that this configuration was fairly well reproduced in the trimer, while the actual structure of the dimer appears to be quite different.

A comparison of the N_2O-N_2O face of the trimer with the ORIENT prediction is interesting. The center-of-mass distance between the N_2O molecules is 3.86 Å, showing

Reproduced with permission of the copyright owner. Further reproduction prohibited without permission.

relatively good agreement with an ORIENT prediction of 3.75 Å. A comparison of the observed and predicted O-M-M-O dihedral angles shows less quantitative agreement, with an observed angle of 75.3° and a prediction of 52.5°. Although the difference between the prediction and experiment is large in this case, the structures are qualitatively similar, with both showing the intermediate T-shaped/crossed configuration described earlier.

Previous experience with trimers involving linear monomers has indicated a preference for configurations where the monomers resemble a slipped-parallel structure.[13, 16, 18, 24] This mimics the configurations of the isolated dimers which often have an anti-parallel, non-polar arrangement.[14, 25] The noticeably different configuration for the N_2O-N_2O face of $(N_2O)_2$•SO_2 seems to indicate that the N_2O-SO_2 interactions in the trimer are strong enough that it is preferable to distort the N_2O dimer portion of the complex and leave the N_2O-SO_2 faces relatively unchanged. Evidence that this is true is gained from an examination of interaction energies for several dimer calculations using the ORIENT program. Table VII.5 shows interaction energies for parallel but distorted

Table VII.5. Contributions to the interaction energy of various N_2O/SO_2 combinations as predicted by the ORIENT program (in mE_h).

	N_2O-N_2O Parallel/T	N_2O-N_2O anti-parallel	N_2O-SO_2 minimum	N_2O-SO_2 symmetric	$(N_2O)_2$•SO_2
Electrostatic	−1.231	−2.998	−4.249		−7.879
Repulsion	1.382	2.541	3.272		7.025
Dispersion	−1.958	−2.905	−3.784		−9.554
Total	−1.808	−3.362	−4.761	−4.559	−10.407

Reproduced with permission of the copyright owner. Further reproduction prohibited without permission.

toward T-shaped and anti-parallel N_2O dimer structures and symmetric and asymmetric N_2O-SO_2 structures. It is obvious that the mixed dimer interactions are much stronger than the N_2O-N_2O interactions. Thus, it is sensible that the N_2O dimer face of the trimer should be distorted from its isolated configuration, while the N_2O-SO_2 faces are relatively unchanged from the isolated structure.

Ab initio calculations on $(N_2O)_2$•SO_2 give varying results. Geometry optimizations were performed at the SCF and DFT levels of calculation. It was found that DFT computations had a very flat potential energy surface, making it difficult to obtain reliable results. SCF calculations with 6-31G* and cc-pVDZ basis sets led to two different structures. The first resembles the experimental configuration, and a similar structure resulted from a B3LYP/6-31G* calculation. For the DFT calculation the forces were negligible at the converged structure, but the step size was slightly larger than the convergence limit. The second SCF result, obtained with the larger basis set, is a cyclic configuration with only the oxygen atoms of the SO_2 out of the plane. Frequency calculations reveal that both SCF structures are true minima. Table VII.4 compares the SCF/6-31G* calculation with the semi-empirical and experimental results. As usual, the *ab initio* structures greatly over-estimate the intermolecular distances.

Acetylene-N_2O

The complex of acetylene with nitrous oxide differs from the other clusters presented in this dissertation, because it is a dimer of linear monomers rather than a more complex trimer. The system is an interesting example of different theoretical models giving different structural results, and thus deserves inclusion in this chapter. Initial studies of the complex, including predictions with Muenter's semi-empirical model,[26, 27] were carried out by several groups,[26, 28, 29] and the data led to the conclusion that the monomers were parallel to each other with a line perpendicular to them connecting their

Reproduced with permission of the copyright owner. Further reproduction prohibited without permission.

Reproduced with permission of the copyright owner. Further reproduction prohibited without permission.

centers of mass. Modeling with the ORIENT program led to contradictory results that tilted the oxygen end of the N_2O toward one of the hydrogen atoms of the HCCH.[30]

Table VII.6. Structural parameters for the HCCH•N_2O complex (units of Å, degrees and MHz). See Figure VI.1 for the atom numbers.

	Expt. [a]	K = 1.0 mE_h [b]	K = 1.225 mE_h [b]	K = 1.35 mE_h induction [c]	K = 1.28 mE_h Dist. Pol. [d]	Prev. Expt'l Struct. [e]	Muenter Model [f]	Muenter DMMs [g]
M_4-M_9	3.2961(8)	3.191	3.301	3.309	3.302	3.305	3.31	3.207
N_2-M_4-M_9	93.9(5)	91.5	91.6	91.2	91.8	90.0	91	91.6
M_4-M_9-C_7	80.3(8)	80.3	80.3	79.6	79.3	90.0	90	89.8
A	9394.2683	9357.9	9368.7	9359.0	9375.1	9281.2	9387(1)	9320.6
B	2831.8564	3027.9	2828.3	2816.1	2827.0	2829.9	2829.6(3)	3005.2
C	2168.0780	2287.7	2172.5	2164.8	2172.0	2168.7	2166.6(2)	2272.5

[a] The quality of the fit was $\Delta I_{rms} = 0.107$ amu•Å^2 where $\Delta I_x = I_x$(obs) - I_x(calc).
[b] ORIENT model without induction, pre-exponential factor K as indicated.
[c] ORIENT model, induction included using monomer polarizabilities, pre-exponential factor K as indicated.
[d] ORIENT model, induction included using distributed polarizabilities, pre-exponential factor K as indicated.
[e] Reference 23. The distance is an average distance while the angles are taken to be equilibrium values. Rotational constants were calculated from structural parameters with monomer structures from Chapter VI.
[f] References 21 and 22.
[g] ORIENT model using DMMs from reference 21, default K.

Both the Muenter model and that used by the ORIENT program employ distributed multipole moments (DMMs) to model the electrostatic part of the intermolecular interaction. The Muenter DMMs are listed in his paper;[26] those used for the current work are given in Appendix F. The Muenter model uses a sum over Lennard-Jones terms to account for the dispersion and repulsion parts of the potential, while the ORIENT model employs the exponential repulsion term given in eq. (VII.1) to describe the dispersion-repulsion part of the potential. The scaling factor K in eq. (VII.1) often underestimates intermolecular distances in dimers when set at the default value of 0.001 E_h. In this work, the values $K = 0.001225\ E_h$, $K = 0.00135\ E_h$ and $K = 0.00128\ E_h$ have been used to best reproduce the center of mass separation when running ORIENT with no induction, point polarizabilities and distributed polarizabilities, respectively. The Muenter model also employs a scaling factor by which the intermolecular separation can be adjusted. This factor multiplies the van der Waals radius of each atom and is chosen to best reproduce experimental results for a specific molecule in a chosen system. The sum of scaled van der Waals radii then multiplies the repulsive term of the potential. For HCCH•N_2O, the factor for N_2O was chosen to best reproduce the center of mass distance of that complex, and that of HCCH reproduced the separation in $(HCCH)_2$. It was found, however, that the chosen value for N_2O did not reproduce the N_2O dimer structure well, so the scaling factor that is designed for one system is not necessarily applicable to others.[26]

While the Muenter model does not include induction effects, the ORIENT program can account for these, as described earlier. For nitrous oxide the polarizabilities used in the point polarizability calculation are $\alpha = 2.93$ Å^3 and $\gamma = 2.83$ Å^3, and for acetylene they are $\alpha = 3.36$ Å^3 and $\gamma = 1.75$ Å^3.[31, 32] A calculation using distributed polarizabilities was also performed.

The results of various HCCH•N_2O structural predictions using the ORIENT semi-empirical model are given in Table VII.6. It can be seen that the predicted structures vary

Reproduced with permission of the copyright owner. Further reproduction prohibited without permission.

little with the inclusion of induction in the calculations. Variation of the pre-exponential term K affects mainly the intermolecular separation while changing the angular relationship within the complex very little. Comparison with the experimental structure, also shown in Table VII.6, indicates angles and rotational constants which are well reproduced. All the $\theta_{N_2\text{-}M_4\text{-}M_9}$ predictions are within 2.7° of the experimental value and within 0.6° of each other. The $\theta_{M_4\text{-}M_9\text{-}C_7}$ values are predicted within 1.0° of the experiment and of each other. A small variation in K also leads to good reproduction of the center-of-mass distance, although the default K of 0.001 E_h predicts a distance that is only 0.1 Å too small. In contrast, the predictions from Muenter's model are within one degree of a parallel structure. This difference seems to be due mainly to the DMMs that were used for the predictions. If the DMMs from Muenter are used with the ORIENT program, a structure that closely resembles that proposed by Muenter is obtained. The structural parameters from this prediction are given in the last column of Table VII.6. Several other sets of DMMs calculated using different basis sets also led to a tilted structure with the ORIENT program, although this aspect was not exhaustively explored.

Ab initio calculations seem to add more evidence to the case for a tilted rather

Table VII.7. Comparison of experimental and *ab initio* structural parameters for HCCH•N_2O (units of Å, degrees and MHz).

	Expt.	SCF/6-31G*	DFT/6-31G*	MP2/6-31G*
M_4-M_9	3.2961(8)	3.524	3.326	3.144
N_2-M_4-M_9	93.9(5)	94.0	93.5	91.2
M_4-M_9-C_7	80.3(8)	74.3	83.7	87.9
A	9394.2683	9841.9	9274.0	8970.9
B	2831.8564	2471.6	2787.4	3132.8
C	2168.0780	1975.5	2143.2	2321.9

Reproduced with permission of the copyright owner. Further reproduction prohibited without permission.

than parallel structure for HCCH•N_2O. Calculations were performed at the SCF, DFT and MP2 levels with a 6-31G* basis set. The results are summarized in Table VII.7. All three calculations give a structure with the oxygen end of N_2O tipped toward one of the hydrogen atoms of the acetylene. Angles are within a few degrees of the experiment, although they are not as closely reproduced as by the ORIENT model. Prediction of the intermolecular separations is less accurate, as seen in the previous *ab initio* calculations. The SCF calculation over estimates the R_{cm} distance by several tenths of an Angstrom, and, surprisingly, the MP2 calculation underestimates this distance by a comparable amount. The DFT intermolecular separation is only about 0.03 Å larger than the experimental value, and this combined with angles within 5° of experiment make the DFT calculation the best prediction.

General Conclusions

The examination of a series of dimers and trimers has made it possible to assess the usefulness of the ORIENT semi-empirical model as a predictive tool for the study of weakly bound complexes. The model is impressively successful, especially considering that induction and anisotropic effects in the dispersion and repulsion terms are not included. Of the five complexes that were examined, only one was significantly different from the semi-empirical prediction. This was the N_2O•SO_2 dimer, whose structure is relatively uncertain and may be much closer to the predictions than it appears. In general, the ORIENT model seems to give angles that are within 10° of experiment, although occasionally the difference is larger. This is sufficient to give qualitatively accurate spectral predictions that are a very useful assignment tool. Occasionally, agreement between the model and experiment is much more quantitative, as in the case of $(CO_2)_2N_2O$. It seems that the exceptionally good reproduction of the experimental structure in this case is purely a chance occurrence, since most predictions are not as

Reproduced with permission of the copyright owner. Further reproduction prohibited without permission.

accurate. The prediction of the correct global minimum configuration for the sulfur dioxide containing trimer, $(N_2O)_2 \bullet SO_2$, is particularly gratifying, since $N_2O \bullet SO_2$ was not modeled well, and other SO_2 containing dimers have also been problematic. It is possible that the constraints caused by the greater number of interactions which must be simultaneously optimized in a trimer system may lead to a better performance on trimers containing SO_2 compared to similar dimers. The study of SO_2 containing species is of atmospheric interest and also pushes toward more complex trimer systems than have previously been examined. The success of the ORIENT model on this first SO_2 containing trimer is encouraging, since it suggests that other trimers containing SO_2 may be modeled accurately, as well. This will facilitate the assignment of more complex species which will lead to a better understanding of intermolecular forces.

The use of *ab initio* calculations to model dimers and trimers is much more complicated than semi-empirical modeling. Even relatively small computations are much more time consuming than semi-empirical ones, and the need to do calculations that account for electron correlation and the polarization of the monomers exacerbates the problem. Nevertheless, for most of the species studied in this thesis a reasonable prediction of the structure could be obtained with a relatively small calculation. The largest problem in using this type of computation in a predictive sense appears to be the overestimation of intermolecular distances, leading to rotational constants that are considerably smaller than the experimental values and making predicted spectra inaccurate. Another major problem is the flatness of the potential energy surfaces for weakly bound complexes which makes it difficult to obtain converged geometry optimizations, either leading to exceedingly long calculations or no results at all in some cases. Presumably, the *ab initio* calculations work as well as they do in the absence of proper treatment of electron correlation, because the anisotropy in the electrostatic interactions (moderately well modeled even at the SCF level) is the key determinant of the basic configuration. It is possible that use of a larger basis set, such as cc-pVDZ,

Reproduced with permission of the copyright owner. Further reproduction prohibited without permission.

would improve the calculations significantly, although a small amount of exploration with this basis in the current work did not indicate that this was the case. Many successful calculations have been done at the MP2 level with cc-pVDZ or cc-pVTZ basis sets,[10 - 12] and this might improve the results significantly enough to make the much greater expenditure in computation time worthwhile.

Full explorations of the potential energy surfaces of the systems studied were beyond the scope of this research. This further exploration would make it possible to determine whether *ab initio* calculations generally find that the global minimum energy structure is similar to the experimental structure.

In general, it seems that as predictive tools the semi-empirical calculations are much more practical and accurate than fairly small *ab initio* calculations. Use of the default parameters in ORIENT gives qualitatively correct configurations, that are also quantitatively quite accurate, and can also lead to useful information on induced dipole components if induction is included in a calculation. *Ab initio* calculations are useful but relatively unreliable, with differing levels of calculation giving the best results for different systems and over estimated distances making accurate prediction of rotational constants difficult. At this time, they probably remain better tools for rationalization rather than prediction of structures.

Reproduced with permission of the copyright owner. Further reproduction prohibited without permission.

References for Chapter VII

[1] C. W. Gillies, J, Z. Gillies, R. D. Suenram, F. J. Lovas, E. Kraka and D. Cremer, J. Am. Chem. Soc. **113**, 2412 (1991).

[2] J. Z. Gillies, C. W. Gillies, R. D. Suenram, F. J. Lovas, W. Stahl, J. Am. Chem. Soc. **111**, 3073 (1989).

[3] A. J. Stone, A. Dullweber, M. P. Hodges, P. L. A. Popelier and D. J. Wales, *ORIENT: A program for studying interactions between molecules, Version 3.2*, University of Cambridge (1995).

[4] A. J. Stone, *The Theory of Intermolecular Forces*; Oxford: Clarendon Press (1996).

[5] *CADPAC: The Cambridge Analytic Derivatives Package Issue 6*, Cambridge (1995). A suite of quantum chemistry programs developed by R. D. Amos with contributions from I. L. Alberts, J. S. Andrews, S. M. Colwell, N. C. Handy, D. Jayatilaka, P. J. Knowles, R. Kobayashi, K. E. Laidig, G. Laming, A. M. Lee, P. E. Maslen, C. W. Murray, J. E. Rice, E. D. Simandiras, A. J. Stone, M.-D. Su and D. J. Tozer.

[6] K. Mirsky in *The Determination of Intermolecular Interaction Energy By Empirical Methods*, R. Schenk, R. Olthof-Hazenkamp, H. Van Koningveld, G. C. Bassi, eds., Delft University Press: Delft, The Netherlands, (1978).

[7] M. A. Spackman, J. Chem. Phys. **85**, 6579 (1986).

[8] S. A. Peebles and R. L. Kuczkowski, J. Mol. Struct. **447**, 151 (1998).

[9] *Gaussian 94, Revision E.2*, M. J. Frisch, G. W. Trucks, H. B. Schlegel, P. M. W. Gill, B. G. Johnson, M. A. Robb, J. R. Cheeseman, T. Keith, G. A. Petersson, J. A. Montgomery, K. Raghavachari, M. A. Al-Laham, V. G. Zakrzewski, J. V. Ortiz, J. B. Foresman, J. Cioslowski, B. B. Stefanov, A. Nanayakkara, M. Challacombe, C. Y. Peng, P. Y. Ayala, W. Chen, M. W. Wong, J. L. Andres, E. S. Replogle, R. Gomperts, R. L. Martin, D. J. Fox, J. S. Binkley, D. J. Defrees, J. Baker, J. P. Stewart, M. Head-Gordon, C. Gonzalez and J. A. Pople, Gaussian, Inc., Pittsburgh, PA (1995).

[10] V. M. Rayón and J. A. Sordo, J. Chem. Phys. **110**, 377 (1999).

[11] Z. Kisiel, E. Białkowska-Jaworska, L. Pszczółkowski, A. Milet, C. Struniewicz, R. Moszynski and J. Sadlej, J. Chem. Phys. **112**, 5767 (2000).

[12] S. S. Xantheas and T. H. Dunning, Jr., J. Chem. Phys **99**, 8774 (1993).

[13] J. P. Connelly, A. Bauder, A. Chisholm and B. J. Howard, Mol. Phys. **88**, 915 (1996).

Reproduced with permission of the copyright owner. Further reproduction prohibited without permission.

[14] R. W. Randall, J. M. Wilkie, B. J. Howard and J. S. Muenter, Mol. Phys. **69**, 839 (1990).

[15] J. M. LoBue, J. K. Rice and S. E. Novick, Chem. Phys. Lett. **112**, 376 (1984).

[16] S. A. Peebles and R. L. Kuczkowski, J. Phys. Chem. **102**, 8091 (1998).

[17] R. A. Peebles and R. L. Kuczkowski, J. Chem. Phys., in press.

[18] S. A. Peebles and R. L. Kuczkowski, J. Chem. Phys. **109**, 5276 (1998).

[19] L. H. Sun, I. I. Ioannou and R. L. Kuczkowski, Mol. Phys. **88**, 255 (1996).

[20] S. A. Peebles, L. H. Sun, I. I. Ioannou and R. L. Kuczkowski, J. Mol. Struct. **485-486**, 211 (1999).

[21] S. A. Peebles, L. H. Sun and R. L. Kuczkowski, J. Chem. Phys. **110**, 6804 (1999).

[22] M. J. Weida and D. J. Nesbitt, J. Chem. Phys. **105**, 10210 (1996).

[23] G. T. Fraser, A. S. Pine, W. J. Lafferty and R. E. Miller, J. Chem. Phys. **87**, 1502 (1987).

[24] R. A. Peebles, S. A. Peebles and R. L. Kuczkowski, Mol. Phys. **96**, 1355 (1999).

[25] Z. S. Huang and R. E. Miller, J. Chem. Phys. **89**, 5408 (1988).

[26] T. A. Hu, L. H. Sun and J. S. Muenter, J. Chem. Phys. **95**, 1537 (1991).

[27] J. S. Muenter, J. Chem. Phys. **94**, 2781 (1991).

[28] H. O. Leung, J. Chem. Phys. **107**, 2232 (1997).

[29] H. O. Leung, Chem. Comm. **22**, 2525 (1996).

[30] S. A. Peebles and R. L. Kuczkowski, J. Phys. Chem. **103**, 3884 (1999).

[31] G. R. Alms, A. K. Burnham and W. H. Flygare, J. Chem. Phys. **63**, 3321 (1975).

[32] C. G. Gray and K. E. Gubbins, *Theory of Molecular Fluids Vol. 1: Fundamentals*, Oxford University Press: Oxford, (1984).

Reproduced with permission of the copyright owner. Further reproduction prohibited without permission.

APPENDICES

Reproduced with permission of the copyright owner. Further reproduction prohibited without permission.

APPENDIX A

This appendix containes tables of transition frequencies for $(OCS)_3$.

Table A.1. Frequencies of measured rotational transitions for $(^{18}OCS)_3$ (in MHz).

$J'_{K_a K_c'}$	$J''_{K_a K_c''}$	Frequency	$\Delta\nu^a$
5_{15}	4_{14}	5731.850	0.001
5_{05}	4_{04}	5733.384	0.000
5_{24}	4_{23}	6117.078	0.002
5_{14}	4_{13}	6160.769	–0.001
5_{33}	4_{32}	6399.617	0.001
5_{42}	4_{41}	6498.074	–0.002
5_{41}	4_{40}	6584.159	0.002
5_{23}	4_{22}	6605.207	0.001
5_{41}	4_{31}	7587.620	–0.002
5_{42}	4_{32}	7692.189	–0.002
5_{50}	4_{40}	7962.711	0.001
5_{51}	4_{41}	7971.907	0.001
6_{16}	5_{15}	6838.528	–0.001
6_{06}	5_{05}	6838.810	–0.001
6_{25}	5_{24}	7237.156	–0.001
6_{15}	5_{14}	7249.494	–0.001
6_{34}	5_{33}	7588.809	0.000
6_{24}	5_{23}	7717.317	–0.001
6_{33}	5_{32}	8073.109	–0.002
6_{51}	5_{41}	9228.634	0.002
6_{52}	5_{42}	9287.679	–0.001

Reproduced with permission of the copyright owner. Further reproduction prohibited without permission.

Table A.1. (continued)

$J'_{Ka'Kc'}$	$J''_{Ka''Kc''}$	Frequency	$\Delta\nu$[a]
6_{60}	5_{50}	9592.597	–0.001
6_{61}	5_{51}	9595.606	0.001
7_{17}	6_{16}	7944.720	0.001
7_{07}	6_{06}	7944.767	0.000
7_{26}	6_{25}	8346.827	0.000
7_{16}	6_{15}	8349.677	0.001
7_{35}	6_{34}	8734.287	–0.001
7_{34}	6_{33}	9270.808	0.001
7_{70}	6_{60}	11220.187	–0.001
7_{71}	6_{61}	11221.096	0.000

[a] $\Delta\nu = \nu_{obs} - \nu_{calc}$ (in MHz).

Reproduced with permission of the copyright owner. Further reproduction prohibited without permission.

Table A.2. Frequencies of measured rotational transitions for $(O^{13}CS)_3$ (in MHz).

$J'_{K_a'K_c'}$	$J''_{K_a''K_c''}$	Frequency	$\Delta\nu^a$
5_{15}	4_{14}	5863.310	0.004
5_{05}	4_{04}	5864.888	0.004
5_{24}	4_{23}	6267.016	–0.001
5_{14}	4_{13}	6312.245	–0.002
5_{33}	4_{32}	6563.758	0.000
5_{42}	4_{41}	6667.702	–0.001
5_{41}	4_{40}	6758.810	0.001
5_{23}	4_{22}	6778.400	0.003
5_{32}	4_{31}	6924.375	0.000
5_{32}	4_{22}	7560.878	0.002
5_{41}	4_{31}	7805.238	0.002
5_{42}	4_{32}	7915.015	0.000
5_{50}	4_{40}	8196.863	0.001
5_{51}	4_{41}	8206.595	–0.002
6_{16}	5_{15}	6994.381	–0.001
6_{06}	5_{05}	6994.668	–0.003
6_{15}	5_{14}	7424.677	–0.002
6_{25}	5_{24}	7411.978	–0.001
6_{34}	5_{33}	7780.888	–0.002
6_{24}	5_{23}	7914.295	0.002
6_{33}	5_{32}	8288.963	–0.002

Reproduced with permission of the copyright owner. Further reproduction prohibited without permission.

Table A.2. (continued)

$J'_{Ka'Kc'}$	$J''_{Ka''Kc''}$	Frequency	$\Delta\nu$[a]
6_{60}	5_{50}	9875.275	0.001
6_{61}	5_{51}	9878.467	–0.004
7_{26}	6_{25}	8546.132	0.002
7_{16}	6_{15}	8549.048	0.001
7_{35}	6_{34}	8952.239	–0.003
7_{25}	6_{24}	9005.194	0.000
7_{34}	6_{33}	9513.868	0.001
7_{70}	6_{60}	11551.262	–0.003
7_{71}	6_{61}	11552.239	0.002
8_{17}	7_{16}	9677.717	0.001

[a] $\Delta\nu = \nu_{obs} - \nu_{calc}$ (in MHz).

Reproduced with permission of the copyright owner. Further reproduction prohibited without permission.

APPENDIX B

This appendix contains tables of transition frequencies for $(CO_2)_2N_2O$.

Table B.1. Transition frequencies (estimated center frequencies) of assigned lines for normal $(CO_2)_2N_2O$ (in MHz).

$J'_{Ka'Kc'}$	$J''_{Ka''Kc''}$	Frequency	Obs. - Calc.
2_{11}	1_{01}	5296.266	0.005
2_{21}	1_{10}	5623.347	–0.013
2_{20}	1_{10}	5820.397	–0.004
2_{20}	1_{01}	6586.757	–0.007
3_{13}	2_{12}	5485.408	0.001
3_{03}	2_{02}	5596.060	0.002
3_{13}	2_{02}	5645.108	0.005
3_{22}	2_{21}	6191.994	–0.005
3_{12}	2_{11}	6621.243	0.026
3_{21}	2_{20}	6787.839	–0.012
3_{22}	2_{11}	7285.441	–0.014
3_{12}	2_{02}	7986.453	–0.012
3_{21}	2_{11}	8078.355	0.015
3_{22}	2_{12}	8490.991	–0.016
3_{30}	2_{20}	8995.270	0.001
3_{21}	2_{02}	9443.597	0.008
4_{04}	3_{13}	7175.098	0.006
4_{14}	3_{13}	7187.440	–0.008
4_{04}	3_{03}	7224.126	–0.012
4_{14}	3_{03}	7236.481	–0.012
4_{23}	3_{22}	8093.055	0.009

Reproduced with permission of the copyright owner. Further reproduction prohibited without permission.

Table B.1. (cont.)

$J'_{K_a K_c'}$	$J''_{K_a K_c''}$	Frequency	Obs. - Calc.
4_{32}	3_{31}	8520.489	–0.003
4_{23}	3_{12}	8757.297	0.013
4_{31}	3_{30}	8855.761	–0.025
4_{22}	3_{21}	9104.327	0.019
4_{13}	3_{03}	10849.614	–0.005
5_{05}	4_{14}	8859.116	0.002
5_{15}	4_{14}	8861.915	0.002
5_{05}	4_{04}	8871.461	–0.009
5_{15}	4_{04}	8874.268	–0.001
5_{24}	4_{23}	9890.987	0.009
5_{14}	4_{13}	10087.841	–0.015
5_{33}	4_{32}	10566.989	0.008
5_{41}	4_{40}	10887.407	0.012
5_{23}	4_{22}	11198.895	–0.016
5_{32}	4_{31}	11344.307	–0.005
6_{06}	5_{15}	10526.245	0.003
6_{16}	5_{15}	10526.838	0.002
6_{06}	5_{05}	10529.040	–0.001
6_{16}	5_{05}	10529.639	0.005
6_{25}	5_{24}	11613.062	0.015
6_{15}	5_{14}	11685.560	–0.019

Reproduced with permission of the copyright owner. Further reproduction prohibited without permission.

Table B.2. Transition frequencies for the $(^{13}CO_2)_2 \cdot N_2O$ isotope (in MHz).

$J'_{K_a'K_c'}$	$J''_{K_a''K_c''}$	Frequency	Obs. – Calc.
2_{11}	1_{01}	5240.920	0.021
2_{20}	1_{10}	5745.449	–0.034
2_{21}	1_{11}	5946.769	–0.020
2_{20}	1_{01}	6500.121	0.017
3_{03}	2_{12}	5373.487	–0.001
3_{03}	2_{02}	5525.165	0.000
3_{13}	2_{02}	5570.667	0.006
3_{22}	2_{21}	6126.834	–0.013
3_{12}	2_{11}	6551.466	0.008
3_{21}	2_{20}	6728.469	0.024
3_{12}	2_{02}	7908.090	–0.020
3_{21}	2_{11}	7987.656	0.006
3_{31}	2_{20}	8800.604	0.005
3_{22}	2_{12}	8390.661	0.001
3_{30}	2_{20}	8872.977	–0.001
3_{31}	2_{21}	9000.963	–0.002
4_{04}	3_{13}	7086.862	0.005
4_{04}	3_{03}	7132.345	–0.008
4_{14}	3_{03}	7143.542	–0.005
4_{23}	3_{22}	8003.079	–0.002
4_{13}	3_{12}	8359.031	0.003
4_{32}	3_{31}	8436.529	–0.010
4_{23}	3_{12}	8637.330	0.021
4_{31}	3_{30}	8781.847	0.004
4_{22}	3_{21}	9017.986	–0.006
4_{22}	3_{12}	10454.188	0.004

Reproduced with permission of the copyright owner. Further reproduction prohibited without permission.

Table B.2. (cont.)

$J'_{K_a K_c'}$	$J''_{K_a K_c''}$	Frequency	Obs. – Calc.
4_{13}	3_{03}	10741.976	0.003
5_{05}	4_{14}	8747.794	0.017
5_{15}	4_{14}	8750.255	0.001
5_{05}	4_{04}	8758.968	–0.004
5_{15}	4_{04}	8761.429	–0.019
5_{24}	4_{23}	9775.516	0.003
5_{14}	4_{13}	9961.680	0.001
5_{33}	4_{32}	10457.701	–0.009
6_{06}	5_{15}	10392.899	0.014
6_{16}	5_{15}	10393.395	–0.004
6_{06}	5_{05}	10395.359	–0.003
6_{16}	5_{05}	10395.872	–0.004

Table B.3. Transition frequencies for the $^{13}CO_2$•$^{12}CO_2$•N_2O isotope (in MHz).

$J'_{K_a K_c'}$	$J''_{K_a K_c''}$	Frequency	Obs. – Calc.
2_{20}	1_{10}	5797.208	–0.009
3_{03}	2_{12}	5394.779	–0.009
3_{13}	2_{12}	5446.898	0.008
3_{03}	2_{02}	5560.573	–0.002
3_{13}	2_{02}	5612.687	0.010
3_{22}	2_{21}	6142.887	0.009
3_{12}	2_{11}	6570.912	0.016
3_{22}	2_{11}	7256.897	–0.004
3_{12}	2_{02}	7926.858	–0.002
3_{30}	2_{20}	8967.180	0.002
3_{31}	2_{21}	9092.277	–0.001

Reproduced with permission of the copyright owner. Further reproduction prohibited without permission.

Table B.3. (cont.)

$J'_{K_aK_c'}$	$J''_{K_aK_c''}$	Frequency	Obs. – Calc.
3_{21}	2_{12}	9220.468	0.003
3_{21}	2_{02}	9386.256	0.004
4_{04}	3_{13}	7125.166	–0.019
4_{14}	3_{13}	7138.606	–0.009
4_{04}	3_{03}	7177.282	–0.005
4_{14}	3_{03}	7190.724	0.006
4_{23}	3_{22}	8032.760	0.002
4_{13}	3_{12}	8404.132	0.009
4_{32}	3_{31}	8448.584	–0.004
4_{31}	3_{30}	8769.664	–0.003
4_{13}	3_{12}	8459.238	0.026
4_{22}	3_{21}	9026.864	0.001
4_{13}	3_{03}	10770.400	–0.009
5_{05}	4_{14}	8799.314	–0.006
5_{15}	4_{14}	8802.428	–0.003
5_{05}	4_{04}	8812.756	0.006
5_{15}	4_{04}	8815.867	0.007
6_{06}	5_{15}	10455.669	0.003
6_{16}	5_{15}	10456.340	0.000
6_{06}	5_{05}	10458.780	0.004
6_{16}	5_{05}	10459.448	–0.004

Reproduced with permission of the copyright owner. Further reproduction prohibited without permission.

Table B.4. Transition frequencies for the $^{12}CO_2$•$^{13}CO_2$•N_2O isotope (in MHz).

$J'_{Ka'Kc'}$	$J''_{Ka''Kc''}$	Frequency	Obs. – Calc.
3_{03}	2_{12}	5414.677	0.006
3_{13}	2_{12}	5457.308	–0.007
3_{03}	2_{02}	5560.382	0.011
3_{13}	2_{02}	5603.014	0.000
3_{22}	2_{21}	6176.037	0.002
3_{12}	2_{11}	6601.464	0.022
3_{12}	2_{02}	7967.683	–0.014
3_{21}	2_{11}	8036.085	–0.004
3_{22}	2_{12}	8434.487	–0.020
3_{30}	2_{20}	8901.081	0.018
3_{31}	2_{21}	9031.310	0.024
4_{04}	3_{13}	7136.350	–0.017
4_{14}	3_{13}	7146.603	–0.003
4_{04}	3_{03}	7178.991	–0.019
4_{14}	3_{03}	7189.246	–0.002
4_{23}	3_{22}	8063.182	0.015
4_{13}	3_{12}	8413.225	0.022
4_{32}	3_{31}	8508.793	0.004
4_{31}	3_{30}	8869.317	0.009
4_{22}	3_{21}	9095.342	0.004
4_{22}	3_{12}	10529.964	–0.021
4_{32}	3_{22}	11364.039	–0.001
4_{41}	3_{30}	12066.242	–0.017
4_{40}	3_{30}	12089.424	–0.001
4_{41}	3_{31}	12142.594	0.006

Reproduced with permission of the copyright owner. Further reproduction prohibited without permission.

Table B.4. (cont.)

$J'_{K_a K_c'}$	$J''_{K_a K_c''}$	Frequency	Obs. – Calc.
5_{05}	4_{14}	8807.201	–0.002
5_{15}	4_{14}	8809.413	–0.002
5_{05}	4_{04}	8817.438	–0.004
5_{15}	4_{04}	8819.647	–0.006
5_{14}	4_{13}	10022.272	–0.013
6_{06}	5_{15}	10463.080	0.002
6_{16}	5_{15}	10463.530	0.005
6_{06}	5_{05}	10465.292	0.003
6_{16}	5_{05}	10465.744	0.007

Table B.5. Transition frequencies for the CO_2•CO_2•$^{15}N_2O$ isotope (in MHz).

$J'_{K_a K_c'}$	$J''_{K_a K_c''}$	Frequency	Obs. – Calc.
2_{11}	1_{01}	5198.727	0.002
2_{21}	1_{10}	5557.881	0.001
2_{20}	1_{10}	5743.531	–0.001
2_{21}	1_{11}	5948.617	–0.001
2_{20}	1_{11}	6134.269	–0.001
2_{20}	1_{01}	6509.227	0.000
3_{12}	2_{20}	5177.669	0.005
3_{03}	2_{12}	5324.761	0.000
3_{13}	2_{12}	5379.147	–0.001
3_{03}	2_{02}	5494.664	–0.002
3_{13}	2_{02}	5549.054	0.001
3_{22}	2_{21}	6063.380	0.001
3_{12}	2_{11}	6488.164	–0.001
3_{21}	2_{20}	6632.002	–0.002

Reproduced with permission of the copyright owner. Further reproduction prohibited without permission.

Table B.5. (cont.)

$J'_{K_a K_c}$	$J''_{K_a K_c}$	Frequency	Obs. – Calc.
3_{22}	2_{11}	7188.230	0.002
3_{12}	2_{02}	7830.245	–0.001
3_{21}	2_{11}	7942.505	0.000
3_{22}	2_{12}	8360.402	0.000
3_{31}	2_{20}	8827.257	0.001
3_{30}	2_{20}	8890.293	0.000
3_{31}	2_{21}	9012.910	0.002
3_{30}	2_{21}	9075.945	0.001
3_{21}	2_{12}	9114.678	–0.002
4_{04}	3_{13}	7036.618	–0.001
4_{14}	3_{13}	7050.900	–0.001
4_{04}	3_{03}	7091.005	–0.001
4_{14}	3_{03}	7105.289	0.000
4_{23}	3_{22}	7931.515	–0.001
4_{13}	3_{12}	8304.925	0.004
4_{32}	3_{31}	8336.309	–0.003
4_{31}	3_{30}	8644.844	0.004
4_{22}	3_{21}	8907.049	–0.003
4_{41}	3_{30}	12067.462	0.007
4_{40}	3_{30}	12085.002	–0.008
4_{41}	3_{31}	12130.489	–0.002
4_{40}	3_{31}	12148.048	0.002
5_{05}	4_{14}	8691.277	0.000
5_{15}	4_{14}	8694.647	0.000
5_{05}	4_{04}	8705.554	–0.005

Reproduced with permission of the copyright owner. Further reproduction prohibited without permission.

Table B.5. (cont.)

$J'_{Ka'Kc'}$	$J''_{Ka''Kc''}$	Frequency	Obs. – Calc.
5_{15}	4_{04}	8708.928	–0.001
5_{14}	4_{13}	9911.516	0.006
6_{06}	5_{15}	10327.506	–0.010
6_{16}	5_{15}	10328.260	–0.002
6_{06}	5_{05}	10330.888	0.002
6_{16}	5_{05}	10331.646	0.014
6_{15}	5_{14}	11476.626	–0.004

Table B.6. Transition frequencies for the $CO_2 \cdot CO_2 \cdot N_2{}^{18}O$ isotope (in MHz)

$J'_{Ka'Kc'}$	$J''_{Ka''Kc''}$	Frequency	Obs. – Calc.
2_{11}	1_{01}	5240.716	0.000
2_{20}	1_{11}	6148.901	–0.004
3_{03}	2_{12}	5403.691	0.012
3_{13}	2_{12}	5451.957	0.018
3_{03}	2_{02}	5560.617	–0.012
3_{13}	2_{02}	5608.891	0.001
3_{12}	2_{11}	6564.457	0.004
3_{21}	2_{11}	7992.772	0.011
3_{22}	2_{12}	8397.503	–0.010
3_{31}	2_{20}	8824.860	–0.010
3_{30}	2_{20}	8892.849	–0.005
3_{31}	2_{21}	9017.569	0.000
3_{30}	2_{21}	9085.566	0.013
4_{04}	3_{13}	7133.345	–0.009
4_{14}	3_{13}	7145.529	0.008
4_{04}	3_{03}	7181.607	–0.007

Reproduced with permission of the copyright owner. Further reproduction prohibited without permission.

Table B.6. (cont.)

$J'_{K_a K_c'}$	$J''_{K_a K_c''}$	Frequency	Obs. – Calc.
4_{14}	3_{03}	7193.783	0.002
4_{32}	3_{31}	8450.221	–0.007
4_{23}	3_{12}	8684.823	0.006
4_{22}	3_{21}	9022.451	–0.016
4_{22}	3_{12}	10450.786	0.011
5_{05}	4_{14}	8809.280	0.000
5_{15}	4_{14}	8812.035	–0.001
5_{05}	4_{04}	8821.442	–0.005
5_{15}	4_{04}	8824.190	–0.013
5_{24}	4_{23}	9820.024	0.006
5_{14}	4_{13}	10013.552	0.000
6_{06}	5_{15}	10468.575	–0.009
6_{16}	5_{15}	10469.163	–0.006
6_{06}	5_{05}	10471.349	0.009
6_{16}	5_{05}	10471.938	0.014

Table B.7. Transition frequencies for the $CO_2 \bullet CO_2 \bullet {}^{15}N^{14}NO$ isotope (in MHz).

$J'_{K_a K_c'}$	$J''_{K_a K_c''}$	Frequency	Obs. – Calc.
2_{11}	1_{01}	5230.877	0.007
2_{20}	1_{11}	6163.883	–0.005
2_{20}	1_{01}	6535.875	0.003
3_{03}	2_{12}	5361.807	–0.002
3_{13}	2_{12}	5414.584	0.000
3_{03}	2_{02}	5528.709	0.004
3_{13}	2_{02}	5581.484	0.004
3_{22}	2_{21}	6105.700	0.001

Reproduced with permission of the copyright owner. Further reproduction prohibited without permission.

Table B.7. (cont.)

$J'_{K_a K_c}$	$J''_{K_a K_c}$	Frequency	Obs. – Calc.
3_{12}	2_{11}	6532.020	–0.005
3_{21}	2_{20}	6682.592	–0.007
3_{22}	2_{11}	7221.634	0.001
3_{12}	2_{02}	7881.450	–0.002
3_{22}	2_{12}	8404.161	–0.002
3_{31}	2_{20}	8861.647	0.004
3_{30}	2_{20}	8926.609	0.001
3_{31}	2_{21}	9050.712	0.002
3_{30}	2_{21}	9115.673	–0.002
3_{21}	2_{12}	9170.135	0.005
4_{04}	3_{13}	7082.887	0.001
4_{14}	3_{13}	7096.578	0.001
4_{04}	3_{03}	7135.660	–0.001
4_{14}	3_{03}	7149.349	–0.002
4_{23}	3_{22}	7984.962	0.000
4_{13}	3_{12}	8356.459	0.001
4_{23}	3_{12}	8674.561	–0.008
4_{31}	3_{30}	8713.046	0.004
4_{22}	3_{12}	10427.072	–0.001
4_{32}	3_{21}	10575.624	0.002
4_{13}	3_{03}	10709.204	–0.001
4_{31}	3_{21}	10957.045	–0.006
5_{05}	4_{14}	8747.484	0.005
5_{15}	4_{14}	8750.672	0.001
5_{05}	4_{04}	8761.171	0.001
5_{15}	4_{04}	8764.356	–0.005

Reproduced with permission of the copyright owner. Further reproduction prohibited without permission.

Table B.7. (cont.)

$J'_{K_aK_c'}$	$J''_{K_aK_c''}$	Frequency	Obs. – Calc.
5_{14}	4_{13}	9970.736	0.004
5_{41}	4_{40}	10714.749	0.001
6_{06}	5_{15}	10394.104	–0.004
6_{16}	5_{15}	10394.799	–0.005
6_{06}	5_{05}	10397.300	0.002
6_{16}	5_{05}	10398.002	0.006

Reproduced with permission of the copyright owner. Further reproduction prohibited without permission.

APPENDIX C

The tunneling motion in $N_2O{\bullet}SO_2$ complicated the spectral assignment by leading to intensity variations and frequency perturbations in the transitions. Some details of the assignment process are given in this appendix, followed by transition frequencies for all the assigned isotopomers of $N_2O{\bullet}SO_2$.

Although the measured dipole moment of $N_2O{\bullet}SO_2$ had all three selection rules, only *a*- and *c*-type transitions were assigned. Besides the missing *b*-dipole transitions, some of the *a*- and *c*-dipole transitions were perturbed. The intensity of the *a*-dipole *R*-branch clusters was unusual. For the higher frequency component of the doublet, the $K_a = 0$ and upper $K_a = 1$ transitions were very strong while the lower $K_a = 1$ was weak. This intensity pattern was reversed for the lower component of the doublet. It has not been possible to propose a completely satisfactory explanation for this intensity variation. The weaker intensity of the lower tunneling doublet transitions has prevented unequivocal assignments of some of the lower frequency components for several isotopic species.

For the normal isotopomer 11 *a*-type and 3 *c*-type transitions were measured for the higher frequency component, and 10 *a*-type transitions were measured for the lower frequency component. The lower $K_a = 1$ transitions for the upper frequency component were perturbed, and their intensities were low. Because of this, they were removed from the fit. Their Stark effects did appear to be consistent with the assignment, although the weaker Stark components could not be definitely observed. One possible *c*-type transition for the lower tunneling component of the normal isotope was also measured, but failure to identify additional *c*-type transitions made it impossible to confirm the assignment. Similar sets of transitions were measured for the upper tunneling components of the other isotopomers, but assignments of the lower component spectra are relatively uncertain and quite incomplete. Although transitions have been observed that are believed to belong to the lower tunneling component of each species, it has been

Reproduced with permission of the copyright owner. Further reproduction prohibited without permission.

impossible to identify enough transitions for any of these spectra to confirm an assignment unequivocally. The use of Stark effect data as an assignment tool was not possible since that type of measurement requires lines that are stronger than most of the lower tunneling doublet transitions. Another contribution to the difficulty of making these assignments was the multitude of lines in some regions where transitions were expected. The close overlap of the upper component of the $^{15}N_2O$-$^{34}SO_2$ species with the lower component of $^{15}N_2O$-$^{32}SO_2$ caused further complication. The $^{15}N_2O$-$^{34}SO_2$ upper component transitions had about the same intensity when measured in natural abundance as was expected for the weak lower tunneling doublets of $^{15}N_2O$-$^{32}SO_2$. Only after a marked increase in intensity was observed upon use of a ^{34}S enriched sample was this species correctly identified and assigned.

One possible *b*-type transition was observed about 900 MHz above the predicted frequency. A tentative identification as the upper component *b*-type $J = 1 \leftarrow 0$ transition of the normal species was based on a Stark effect measurement and the fact that a small quadrupole splitting similar to that of the *c*-type $J = 1 \leftarrow 0$ transition was observed. (The splitting is probably ^{14}N quadrupole related, since the *c*-dipole transitions for the $^{15}N_2O$ species were unsplit.) Attempts at finding the corresponding $J = 2 \leftarrow 1$ transition were unsuccessful, so there is not conclusive proof that this is a *b*-type transition. The large perturbation from the predicted frequency is not unexpected. Since the direction of the μ_b-component of the dipole moment is presumably reversed by the proposed tunneling motion, this is a tunneling-rotation transition rather than a pure rotational transition with perturbation due to the tunneling motion.

Reproduced with permission of the copyright owner. Further reproduction prohibited without permission.

Reproduced with permission of the copyright owner. Further reproduction prohibited without permission.

Table C.1. Upper frequency tunneling doublet transition frequencies for $N_2O{\bullet}SO_2$ (in MHz).

	$^{14}N_2O{\bullet}^{32}SO_2$		$^{15}N_2O{\bullet}^{32}SO_2$		$^{14}N_2{}^{18}O{\bullet}^{32}SO_2$		$^{15}N_2O{\bullet}^{34}SO_2$		$^{15}N_2O{\bullet}^{32}S^{18}O_2$	
$J'_{Ka'Kc'}$ - $J''_{Ka''Kc''}$	Frequency	Obs – Calc	Frequency	Obs – Calc	Frequency	Obs – Calc	Frequency	Obs – Calc	Frequency	Obs – Calc
1_{10}-0_{00}	7616.778	0.001	7513.705	0.000	7401.054	–0.006	7498.897	0.001	7076.934	0.071[a]
2_{12}-1_{11}	5822.803	32.989[a]	5659.137	29.736[a]						
2_{02}-1_{01}	5857.240	−0.002	5684.244	−0.002	5757.932	0.004	5593.487	0.001	5552.995	−0.003
2_{11}-1_{10}	5907.940	0.000	5727.631	0.000	5796.367	–0.004	5634.735	0.005	5616.971	0.003
2_{11}-1_{01}	10594.966	−0.014[a]	10398.170	0.000	10317.467	0.008	10335.889	0.000	9915.934	0.006
3_{13}-2_{12}	8728.397	48.312[a]	8484.458	44.916[a]	8604.859	46.156[a]	8356.687	44.820[a]	8244.266	48.537[a]
3_{03}-2_{02}	8780.154	0.000	8521.059	0.002	8631.748	–0.003	8385.156	−0.006	8322.315	−0.005
3_{12}-2_{11}	8857.254	0.001	8586.848	0.000	8689.991	–0.001	8447.618	−0.004	8420.115	0.002
3_{12}-2_{02}	13594.991	−0.001	13300.772	0.000	13249.520	–0.002	13190.024	−0.002	12783.037	−0.006
4_{14}-3_{13}	11630.664	66.182[a]	11305.571	61.572[a]	11468.537	65.594[a]	11133.493	59.466[a]	10982.507	65.061[a]
4_{04}-3_{03}	11695.862	0.000	11351.218	−0.001	11499.112	0.001	11170.493	0.004	11082.591	0.003
4_{13}-3_{12}	11800.605	0.000	11400.224	0.006[a]	11577.784	0.002	11254.808	0.003	11216.366	0.003
5_{05}-4_{04}	14601.447	0.069[a]	14172.060	0.000	14357.366	0.000	13946.900	−0.001	13830.072	−0.001
5_{14}-4_{13}	14735.386	0.000	14285.233	0.000	14457.184	0.000	14053.796	−0.001	14002.589	−0.001

[a] not included in fit

Reproduced with permission of the copyright owner. Further reproduction prohibited without permission.

Table C.2. Lower frequency tunneling doublet transition frequencies for $N_2O{\bullet}SO_2$ (in MHz).

	$^{14}N_2O{\bullet}^{32}SO_2$		$^{15}N_2O{\bullet}^{32}SO_2$		$^{14}N_2{}^{18}O{\bullet}^{32}SO_2$		$^{15}N_2O{\bullet}^{34}SO_2$		$^{15}N_2O{\bullet}^{32}S^{18}O_2$	
$J'_{Ka'Kc'}$ - $J''_{Ka''Kc''}$	Frequency	Obs – Calc	Frequency	Obs – Calc	Frequency	Obs – Calc	Frequency	Obs – Calc	Frequency	Obs – Calc
2_{12}-1_{11}	5729.422	–0.020	5565.307	0.226[a]	5648.462	–0.102				
2_{02}-1_{01}	5766.268	0.079[a]	5594.354	–0.028						
2_{11}-1_{10}	5814.633	–0.020	5643.093	0.302[a]						
3_{13}-2_{12}	8589.272	0.014	8343.024	0.017	8470.648	0.117	8209.988	–0.024	8097.268	–0.993
3_{03}-2_{02}	8643.923	0.033	8386.713	–0.050	8496.179	3.754[a]	8240.765	0.077	8185.836	11.810[a]
3_{12}-2_{11}	8717.364	0.013	8460.257	0.041			8304.566	–0.054	8282.189	0.006
4_{14}-3_{13}	11443.223	0.410[a]	11114.783	–0.232[a]	11289.299	–0.037	10940.625	0.018	10788.972	0.740
4_{04}-3_{03}	11514.703	–0.033	11173.030	0.052	11318.749	0.000	10981.417	–0.058	10900.559	13.079[a]
4_{13}-3_{12}	11614.319	0.205[a]	11272.461	–0.030			11067.991	0.040		
5_{15}-4_{14}			13878.488	–0.011	14102.301	–0.990[a]	13667.723	2.544[a]	13477.409	8.106[a]
5_{05}-4_{04}	14375.817	0.007								

[a] not included in fit.

APPENDIX D

This appendix containes tables of transition frequencies for $(N_2O)_2 \bullet SO_2$.

Table D.1. Transition frequencies for $(N_2O)_2 \bullet SO_2$ (in MHz).

$J'_{K_a K_c'}$	$J''_{K_a K_c''}$	Frequency	Obs. – Calc.
3_{12}	2_{11}	5904.0641	0.0032
3_{31}	2_{20}	7661.4899	–0.0011
3_{30}	2_{21}	7980.0246	0.0022
3_{21}	2_{12}	8299.2614	–0.0079
4_{04}	3_{13}	6328.6880	–0.0025
4_{14}	3_{13}	6332.9576	0.0023
4_{04}	3_{03}	6350.3397	0.0021
4_{14}	3_{03}	6354.6058	0.0034
4_{13}	3_{22}	7058.0525	–0.0017
4_{23}	3_{22}	7197.0219	–0.0012
4_{13}	3_{12}	7452.8596	0.0005
4_{23}	3_{12}	7591.8259	–0.0021
4_{22}	3_{21}	8196.0130	–0.0052
4_{32}	3_{21}	9165.0839	–0.0016
4_{41}	3_{30}	10481.6097	0.0053
4_{31}	3_{22}	10527.2685	0.0124
4_{40}	3_{31}	10613.4085	0.0005
4_{22}	3_{13}	11649.2828	–0.0001
5_{05}	4_{14}	7799.4656	–0.0005
5_{15}	4_{14}	7800.2223	–0.0005
5_{05}	4_{04}	7803.7326	0.0017
5_{15}	4_{04}	7804.4889	0.0014

Reproduced with permission of the copyright owner. Further reproduction prohibited without permission.

Table D.1. (cont.)

$J'_{K_a K_c'}$	$J''_{K_a K_c''}$	Frequency	Obs. – Calc.
5_{14}	4_{23}	8716.1871	–0.0076
5_{24}	4_{23}	8752.4806	–0.0007
5_{14}	4_{13}	8855.1526	–0.0109
5_{24}	4_{13}	8891.4443	–0.0059
5_{23}	4_{22}	9957.3743	–0.0042
5_{33}	4_{22}	10426.1083	0.0080
5_{42}	4_{31}	12103.6321	–0.0121
5_{51}	4_{40}	13261.9637	–0.0071
5_{50}	4_{41}	13308.2107	0.0081
6_{06}	5_{15}	9262.1682	0.0031
6_{16}	5_{15}	9262.2918	0.0009
6_{06}	5_{05}	9262.9221	0.0004
6_{16}	5_{05}	9263.0436	–0.0040
6_{15}	5_{24}	10238.2039	0.0112
6_{25}	5_{24}	10246.1632	–0.0020
6_{15}	5_{14}	10274.4945	0.0152
6_{25}	5_{14}	10282.4544	0.0026
7_{07}	6_{16}	10723.2229	–0.0016
7_{17}	6_{06}	10723.3717	0.0013
7_{26}	6_{25}	11715.0731	–0.0057
7_{16}	6_{15}	11721.4729	–0.0009
7_{26}	6_{15}	11723.0536	0.0023
8_{08}	7_{17}	12183.9324	–0.0046
8_{18}	7_{07}	12183.9623	0.0022

Reproduced with permission of the copyright owner. Further reproduction prohibited without permission.

Table D.2. Transition frequencies for $(^{15}N_2O)_2 \cdot SO_2$ (in MHz).

$J'_{K_a K_c'}$	$J''_{K_a K_c''}$	Frequency	Obs. – Calc.
3_{22}	2_{21}	5322.1788	0.0009
3_{21}	2_{20}	5901.8778	0.0035
3_{22}	2_{11}	6122.4698	–0.0012
3_{31}	2_{20}	7476.0541	0.0007
3_{30}	2_{21}	7760.1680	–0.0040
3_{21}	2_{12}	8003.7088	–0.0027
4_{04}	3_{13}	6096.9817	–0.0037
4_{14}	3_{13}	6102.5986	–0.0034
4_{04}	3_{03}	6123.3530	0.0006
4_{14}	3_{03}	6128.9682	–0.0007
4_{13}	3_{22}	6760.3826	0.0037
4_{23}	3_{22}	6927.1549	0.0003
4_{13}	3_{12}	7198.2106	0.0002
4_{32}	3_{31}	7356.2838	0.0006
4_{23}	3_{12}	7364.9873	0.0013
4_{31}	3_{30}	7727.2478	–0.0041
4_{22}	3_{21}	7871.9771	0.0036
4_{32}	3_{21}	8930.4626	0.0003
4_{31}	3_{22}	10165.2482	0.0022
4_{41}	3_{3c}	10227.9629	–0.0005
4_{40}	3_{31}	10338.5078	0.0018
5_{05}	4_{14}	7516.1523	0.0015
5_{15}	4_{14}	7517.2275	–0.0003
5_{05}	4_{04}	7521.7678	0.0004
5_{15}	4_{04}	7522.8465	0.0021
5_{14}	4_{23}	8387.1822	–0.0005

Reproduced with permission of the copyright owner. Further reproduction prohibited without permission.

Table D.2. (cont.)

$J'_{K_a K_c'}$	$J''_{K_a K_c''}$	Frequency	Obs. – Calc.
5_{24}	4_{23}	8434.4970	0.0016
5_{14}	4_{13}	8553.9578	–0.0006
5_{24}	4_{13}	8601.2691	–0.0019
5_{33}	4_{32}	9090.1831	–0.0009
5_{23}	4_{22}	9600.1728	0.0005
5_{32}	4_{31}	9878.0967	0.0001
5_{33}	4_{22}	10148.6751	0.0023
5_{42}	4_{31}	11805.9555	0.0004
5_{41}	4_{32}	12469.8844	–0.0006
5_{51}	4_{40}	12939.1474	–0.0001
5_{50}	4_{41}	12975.4971	–0.0007
6_{06}	5_{15}	8925.7068	–0.0002
6_{16}	5_{15}	8925.9002	–0.0004
6_{06}	5_{05}	8926.7825	–0.0015
6_{16}	5_{05}	8926.9769	–0.0006
6_{15}	5_{24}	9868.0332	–0.0018
6_{25}	5_{24}	9879.2971	–0.0004
6_{15}	5_{14}	9915.3479	0.0003
6_{25}	5_{14}	9926.6118	0.0016
6_{34}	5_{33}	10705.9238	–0.0024
6_{24}	5_{23}	11045.7324	0.0004
7_{07}	6_{16}	10333.1614	–0.0001
7_{17}	6_{06}	10333.3900	0.0017

Reproduced with permission of the copyright owner. Further reproduction prohibited without permission.

Table D.3. Transition frequencies for $^{15}N_2O$•$^{14}N_2O$•SO_2.

$J'_{Ka'Kc'}$	$J''_{Ka''Kc''}$	Frequency	Obs. – Calc.
3_{12}	2_{11}	5777.1970	–0.0009
3_{22}	2_{11}	6241.6666	0.0086
3_{31}	2_{20}	7623.2845	0.0020
3_{30}	2_{21}	7901.8384	–0.0032
3_{21}	2_{12}	8122.7428	–0.0018
4_{04}	3_{13}	6208.9272	–0.0048
4_{14}	3_{13}	6215.2660	–0.0009
4_{04}	3_{03}	6237.8628	0.0032
4_{13}	3_{22}	6862.2881	0.0034
4_{23}	3_{22}	7044.1787	–0.0077
4_{22}	3_{21}	7990.5883	0.0021
4_{13}	3_{12}	7326.7403	–0.0045
4_{23}	3_{12}	7508.6555	0.0090
4_{32}	3_{21}	9107.3353	0.0073
4_{31}	3_{22}	10324.8721	–0.0079
4_{41}	3_{30}	10427.8680	–0.0049
4_{40}	3_{31}	10533.7989	0.0003
4_{22}	3_{13}	11361.6946	0.0042
5_{05}	4_{14}	7656.1108	–0.0011
5_{15}	4_{14}	7657.3523	–0.0079
5_{05}	4_{04}	7662.4512	0.0044
5_{15}	4_{04}	7663.6960	0.0009
5_{14}	4_{23}	8529.5373	0.0027
5_{24}	4_{23}	8582.6832	–0.0007
5_{23}	4_{32}	8642.9879	0.0086
5_{14}	4_{13}	8711.4378	0.0016

Reproduced with permission of the copyright owner. Further reproduction prohibited without permission.

Table D.3. (cont.)

$J'_{K_a K_c'}$	$J''_{K_a K_c''}$	Frequency	Obs. – Calc.
5_{24}	4_{13}	8764.5835	–0.0020
5_{23}	4_{22}	9759.7079	–0.0132
5_{33}	4_{22}	10352.2664	0.0020
5_{51}	4_{40}	13190.6230	–0.0041
5_{50}	4_{41}	13224.6447	0.0071
6_{06}	5_{15}	9092.8392	0.0004
6_{16}	5_{15}	9093.0693	0.0000
6_{06}	5_{05}	9094.0878	0.0008
6_{16}	5_{05}	9094.3201	0.0026
6_{15}	5_{24}	10044.0582	–0.0058
6_{15}	5_{14}	10097.2199	0.0066
6_{25}	5_{14}	10110.2209	–0.0075
7_{07}	6_{16}	10527.2053	–0.0080
7_{17}	6_{06}	10527.4925	0.0079
7_{16}	6_{15}	11512.6710	0.0024

Table D.4. Transition frequencies for $^{14}N_2O$•$^{15}N_2O$•SO_2.

$J'_{K_a K_c'}$	$J''_{K_a K_c''}$	Frequency	Obs. – Calc.
3_{12}	2_{11}	5806.0301	–0.0008
3_{22}	2_{11}	6182.6247	0.0000
3_{31}	2_{20}	7520.8735	–0.0096
3_{30}	2_{21}	7842.2529	0.0106
3_{21}	2_{12}	8174.1772	0.0020
4_{04}	3_{13}	6213.0725	–0.0049
4_{14}	3_{13}	6216.9745	0.0065

Reproduced with permission of the copyright owner. Further reproduction prohibited without permission.

Table D.4. (cont.)

$J'_{Ka'Kc'}$	$J''_{Ka''Kc''}$	Frequency	Obs. – Calc.
4_{04}	3_{03}	6233.2312	0.0004
4_{14}	3_{03}	6237.1320	0.0106
4_{13}	3_{22}	6944.1769	–0.0141
4_{32}	3_{21}	8994.9416	–0.0077
4_{41}	3_{30}	10290.4837	0.0000
4_{40}	3_{31}	10425.5269	0.0023
5_{05}	4_{14}	7655.6140	–0.0038
5_{15}	4_{14}	7656.2998	0.0055
5_{05}	4_{04}	7659.5113	0.0029
5_{15}	4_{04}	7660.1838	–0.0011
5_{24}	4_{23}	8598.6061	0.0059
6_{06}	5_{15}	9090.5905	–0.0086
6_{25}	5_{14}	10096.0981	0.0025
7_{26}	6_{15}	11510.7602	0.0016

Table D.5. Transition frequencies for $(^{15}N_2O)_2 \bullet {}^{34}SO_2$.

$J'_{Ka'Kc'}$	$J''_{Ka''Kc''}$	Frequency	Obs. – Calc.
3_{12}	2_{11}	5650.9998	0.0008
3_{22}	2_{11}	6037.6380	–0.0028
3_{30}	2_{21}	7663.7363	–0.0008
3_{21}	2_{12}	7966.4774	0.0020
4_{04}	3_{13}	6043.5743	0.0034
4_{14}	3_{13}	6047.8165	–0.0001
4_{04}	3_{03}	6064.9623	0.0026
4_{14}	3_{03}	6069.2053	–0.0002
4_{13}	3_{22}	6744.9710	–0.0018

Reproduced with permission of the copyright owner. Further reproduction prohibited without permission.

Table D.5. (cont.)

$J'_{K_a K_c}$	$J''_{K_a K_c}$	Frequency	Obs. – Calc.
4_{23}	3_{22}	6882.0997	–0.0038
4_{13}	3_{12}	7131.6169	0.0023
4_{23}	3_{12}	7268.7421	–0.0032
4_{22}	3_{21}	7845.9183	0.0005
4_{32}	3_{21}	8793.6010	0.0031
4_{41}	3_{30}	10068.4296	–0.0005
4_{31}	3_{22}	10102.6782	0.0000
4_{40}	3_{31}	10194.1896	–0.0027
5_{05}	4_{14}	7447.0036	–0.0034
5_{15}	4_{14}	7447.7638	–0.0022
5_{15}	4_{04}	7452.0112	–0.0006
5_{14}	4_{23}	8331.9063	0.0024
5_{24}	4_{23}	8367.9979	0.0011
5_{14}	4_{13}	8469.0359	0.0014
5_{24}	4_{13}	8505.1280	0.0005
5_{23}	4_{22}	9532.9665	–0.0004
5_{33}	4_{22}	9994.4360	0.0031
5_{42}	4_{31}	11619.3386	–0.0017
5_{51}	4_{40}	12740.1254	0.0051
5_{50}	4_{41}	12783.9694	–0.0037
6_{06}	5_{15}	8842.4806	–0.0034
6_{16}	5_{05}	8843.3766	0.0063
6_{15}	5_{24}	9785.9082	0.0005
6_{25}	5_{14}	9829.9887	–0.0042

Reproduced with permission of the copyright owner. Further reproduction prohibited without permission.

APPENDIX E

This appendix contains tables of transition frequencies for HCCH•N_2O.

Table E.1. Transition frequencies of HCCH•N_2O measured in this work (in MHz).

$J'_{Ka'Kc'}$	$J''_{Ka''Kc''}$	HCCH•$^{15}N_2O$		$H^{13}C^{12}CH•^{15}N_2O$		$H^{12}C^{13}CH•^{15}N_2O$		$H^{12}C^{12}CH•^{15}N^{14}NO$		$H^{12}C^{12}CD•^{15}N_2O$	
		Frequency	Obs. – Calc.	Frequency	Obs. – Calc.	Frequency	Obs. – Calc.	Frequency	Obs. – Calc.	Frequency	Obs. – Calc.
1_{10}	1_{01}	7024.498	0.001	7011.793	-0.005	7006.335	-0.001	7011.904	0.000	6664.025	0.000
1_{11}	0_{00}	11281.909	-0.001	11183.009	0.003	11185.280	0.003	11294.896	0.000	10814.661	0.002
2_{11}	2_{02}	7730.701	0.000	7689.034	0.000	7686.870	0.000	7728.733	0.000	7374.085	-0.001
2_{12}	1_{11}	9172.487	0.002	8974.765	0.005	8993.067	-0.006	9232.787	0.000	8959.903	0.006
2_{02}	1_{01}	9782.297	0.001	9562.873	-0.004	9583.602	-0.004	9850.269	0.000	9567.775	-0.005
2_{11}	1_{10}	10488.498	-0.002	10240.116	0.003	10264.148	0.008	10567.099	0.000	10277.838	-0.002
2_{12}	1_{01}							15577.456	0.000		
3_{03}	2_{12}	8796.857	0.000	8442.289	-0.004	8483.026	-0.001	8924.629	0.000	8827.699	0.003
3_{12}	3_{03}	8877.647	0.001	8786.076	0.002	8789.659	-0.004	8894.217	0.000	8531.793	0.002
3_{13}	2_{12}	13728.994	-0.001	13434.585	-0.004	13461.795	0.002	13818.563	0.000	13408.450	-0.002
3_{03}	2_{02}							14651.816	0.001		

Reproduced with permission of the copyright owner. Further reproduction prohibited without permission.

Reproduced with permission of the copyright owner. Further reproduction prohibited without permission.

Table E.1. (cont.)

$J'_{Ka'Kc'}$	$J''_{Ka''Kc''}$	$HCCH{\bullet}^{15}N_2O$		$H^{13}C^{12}CH{\bullet}^{15}N_2O$		$H^{12}C^{13}CH{\bullet}^{15}N_2O$		$H^{12}C^{12}CH{\bullet}^{15}N^{14}NO$		$H^{12}C^{12}CD{\bullet}^{15}N_2O$	
		Frequency	Obs. – Calc.	Frequency	Obs. – Calc.	Frequency	Obs. – Calc.	Frequency	Obs. – Calc.	Frequency	Obs. – Calc.
3_{22}	2_{21}							14848.255	0.000		
3_{21}	2_{20}							15045.833	0.000		
3_{12}	2_{11}							15817.300	0.001		
3_{21}	3_{12}							18312.559	0.000		
4_{13}	4_{04}	10557.737	0.000	11389.275	-0.001	10401.829	0.001	10603.136	0.000	10233.450	0.000
4_{04}	3_{13}	14258.122	0.000	13786.249	0.003	13837.908	0.000	14421.345	0.000		
4_{22}	4_{13}							17528.244	0.000		
4_{14}	3_{13}							18370.793	0.000		
5_{14}	4_{23}							9369.400	0.000		
5_{14}	5_{05}	12862.317	0.000					12948.239	0.000	12570.811	0.000
5_{23}	5_{14}							16914.301	0.000		

APPENDIX F

This appendix contains tables of the DMMs used in ORIENT calculations.

Table F.1. DMMs for OCS calculated with and without bond centers (in a.u.).

	Q_{00}	Q_{10}	Q_{20}	Q_{30}	Q_{40}
O	–0.519	–0.083	0.277	0.437	0.708
C	0.646	–0.458	0.287	1.753	7.088
S	–0.127	0.080	1.659	–0.755	2.341
O	–0.169	0.218	0.354	0.185	0.068
O-C [a]	–0.672	0.024	0.476	0.054	0.066
C	1.186	–0.668	0.416	0.189	0.634
C-S [a]	–0.778	0.212	0.848	–0.305	0.669
S	0.433	–0.720	2.371	–0.704	0.209

[a]Calculated at the bond center

Table F.2. Multipole moments for CO_2 and N_2O (in a.u.) used in $(CO_2)_2N_2O$ calculations and $HCCH{\bullet}N_2O$ calculations.

	z[a]	Q_{00}	Q_{10}	Q_{20}	Q_{30}	Q_{40}
C	0.0000	1.3975	0.0000	–0.2773	0.0000	1.9108
O	2.1959	–0.6988	0.3949	–0.1688	0.2869	–0.2226
O	–2.1959	–0.6988	–0.3949	–0.1688	–0.2869	–0.2226
N	0.0000	0.6260	0.4547	0.0240	–0.5179	2.3912
N	–2.1278	–0.1349	0.0879	–0.0657	0.3688	0.9279
O	2.2507	–0.4911	0.0044	0.4962	0.3722	–0.7351

[a] z-coordinate in a.u.

Reproduced with permission of the copyright owner. Further reproduction prohibited without permission.

Table F.3. Distributed multipole moments for SO_2. The coordinates of SO_2 are x(S) = 0.00000, y(S) = 0.00000; x(O) = ±2.33328, y(O) = −1.36619; x(BC) = ±1.16962, y(BC) = −0.68324. All quantities are in atomic units. Used for $N_2O{\bullet}SO_2$ and $(N_2O)_2{\bullet}SO_2$ calculations.

	S	O	O	BC1	BC2
Q_{00}	1.90811	−0.08198	−0.08198	−0.87208	−0.87208
Q_{11c}	0.00000	−0.42845	0.42845	−0.19928	0.19928
Q_{11s}	−1.78374	0.41797	0.41797	0.16783	0.16783
Q_{20}	−0.20267	−0.25003	−0.25003	−0.66404	−0.66404
Q_{22c}	1.32120	0.35691	0.35691	−0.24356	−0.24356
Q_{22s}	0.00000	−0.85711	0.85711	−0.69849	0.69849
Q_{31c}	0.00000	0.43857	−0.43857	−0.37498	0.37498
Q_{31s}	0.19447	−0.32947	−0.32947	0.12772	0.12772
Q_{33c}	0.00000	0.30226	−0.30226	−0.00423	0.00423
Q_{33s}	0.43277	0.60714	0.60714	−0.46519	−0.46519
Q_{40}	0.27140	0.26853	0.26853	0.08971	0.08971
Q_{42c}	−0.19708	−0.08980	−0.08980	0.09319	0.09319
Q_{42s}	0.00000	0.38557	−0.38557	0.45509	−0.45509
Q_{44c}	−0.42292	−0.46765	−0.46765	−0.63153	−0.63153
Q_{44s}	0.00000	−0.20926	0.20926	−0.12204	0.12204

Reproduced with permission of the copyright owner. Further reproduction prohibited without permission.

Table F.4. Distributed multipole moments for N_2O with bond centers (in a.u.). Used for $N_2O \cdot SO_2$ and $(N_2O)_2 \cdot SO_2$ calculations.

Atom	z[a]	Q_{00}	Q_{10}	Q_{20}	Q_{30}	Q_{40}
N	0.000	1.35199	0.17842	0.07026	–0.37472	0.25430
N	–2.132	0.47621	0.66166	0.22873	0.19597	0.08704
O	2.239	–0.12595	–0.39704	0.90124	–0.13432	0.02099
BC1	–1.066	–1.13777	–0.00414	0.58964	0.13092	0.44128
BC2	1.121	–0.56448	0.03124	0.19886	0.03267	–0.05722

[a] z refers to the *z*-coordinate of the atom.
[b] BC1 and BC2 refer to the midpoints of the bonds.

Table F.5. Distributed multipole moments for acetylene used in $HCCH \cdot N_2O$ calculations.[a]

Atom	Coordinate[b]	Q_{00}	Q_{10}	Q_{20}	Q_{30}	Q_{40}
H	3.14167	0.03324	0.30454	–0.13257	0.06960	–0.04614
C	1.13667	–0.03324	0.42291	–0.30230	–1.60327	2.11596
C	–1.13667	–0.03324	–0.42291	–0.30230	1.60327	2.11596
H	–3.14167	0.03324	–0.30454	–0.13257	–0.06960	–0.04614

[a] All quantities are in atomic units.
[b] *z* coordinate of atom in Bohr.

Reproduced with permission of the copyright owner. Further reproduction prohibited without permission.